# Development and Characterization of New Test Materials with Adjustable Relaxation and Diffusion Properties for Magnetic Resonance Imaging

**Dissertation**

der Mathematisch-Naturwissenschaftlichen Fakultät

der Eberhard Karls Universität Tübingen

zur Erlangung des Grades eines

Doktors der Naturwissenschaften

(Dr. rer. nat.)

vorgelegt von

Victor Niels Ulrich Fritz

aus Herrenberg

Tübingen

2025

Gedruckt mit Genehmigung der Mathematisch-Naturwissenschaftlichen Fakultät der Eberhard Karls Universität Tübingen.

| | |
|---|---|
| Tag der mündlichen Qualifikation: | 19.12.2025 |
| Dekan: | Prof. Dr. Thilo Stehle |
| 1. Berichterstatter/-in: | Prof. Dr. Dr. Fritz Schick |
| 2. Berichterstatter/-in: | Prof. Dr. Klaus Scheffler |

# Abstract

This thesis focuses on the characterization and development of test materials for quantitative magnetic resonance imaging (MRI), with particular emphasis on materials for fat-water quantification, diffusion-weighted imaging (DWI), and relaxometry at 3 Tesla. The research culminated in four peer-reviewed publications and addressed critical challenges in the design of test materials, including temporal stability, spectral purity, non-toxicity, biomimetic properties, and the ability to independently adjust multiple MR parameters within a single material.

The first part of this thesis (Publication 1) comprehensively evaluated the suitability of three common emulsifiers (polysorbate 60, SDS, and soy lecithin) for preparing oil-in-water emulsions used as tissue analogues for MRI. The study critically assessed the impact of these substances on emulsion stability, spectral properties, and the relaxation and diffusion characteristics of the aqueous phase. The results reveal that emulsifiers influence not only the physical stability of emulsions but also substantially affect the material's signal characteristics, as well as its relaxation and diffusion properties. Among the emulsifiers tested, soy lecithin has been identified as the most suitable candidate for fat-water phantom formulations due to its high stabilizing ability, spectral invisibility, and promising effects on relaxation and diffusion.

Build upon previous findings, the second part of this thesis (Publication 2) positioned soy lecithin as a promising, inexpensive, and non-hazardous alternative that effectively overcomes drawbacks associated with conventional water-diffusion-modifying agents such as polymers and sugars. The study showed that aqueous soy lecithin solutions provide a remarkably wide range of adjustable apparent diffusion coefficient (ADC) values ($2.02 \cdot 10^{-3}$ mm²/s to $0.48 \cdot 10^{-3}$ mm²/s) covering almost the entire physiological spectrum of body parts, and this at relatively low concentrations (0 – 10%) compared to other substances. With the addition of agar, ADC and T2 can be adjusted almost independently. The observation of non-Gaussian diffusion behavior at higher b-

values also underscored the potential for more bio-realistic diffusion characteristics.

In the third part of this work (Publication 3), soy lecithin was introduced and evaluated as a viable and safe alternative to paramagnetic additives for the development of relaxometry phantoms. This work addressed the need for non-toxic, biocompatible materials capable of reproducing tissue-specific T1 and T2 relaxation times. By demonstrating the compatibility of soy lecithin and agar and validating their nearly independent T1 and T2 modifying effects, a preparation protocol (based on simple calculation models) was established for formulating soy lecithin-agar hydrogels with specific relaxation times. Test gels mimicking relaxation times of different tissues, including gray and white matter, kidney, spleen, and muscle, were successfully and reproducibly produced. Deviations between measured and target values were less than 3% for T1 and 6.5% for T2. A significant limitation observed was their poor temporal stability due to material biodegradation, which may restrict their utility in long-term or multi-center studies.

The final part of this thesis (Publication 4) addressed a fundamental challenge in the development of quantitative MRI phantoms: the simultaneous and independent control of T1, T2, and ADC values within a single material. Building upon insights from previous work regarding the individual properties of key components, a three-component system using Gd-DTPA, agarose, and soy lecithin was established. This approach allowed for the creation of hydrogels with precisely adjustable relaxation and diffusion properties. The work introduced a detailed, step-by-step protocol for preparing these hydrogels utilizing concentration dependent models for T1, T2, and ADC. Values of almost all biological tissues could be mimicked with reasonable accuracy, as evidenced by the consistently low deviations between measured and targeted values (less than 8% for T1, 7.5% for T2, and 11.5% for ADC). The developed protocol also demonstrated high reproducibility across different batches, and the resulting gels exhibited acceptable temporal stability over a 12-week storage period.

Overall, this thesis contributed to the advancement of MRI phantom research by addressing multiple questions related to test material characterization and development. Soy lecithin played a key role in this effort, proving to be a new, flexible and effective phantom material that fulfills key criteria such as ADC-

tunability, a single-line spectrum, and biomimetic properties; thus broadening the spectrum of usable and interesting parameter modifying substances.

# Zusammenfassung

Das Ziel dieser Arbeit besteht in der Entwicklung und Charakterisierung von Testmaterialien für die quantitative Magnetresonanztomographie (MRT) mit Schwerpunkt auf Materialien für die Fett-Wasser-Quantifizierung, die diffusionsgewichtete Bildgebung (DWI) und die Relaxometrie bei 3 Tesla. Die Forschungsarbeit mündete in vier begutachteten Publikationen und befasste sich mit kritischen Herausforderungen bei der Herstellung von Testmaterialien, darunter Materialstabilität, spektrale Reinheit, Giftigkeit, biomimetische Eigenschaften und die Möglichkeit, mehrere MR-Parameter innerhalb eines einzigen Materials unabhängig voneinander anzupassen.

Der erste Teil dieser Arbeit (Veröffentlichung 1) analysierte die Eignung von drei gängigen Emulgatoren (Polysorbat 60, SDS und Sojalecithin) für die Herstellung von Öl-in-Wasser-Emulsionen, die als Gewebesurrogate für die MRT verwendet werden. Dabei wurde der Einfluss dieser Substanzen auf die Emulsionsstabilität, die spektralen Eigenschaften sowie die Relaxations- und Diffusionseigenschaften der wässrigen Phase systematisch untersucht. Die Ergebnisse zeigten, dass Emulgatoren nicht nur die physikalische Stabilität von Emulsionen, sondern auch das Signalspektrum des Materials sowie dessen Relaxations- und Diffusionseigenschaften erheblich beeinflussen. Unter den getesteten Emulgatoren wurde Sojalecithin aufgrund seiner hohen Stabilisierungsfähigkeit, spektralen Unsichtbarkeit sowie seiner vielversprechenden Auswirkungen auf Relaxation und Diffusion als am besten geeignet für Fett-Wasser-Phantome identifiziert.

Aufbauend auf diesen Erkenntnissen präsentiert der zweite Teil dieser Arbeit (Veröffentlichung 2) Sojalecithin als vielversprechende, kostengünstige und sichere Alternative zu herkömmlichen Wasserdiffusions-modifizierenden Stoffen wie Polymere und Zucker. Die Studie zeigte, dass wässrige Sojalecithinlösungen bereits bei vergleichsweise niedrigen Konzentrationen (0 – 10 %) einen außergewöhnlich breiten Bereich an scheinbaren Diffusionskoeffizienten ($2{,}02 \cdot 10^{-3}$ mm²/s – $0{,}48 \cdot 10^{-3}$ mm²/s) abdecken und damit nahezu das gesamte physiologische Spektrum abbilden. Zudem ließen sich durch Zugabe von Agar der scheinbare Diffusionskoeffizient (ADC-Wert) und der T2-Wert weitgehend

unabhängig voneinander einstellen. Die Beobachtung nicht-gaußscher Diffusion bei höheren b-Werten unterstreicht darüber hinaus das Potenzial dieser Materialien für die Nachbildung bio-realistischer Diffusionseigenschaften.
Im dritten Teil dieser Arbeit (Veröffentlichung 3) wurde Sojalecithin als praktikable und sichere Alternative zu paramagnetischen Zusätzen für die Entwicklung von Relaxometrie-Phantomen vorgestellt und bewertet. Diese Arbeit befasste sich mit dem Bedarf an ungiftigen, biokompatiblen Materialien, die gewebespezifische T1- und T2-Relaxationszeiten reproduzieren können. Durch die nachgewiesene Kompatibilität von Sojalecithin und Agar sowie deren weitgehend unabhängige Wirkung auf T1- und T2-Werte konnte ein einfaches, modellbasiertes Protokoll für die Herstellung von Sojalecithin-Agar-Hydrogelen entwickelt werden. Test-Gele zur Simulation der Relaxationszeiten verschiedener Gewebe, darunter graue und weiße Hirnsubstanz, Niere, Milz und Muskel, konnten erfolgreich und reproduzierbar hergestellt werden. Die Abweichungen von den Zielwerten lagen bei T1 unter 3 % und bei T2 unter 6,5 %. Eine wesentliche Einschränkung zeigte sich jedoch in der begrenzten Stabilität der Materialien, was ihren Einsatz in longitudinalen oder multizentrischen Studien derzeit noch limitiert.

Der letzte Teil dieser Arbeit (Veröffentlichung 4) befasste sich mit der Herausforderung, T1-, T2- und ADC-Werte innerhalb einer einzigen Probe unabhängig voneinander einstellen zu können. Aufbauend auf Erkenntnissen aus vorherigen Arbeiten wurde ein Dreikomponentensystem aus Gd-DTPA, Agarose und Sojalecithin entwickelt, das die Herstellung von Hydrogelen mit präzise abgestimmten Relaxations- und Diffusionseigenschaften ermöglichte. Die Arbeit präsentierte ein schrittweises Herstellungsprotokoll, das auf empirisch ermittelten, konzentrationsabhängigen Modellen für T1, T2 und ADC basiert. Die Werte der meisten biologischen Gewebe konnten nachgebildet werden, was durch geringe Abweichungen von den angestrebten Zielwerten belegt wurde. Das Herstellungsverfahren zeigte eine hohe Reproduzierbarkeit und die resultierenden Gele blieben über einen Zeitraum von zwölf Wochen hinweg stabil.

Insgesamt leistete diese Arbeit einen Beitrag zum Fortschritt bei der Herstellung von geeigneten MR-Testmaterialien, indem sie verschiedene Fragestellungen zur Entwicklung und Charakterisierung adressierte. Sojalecithin spielte dabei eine

zentrale Rolle und erwies sich als vielseitiger und effektiver Stoff, der zentrale Anforderungen wie ADC-Einstellbarkeit, das Fehlen störender Zusatzsignale im Spektrum und biomimetische Eigenschaften erfüllt; und damit die Möglichkeiten des Einsatzes parametermodifizierender Substanzen sinnvoll erweitert.

# List of Publication

**Publication 1**

**Fritz, V**., Martirosian, P., Machann, J., Daniels, R., Schick, F. (2022)

*A comparison of emulsifiers for the formation of oil-in-water emulsions: stability of the emulsions within 9 h after production and MR signal properties.*

Magnetic Resonance Materials in Physics, Biology and Medicine
DOI: https://doi.org/10.1007/s10334-021-00970-9

**Publication 2**

**Fritz, V**., Martirosian, P., Machann, J., Thorwarth, D., Schick, F. (2023)

*Soy lecithin: A beneficial substance for adjusting the ADC in aqueous solutions to the values of biological tissues.*

Magnetic Resonance in Medicine
DOI: https://doi.org/10.1002/mrm.29543

**Publication 3**

**Fritz, V**., Eisele, S., Martirosian, P., Machann, J., Schick, F. (2024)

*A straightforward procedure to build a non-toxic relaxometry phantom with desired T1 and T2 times at 3T.*

Magnetic Resonance Materials in Physics, Biology and Medicine
DOI: https://doi.org/10.1007/s10334-024-01166-7

**Publication 4**

**Fritz, V**., Schick, F. (2026)

*Recipe for hydrogels with tunable relaxation and diffusion properties for use as MRI test materials.*

Magnetic Resonance in Medicine
DOI: https://doi.org/10.1002/mrm.70120

# List of contents

# Introduction and Objectives

This chapter briefly explains the key concepts and background needed to understand the work and presents the research questions on which the thesis is based.

Reference materials for phantoms are becoming increasingly important with the growing role of quantitative magnetic resonance imaging (MRI) [1-4]. By measuring specific tissue parameters such as relaxation times (T1, T2), diffusion, fat fraction, etc., quantitative MRI allows detailed characterization of tissue properties and is of great importance in the diagnosis and monitoring of many diseases, including tumors, stroke, multiple sclerosis, and hepatic steatosis [5-8].

The development of new imaging sequences requires thorough validation and testing. Appropriate validation mechanisms are critical to ensure that the proposed technique provides reproducible and, most importantly, accurate quantitative measurements. This is where phantoms play a crucial role: Phantoms are specially designed test objects containing materials with stable and well-defined MR properties, such as relaxation times (T1 and T2) or the apparent diffusion coefficient (ADC) [4]. They provide controlled conditions with known reference values, reproducibility, and the absence of biological variability, making them ideal for rapidly testing and optimizing new imaging techniques. The composition and production of such test materials have therefore become an important area of research [9-24].

This cumulative thesis focuses on the development and characterization of test materials suitable for relaxometry-, diffusion-weighted imaging- (DWI), and fat quantification techniques. The following sections will briefly introduce the relevant quantitative MR parameters and the respective imaging techniques used to measure them. Typical phantom materials, which are designed to mimic specific MR properties of biological tissues, are presented and critically analyzed.

## Origin of the MR signal

For a comprehensive understanding of the MR parameters and methods discussed in this thesis, this section provides a brief overview of the origin of the MR signal. A more detailed introduction to MRI and theoretical fundamentals can be found in the textbooks [25-27], on which this subchapter is based.

MRI is based on the physical principle of nuclear magnetic resonance (NMR). Atomic nuclei, which have a non-zero nuclear spin and thus a magnetic moment, are MR-active or MR-detectable. This allows them to interact with an external magnetic field and be excited by radio frequency fields.

In clinical MRI, hydrogen nuclei ($^1$H) are used almost exclusively for imaging. These are particularly suitable due to their high natural abundance in human tissue and their excellent nuclear spin properties: $^1$H-nuclei (protons) have a half-integer spin (spin ½) and have the largest gyromagnetic ratio of all stable atomic nuclei with $\gamma = 26{,}752 \cdot 10^7$ rad $T^{-1}$ $s^{-1}$. In the following, therefore, only protons and their magnetic moments, are considered.

When a sample containing an ensemble of protons is placed in a strong static magnetic field $\vec{B}_0$ (e.g., inside a MR tomograph), their magnetic moments are preferentially oriented along the direction of the field, resulting in the formation of a macroscopic nuclear magnetization. For the following considerations, the z-axis of the reference system is selected along the external magnetic field: $\vec{B}_0 = (0,0,B_0)$. In thermal equilibrium, the net magnetization is aligned with the field (longitudinal magnetization $M_z$) and not directly detectable. To generate a measurable signal, it must first be tipped into the transverse plane. This is achieved by applying a resonant radio frequency (RF) pulse, also referred to $B_1$ field. By applying a resonant RF pulse orthogonal to the static magnetic field $\vec{B}_0$, the thermal equilibrium can be disturbed and the magnetization increasingly shifted from its equilibrium state. This leads to a precession in which the magnetization vector rotates around the main magnetic field at the Larmor frequency ($w_l = \gamma \cdot B_0$). Note: the resonance condition is fulfilled only if the frequency of the RF pulse is very close to the Lamor frequency ($\omega_{RF} \approx \omega_0$). The rotating transverse magnetization $M_{xy}$ creates a time-varying magnetic flux that induces a detectable alternating voltage – the MR signal – in a receiver coil. The

amplitude of the MR signal depends on the flip angle $\alpha$ by which the magnetization has been deflected, which in turn is determined by the strength and duration of the RF pulse.

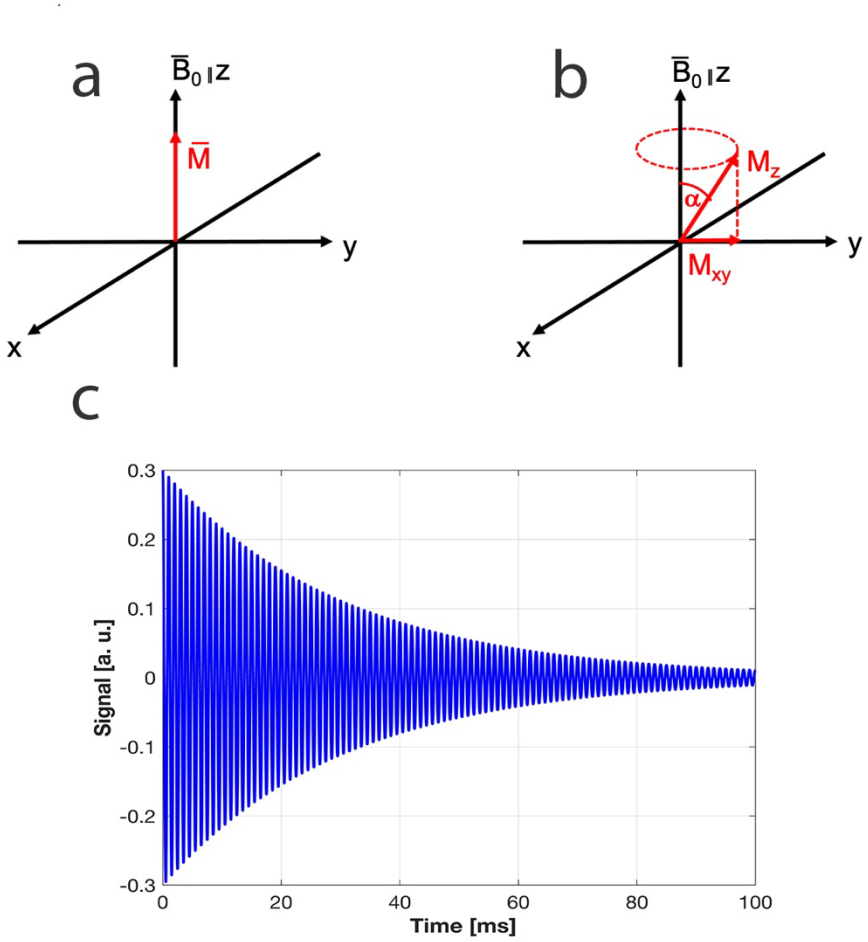


*Figure 1. (a) Net magnetization at equilibrium, oriented parallel to the main magnetic field in the z-direction. (b) After RF excitation by an angle $\alpha$, the magnetization precesses around $\vec{B}_0$ (z-axis) and is separated into a longitudinal ($M_z$) and transversal component ($M_{xy}$). (c) The precessing transverse magnetization induces an alternating voltage in the receiver coil, which is recorded as Free Induction Decay (FID) signal.*

After the RF pulse is turned off, the magnetization returns to its equilibrium state $M_0$. While the transverse component $M_{xy}$ decreases over time (Figure 1c), the longitudinal component $M_z$ increases again and approaches its equilibrium value ($M_0$). The equation of motion for magnetization is described by the Bloch equations, which were formulated by Felix Bloch in 1946 [28]:

$$\frac{dM_x}{dt} = \omega_0 M_y - \frac{M_x}{T2} \quad (1)$$

$$\frac{dM_y}{dt} = -\omega_0 M_x - \frac{M_y}{T2} \quad (2)$$

$$\frac{dM_z}{dt} = \frac{(M_0 - M_z)}{T1} \quad (3)$$

T1 and T2 are the longitudinal and transverse relaxation times, which are described in more detail in the following sections (see *Introduction and Objectives; Relaxometry*).

# Fat-water quantification

## Principles

Magnetic resonance fat quantification techniques are based on the principle of chemical shift between fat and water protons [29-34]. Nuclei or protons are surrounded by an electron shell, which possesses magnetic properties and shields the external magnetic field around the nucleus. Protons in different molecular environments experience differing levels of shielding, resulting in slightly different resonance frequencies [32]. For instance, water protons, bound to strongly electronegative oxygen atoms, are less shielded than fat protons within hydrocarbon chains, leading to a chemical shift of 3.4 ppm (448 Hz at 3T) between water (-OH) and methylene fat ($-CH_2$) protons [32,34,35].

This resonance shift allows MRI and MR-spectroscopy (MRS) to separate the signals originating from water and fat protons and to determine their relative proportions within the tissue based on their signal intensities [35-37]. Specifically, MRS provides a localized spectrum from a small volume (voxel) by converting the time-dependent MR signal (Figure 1c) into a frequency-domain spectrum using a Fourier transform [32]. The fat fraction is then quantified based on the relative amplitudes of the water and fat resonances in the acquired spectrum [35,36].

In contrast, MRI techniques such as 2-point Dixon imaging [29,38] exploit the frequency difference between fat and water to calculate fat-only and water-only images, from which the fat or water fraction can be computed: Because of the frequency difference, water and fat signals undergo a phase shift over time. By acquiring images at specific echo times, one when water and fat signals are in phase (e.g. 2.23 ms) and another when they are out of phase (e.g. 1.12 ms), water and fat signals can be separated to generate distinct water- and fat-only images [38]. As the 2-point Dixon technique do not consider the complexity of fat spectra and T2* signal decay, more advanced multi-point Dixon techniques (e.g 3-point or 6-point Dixon) have been developed, where multiple echoes are acquired to improve the accuracy of fat quantification by accounting for these factors [38-42].

## Test materials for Fat-Water Quantification

[*]Emulsions are the most commonly used test objects for fat-water quantification techniques [19,21,44-49]. These are dispersed systems consisting of two immiscible liquids, typically oil and water, where one phase (e.g. oil) is present in the form of fine droplets dispersed in the other phase (e.g. water) [50]. Their fat content can be precisely varied, making them suitable for creating phantoms with realistic fat fractions comparable to that of human tissue of clinical relevance.

Typically, oil-in-water (o/w) emulsions are used, in which vegetable or synthetic oils are stabilized with suitable emulsifiers and/or thickening agents. Among these, peanut oil is the most commonly chosen fat source for fat-water phantoms [51] because its $^{1}H$ spectrum closely resembles that of triglycerides found in adipose tissue [52]. However, other sources have also been successfully employed: different groups used canola, sunflower, or soybean oils, as well as porcine fat, which offer alternatives with slightly different compositions of saturated and unsaturated fatty acids [51]. In addition to homemade phantom approaches, there are commercially available products for researchers. These include specially designed fat-water phantoms, which contain vials with different

[*] This chapter contains material reproduced and adapted from [43], licensed under CC BY 4.0.

fat fractions, as well as readily available materials like dairy cream or mayonnaise [51,53,54].

However, the creation of oil-in-water emulsions presents challenges related to stability. By nature, emulsions are inherently unstable systems, tending to separate over time due to the high interfacial tension between the oil and water phases [50]. The oil droplets coalesce with each other, resulting in complete separation of the fat and water fraction of the emulsion. Therefore, to create stable emulsions with small oil droplets, stabilizers, also known as emulsifiers or surface active agents (surfactants), need to be added [50,55]. Emulsifiers are amphiphilic molecules, that reduce the surface tension between oil and water phases and prevent emulsions from breakdown. Amphiphilic molecules possess both hydrophilic and hydrophobic moieties. This dual affinity allows them to adsorb at the oil-water interface, reducing the interfacial tension and forming a protective layer around the oil droplets to prevent them from coalescence [50]. Due to their amphiphilic nature, emulsifiers can also form complex self-assembled aggregates, such as micelles or liposomes in aqueous solutions. The specific type of aggregate formed depends on the molecular structure of the emulsifier but also on environmental factors such as temperature and concentration [55].

Nevertheless, those substances are usually not present in human tissue and their inclusion in phantom materials might lead to undesired signal contributions. Micellization of emulsifier molecules may influence the state of water and thus also MR parameters such as relaxation and diffusion properties. It is particularly critical when emulsifiers have similar spectral properties to fat, which can impair fat-water separation and bias quantitative results.

Various emulsifiers have been used to stabilize fat-water phantoms, including sodium dodecyl sulfate (SDS), polysorbates and lecithin [19,21,24,46-49]. However, to the best of the author’s knowledge, the potential impact of surfactants on various MR parameters and confounding factors has not yet been systematically investigated.

Publication 1 of this thesis addresses this research question and examined three common emulsifiers (polysorbate 60, SDS, soy lecithin) for their properties and influences. They were tested with regard to the following criteria: (1) Their ability to stabilize oil-in-water emulsions with the preparation method (ultrasound

emulsification) presented in this study, (2) whether and which signal properties the emulsifiers show by themselves and (3) what influences they have on MR parameters such as relaxation times and diffusivity of the aqueous phase. For these purposes, the emulsifiers were examined both as an additive in o/w emulsions and individually in aqueous solutions (without the presence of fat).

# Diffusion-Weighted Imaging (DWI)

## Principles

Diffusion-weighted imaging (DWI) is an MRI technique that probes the random, microscopic motion of water molecules within biological tissues [56,57]. This motion, driven by thermal energy, leads to translational displacements of the molecules over time - a process known as Brownian motion or molecular diffusion [57]. In a homogeneous, free medium, these displacements follow a Gaussian distribution with a mean square displacement $\langle r^2 \rangle$ that increases linearly with time, as described by Einstein [58]:

$$\langle r^2 \rangle = 6Dt \qquad (4)$$

where $\langle r^2 \rangle$ is the mean square displacement in a three-dimensional space, D is the diffusion coefficient, and t is the diffusion time. MRI can non-invasively make this displacement of water molecules (or proton spins) visible and quantifiable. However, unlike pure liquids, the diffusion of water molecules in biological tissue is not free but is hindered and restricted by cellular structures such as cell membranes, macromolecules, organelles, and other microstructural elements [57]. Therefore, the diffusion coefficient measured in MRI is referred to as the ‘apparent’ diffusion coefficient (ADC). This is particularly valuable in detecting various diseases, since changes in tissue structure, such as increased cellularity or edema, can restrict or enhance water diffusion [56,57].

To make MRI pulse sequences sensitive to molecular diffusion, a pair of symmetric magnetic field gradients (diffusion-encoding gradients) are employed [59]. Figure 2 illustrates exemplarily the fundamental concept of diffusion

sensitization within a spin echo-based pulse sequence: Following a RF excitation pulse, a strong magnetic field gradient pulse is applied for a defined duration $\delta$. This imparts a spatially dependent phase shift (dephasing) of the spins along the direction of the gradient. After the 180° refocusing pulse, a second identical gradient pulse is applied to rephase stationary spins. However, if the proton spins of water molecules have moved due to Brownian motion during the diffusion-sensitive time $\Delta$ the rephasing is incomplete. This results in a net phase shift and a corresponding attenuation of the MR signal. The degree of signal attenuation is directly related to the diffusion coefficient and the strength and duration of the applied gradient pulses [56,59]:

$$\mathrm{S(b)} = \mathrm{S_0} \cdot \exp(-\mathrm{b} \cdot \mathrm{ADC}) \tag{5}$$

with

$$\mathrm{b} = \gamma^2 \mathrm{G_D^2} \left[\delta^2 \left(\Delta - \frac{\delta}{3}\right)\right] \tag{6}$$

for rectangular diffusion-encoding gradients [59]. $S_0$ represents the signal intensity without diffusion weighting (b = 0 s/mm²), $S$ is the signal intensity with a non-zero diffusion weighting b-value, and ADC is the apparent diffusion coefficient.

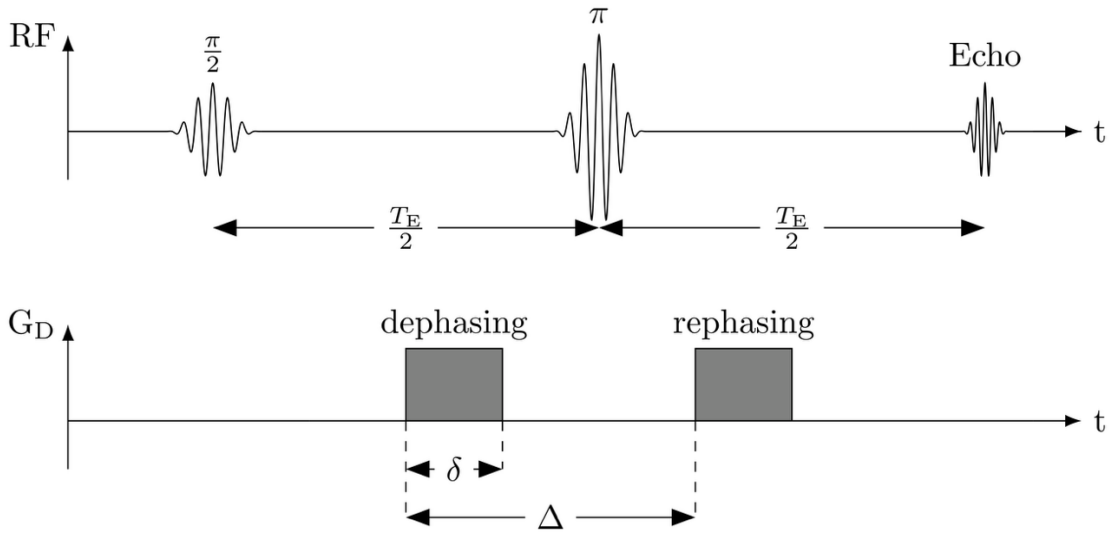


*Figure 2. Fundamental concept of diffusion sensitization within a spin echo-based pulse sequence. Symmetric diffusion-encoding gradients are applied before and after the 180°*

*refocusing pulse to impart and then attempt to rephase a spatially dependent phase shift. If spins undergo Brownian motion during the diffusion-sensitive time $\Delta$, their rephasing is incomplete, resulting in a net phase shift and attenuation of the MR signal. The diffusion-weighting is determined by the gradient's amplitude $G_D$, the gradient's duration $\delta$, and the diffusion-sensitizing time $\Delta$.*

To measure the ADC value, images with different diffusion-weightings (b-values) are acquired and the signal intensities are fitted to the mono-exponential model in Eq. 5.

However, it is important to note that the commonly used mono-exponential model is a simplification of the complex diffusion behavior in biological tissues. This model is only valid for moderate b-values (≤1000 s/mm²), where the diffusion of water molecules can be approximated as Gaussian [56,57]. At higher b-values, deviations from Gaussian diffusion become increasingly significant due to structural hindrance and microstructural complexity. To account for these effects, a second-order correction term need to be introduced to incorporate diffusion kurtosis, or non-Gaussian diffusion [60,61]:

$$\mathrm{S(b)} = \mathrm{S_0} \cdot \exp\left(-\mathrm{b} \cdot \mathrm{ADC} + \frac{1}{6}\mathrm{b}^2 \cdot \mathrm{ADC}^2 \cdot \mathrm{K}\right) \tag{7}$$

where $K$ denotes the kurtosis coefficient, which quantifies the degree of non-Gaussian diffusion of tissue. The mean kurtosis value for biological tissue is in the range of 0.5 to 1.5 [62,63].

## Test materials for DWI

*Tofts et al. [65] outlined several criteria for reliable DWI test objects. These include: (1) covering a wide range of ADC values, preferably comparable to in-vivo values, (2) being chemically stable, readily available, and easy to handle, (3) having a $^1$H spectrum with a single proton peak, since undesired lines from the phantom material can cause artifacts and complicate ADC quantification, (4) Relaxation times (T1 and T2) comparable to values found in biological tissue, and

*This chapter contains material reproduced and adapted from [64], licensed under CC BY 4.0.

(5) exhibiting high viscosity to minimize the effects of bulk motion. Ideally, the materials should replicate the diffusion characteristics of tissue, i.e., Gaussian diffusion at low b-values and measurable non-Gaussianity at higher b-values (>1000 s/mm²).

The search for materials that meet all the above criteria is an ongoing challenge. Various materials have been proposed and evaluated. For example, organic liquids such as alkanes were introduced by Tofts et al. [65] as reference media, offering well-defined and stable diffusion properties. However, their practical application is limited, as they are not readily available and potentially toxic. In addition, these substances cannot be easily doped with paramagnetic agents to adjust their relaxation times to values representative of human tissue [65].

Water-based diffusion phantoms have proven to be more practical and versatile. In such phantoms, different solutes are added to water in order to modulate its diffusion properties. Common additives include sugars such as sucrose or polymeric substances like polyvinylpyrrolidone (PVP) and polyethylene glycol (PEG) [13,15,66,67]. The reduction in water diffusivity in such systems is generally attributed to molecular interactions between the solute and surrounding water molecules: The dissolved macromolecules form hydrogen bonds with the surrounding water molecules, thereby inhibiting their mobility [68,69]. PEG, for example, contains repeating ether oxygen groups (-$CH_2$-$CH_2$-O-) [70] that act as hydrogen bond acceptors, binding water molecules in hydrate shells. This reduces the fraction of “free” water available for diffusion and leads to a measurable decrease in the ADC value [63,68]. In addition, the presence of large macromolecules imposes physical constraints on diffusing water molecules by acting as obstacles within the solution [63,68]. The ADC can be systematically adjusted, within a certain range, by varying the concentration of the dissolved substance. Higher concentrations lead to more hydrogen bonding, hydrate shells, and greater steric hindrance by macromolecules, which overall contributes to a further reduction in water mobility.

However, sucrose, PEG, and PVP-based aqueous solutions introduce different undesired secondary effects, such as multiple spectral lines in the $^1$H spectrum, relaxation times that are not representative of those found in biological tissues, and/or fail to replicate the non-gaussian diffusion behavior observed in tissue for high b-values [63,67,71].

Furthermore, the physical origin of diffusion restriction in these phantoms is fundamentally different from that in biological tissue. In tissue, diffusion is shaped by a complex microstructure that includes cell membranes and other subcellular structures (organelles, macromolecules) acting as semipermeable barriers or confining geometries [57]. These structures, which range in size from approximately 0.5 μm to 30 μm [72], lead to compartmentalization and restricted diffusion of water; features that are not present in homogeneous macromolecular aqueous solutions, where diffusion mainly arises from hydrogen bonding and collisions with molecules [57,68].

An alternative approach might involve using surfactants [63]. Given their amphiphilic nature, surfactants spontaneously form self-assembled organized aggregates, such as vesicles and liposomes in aqueous solution [55]. These aggregates, which can range in size from 0.1 to 5 μm [73,74], could provide a more realistic representation of diffusion restriction by forming structures analogous to the compartments and barriers found in biological tissues, potentially offering a more bio-realistic phantom material design. Soy lecithin, a naturally occurring amphiphile composed of a mixture of phospholipids [72,73], has emerged as a promising candidate: Publication 1 showed that adding small amounts of soy lecithin to water significantly restricts the mobility of water molecules without producing any additional spectral signals (see *Publication 1*). Building on these findings, Publication 2 investigated soy lecithin as a substance suitable for creating diffusion MRI test materials, which could overcome the disadvantages of other ADC-modifying substances. For this purpose, aqueous soy lecithin dispersions with different concentrations were prepared and evaluated using the criteria described above. Specifically, the range of achievable ADC values, the degree of non-Gaussianity, simultaneous effects on relaxation times, and the question of whether the materials exhibit a single-line $^{1}H$ spectrum from water protons only even at high soy lecithin concentrations were systematically investigated.

# Relaxometry

## Principles

Relaxation refers to the tendency of magnetization to return to its equilibrium state $M_0$ after RF excitation [25-27]. Interactions between the magnetic moments and their environment cause a decrease in transverse magnetization and an increase in longitudinal magnetization until thermal equilibrium is reached [25-27]. There are two types of relaxation: longitudinal and transverse relaxation. Both relaxation mechanisms are significantly influenced by the thermal mobility of the molecules in their environment and vary between different tissues [25-27].

## Longitudinal relaxation

Longitudinal relaxation, also known as spin-lattice relaxation, describes the buildup of the longitudinal magnetization along the direction of the external magnetic field. Starting from an initial value of $M_z(0)$, the longitudinal magnetization, $M_z$, relaxes exponentially toward thermal equilibrium $M_0$ (Eq. 8) [75].

$$\mathrm{M_z(t) = M_0 + (M_z(0) - M_0) \cdot \exp\left(-\frac{t}{T_1}\right)} \qquad (8)$$

The rate of this recovery is characterized by the relaxation time T1. During longitudinal relaxation, the excited spins release energy to their surroundings ("the lattice") by returning to the energetically more favorable state (spin-up, parallel to $\vec{B}_0$) [25-27]. The driving force behind this process is the molecular motion (tumbling, vibrations, and collisions) which causes magnetic field fluctuations at the location of a nucleus [27,76]. Relaxation is most effective when the frequency of the local magnetic fluctuations (perpendicular to $\vec{B}_0$) is at or near the resonance frequency. This resonance condition increases the likelihood of spin transitions from the higher- to the lower-energy state, thereby accelerating the return to equilibrium [27,76]. Therefore, T1 is critically dependent on the molecular structure and composition of the tissue, particularly its water content

and macromolecule concentration. Rapidly tumbling of free or unbound water molecules, for example, is really ineffective for longitudinal relaxation [27,76]. However, the presence of macromolecules leads to more efficient relaxation and shorter T1 times. Macromolecules bind water molecules, restricting their mobility and bringing the fluctuation spectrum closer to the Larmor frequency [26,27]. In tissues, T1 values typically range from 700 ms to 1800 ms at typical clinical field strengths (1.5T, 3T) [75].

The gold standard for measuring T1 is the inversion recovery technique [25,77,78], which is illustrated in Figure 3. The magnetization is first completely inverted by a 180° inversion pulse. As described above, it then returns to its equilibrium state with the time constant T1. After a specified inversion time TI, a RF excitation pulse is applied, which converts the existing longitudinal magnetization into transverse magnetization for signal acquisition. To determine T1, the IR sequence is recorded several times with different inversion times TI. This allows the sampling of the longitudinal magnetization point by point and determination of T1 using Eq. 8 [25,75].

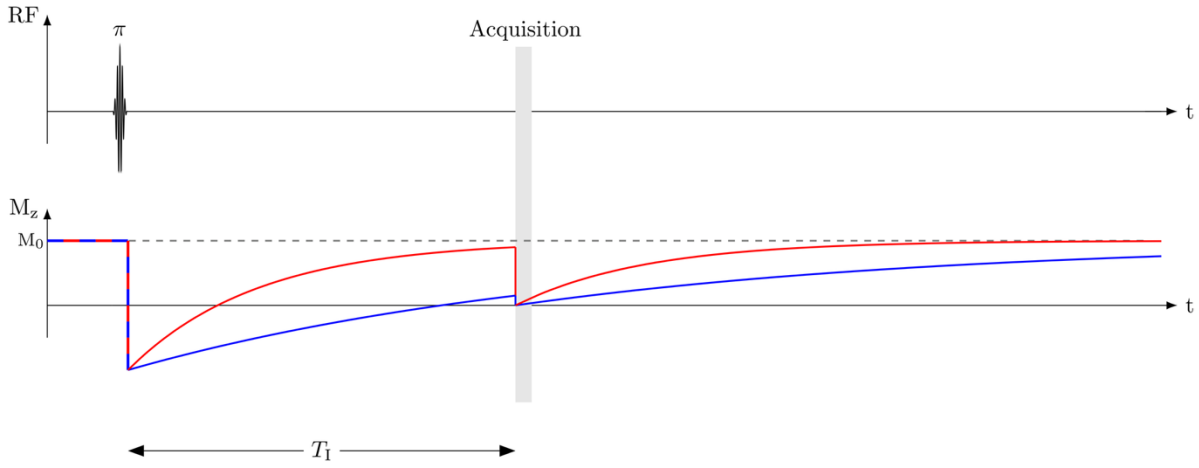


*Figure 3. Scheme of an Inversion Recovery (IR) pulse sequence. This technique utilizes an initial 180° inversion pulse followed by a 90° excitation pulse to convert the longitudinal magnetization into the transverse plane for signal acquisition. By recording the sequence several times with different inversion times TI, the recovery of longitudinal magnetization is sampled point by point, allowing for the determination of T1. The blue and red curves represent the longitudinal magnetization during an IR sequence for two tissues with different T1 times (blue: long T1, red: short T1).*

## Transverse relaxation

Transverse relaxation, also known as spin-spin relaxation, describes the exponential decay of the transverse magnetization $M_{xy}$ resulting from the loss of phase coherence among spins [25,27]. Magnetic field fluctuations parallel to the external magnetic field lead to slightly variations in local Larmor frequencies. These frequency differences result in dephasing of the proton spins, causing the net transverse signal to decay exponentially over time (Eq. 9) [25,75].

$$\mathrm{M_{xy}(t) = M_{xy}(0) \cdot \exp\left(-\frac{t}{T_2}\right)} \qquad (9)$$

The decay rate is characterized by the relaxation time T2. T2 is the time it takes for the transverse magnetization to decrease to 37% of its initial value [75].
The extent of dephasing depends on the tissue's mobility and molecular structure. In fluids with high molecular mobility, such as free water, fluctuations are effectively averaged out, leading to prolonged coherence of spins and, consequently, longer T2 times [27]. Conversely, in tissues where molecular motion is restricted, such as those with abundant macromolecular structures, local field differences persist, resulting in faster dephasing and shorter T2 relaxation times [27]. In most biological tissues, T2 times are generally much shorter than T1 times, typically ranging between 30 and 150 milliseconds depending on the tissue [75].
T2 is typically measured using the Carr-Purcell-Meiboom-Gill (CPMG) pulse sequence [25,75,79-82] (Figure 4). After a 90° excitation pulse, a series of 180° refocusing pulses are applied at defined time intervals. These pulses generate a train of spin echoes at specific echo times (TE), determined by the timing of the refocusing pulses. This allows the decay of transverse magnetization to be monitored over time. The T2 time is then calculated by fitting the signal intensities from these echoes as a function of TE using Eq. 9 [75].

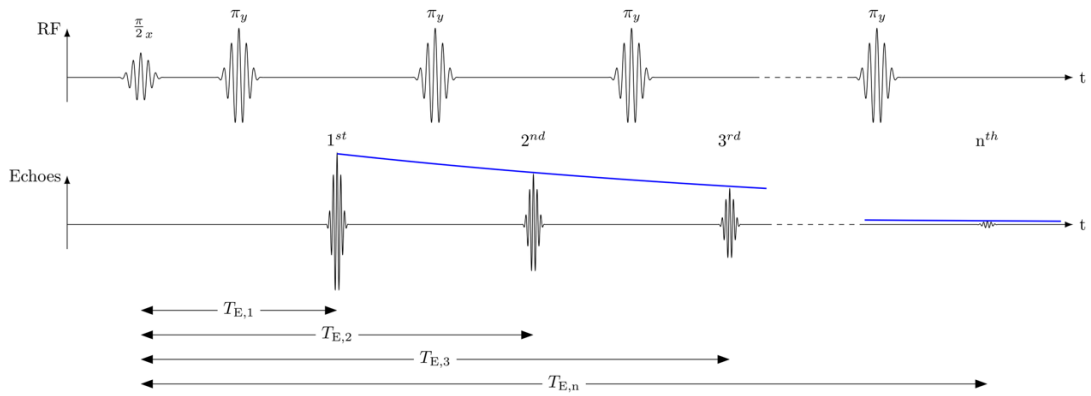


*Figure 4. Scheme of the Carr-Purcell-Meiboom-Gill (CPMG) pulse sequence. This sequence utilizes a 90° excitation pulse followed by a series of 180° refocusing pulses to generate a train of spin echoes. By monitoring the signal intensities of these echoes at varying echo times ($TE_1$, $TE_2$,.. $TE_n$), the exponential decay of transverse magnetization is measured, allowing for the calculation of T2.*

## Test materials for Relaxometry

*Test materials for relaxometry are often formulated as two-component systems to enable independent control of the T1 and T2 relaxation times. These systems typically combine a paramagnetic dopant (e.g. nickel chloride, copper sulfate, manganese chloride, or gadolinium salts) to primarily shorten T1, and a gelling agent (agar or agarose) to primarily modulate T2, both dissolved in water, the base material [4,11,12]. Paramagnetic substances possess unpaired electrons with large magnetic moments, which generate strong time-varying magnetic fields at the location of nearby water protons, thus accelerating both T1 and T2 relaxation [84]. Gelling agents, on the other hand, primarily affect T2 by forming semi-solid matrices that increase spin dephasing [9,17]. Adjusting the concentrations of the paramagnetic dopant and the gelling agent allows one to independently tailor the material's T1 and T2 times. The concentrations required to achieve specific relaxation times can be determined using established models described by Tofts et al. [4,12]:

* This chapter contains material reproduced and adapted from [83], licensed under CC BY 4.0.

$$C_x = \frac{R2 - R2_w - \left(r_2^{(y)}/r_1^{(y)}\right)(R1 - R1_w)}{r_2^{(x)} - \left(r_2^{(y)}/r_1^{(y)}\right) r_1^{(x)}} \quad (10)$$

$$C_y = \frac{R1 - R1_w - \left(r_1^{(x)}/r_2^{(x)}\right)(R2 - R2_w)}{r_1^{(y)} - \left(r_1^{(x)}/r_2^{(x)}\right) r_2^{(y)}} \quad (11)$$

where $C_x$ and $C_y$ represent the concentrations of components x and y, $R1 = 1/T1$ and $R2 = 1/T2$ denote the target relaxation rates, $R1_w$ and $R2_w$ are the relaxation rates of pure water, and $r_1$ and $r_2$ are the relaxivities of components x and y. The relaxivity of a substance is a measure of how effectively the substance enhances the relaxation rate of water and is defined as the change in relaxation rate ($R1 = 1/T1$ or $R2 = 1/T2$) per unit concentration of the substance [4].

To effectively achieve independent control over T1 and T2, the combined components should have distinct relaxivity profiles. The most useful combinations involve one component with a high $r_2$ (significantly greater than $r_1$, such as agar, agarose or MnCl2) and another with a low $r_2$ (where $r_2 \approx r_1$, such as Gd-DTPA and Ni-DTPA) [4]. Examples of such effective mixtures include Gd-DTPA and agarose, Ni2+ and agarose, Ni-DTPA and agarose, and Ni2+ and Mn2+ in aqueous solution [4].

While these paramagnetically doped gels/liquids can be reproducibly produced and exhibit high temporal stability [4,11,12], the use of paramagnetic substances remains somewhat controversial due to concerns about their toxicity. Paramagnetic salts are quite toxic, which complicates the production, handling and disposal of such test materials. Furthermore, the presence of paramagnetic salts can strongly affect the magnetic susceptibility of the phantom material [85]. This could lead to adverse effects, especially for gradient echo sequences, as undesirable magnetic field inhomogeneities occur depending on the geometry and composition of the phantom.

There are no known safer alternatives that could effectively replace paramagnetic agents for controlling T1 in the preparation of relaxometry phantoms. Sewskowa et al. [86] investigated the use of detonation diamond nanoparticles (DNDs) as a

potential substitute for paramagnetic salts. The phantoms composed of agar, carageen, and DND particles suspended in dimethyl sulfoxide have been shown to successfully mimic the relaxation times of liver tissue. However, the data from the study suggests that phantoms with T1 values above 950 ms cannot be fabricated, at least not with the fabrication method presented – which is a disadvantage, as many tissues (e.g. gray matter, kidney, spleen, etc.) have T1 values in the range of 1000 – 2000 ms and therefore cannot be covered [75].

Within the scope of this thesis, the potential of soy lecithin as a non-hazardous and inexpensive alternative was investigated. In line with Tofts' concept [4] of combining agents with markedly differently relaxivity profiles, soy lecithin emerges as a promising alternative to paramagnetic salts. Due to its balanced relaxivities ($r_2 \approx r_1$, see *Publication 1 and Publication 2*), it could form an effective pair with agar or agarose. Publication 3 therefore investigated soy lecithin-agar gels as an alternative phantom material for the construction of relaxometry phantoms without safety and toxicity issues. This study specifically checked the compatibility between soy lecithin and agar, determining whether Eqs. 10 and 11 were applicable for this pair of substances. To validate their utility, test phantoms designed to mimic relaxation times of different tissues were prepared and subsequently evaluated for reproducibility and temporal stability.

## Test materials mimicking multiple MR properties

*Biological tissues are characterized not by a single MR property but by a complex interplay of multiple parameters, including longitudinal and transverse relaxation times (T1, T2), ADC value, fat fraction, and magnetization transfer effects, among others [24,51]. All these parameters contribute to the measured MR signal, often in interdependent and in sequence-specific ways.

However, as described in the previous sections, most phantom materials are designed with a single, well-defined purpose in mind, such as simulating fat fraction in emulsions for calibration of fat quantification techniques, or providing specific T1 or T2 times for relaxometry, or defined diffusion properties for DWI. In these cases, the material closely replicates one or two target MR properties, while

* This chapter contains material reproduced and adapted from [87], licensed under CC BY 4.0.

other tissue-relevant parameters often remain uncontrolled. This limitation becomes critical because MR techniques designed to measure a specific property can be influenced by confounding factors; for instance, T2 mapping might be biased by underlying diffusion effects or the tissues' T1 time [88].

Traditional single-purpose phantoms cannot adequately address these interactions, as they inherently lack control over secondary MR parameters. To overcome this, multi-parametric phantoms have emerged as a promising solution. By integrating multiple, well characterized MR properties into a single-material, these phantoms enable more realistic tissue simulations, better reflecting biological complexity [2].

Very few approaches have been reported allowing the simultaneous and independent adjustment of multiple MRI parameters within a single test material. Most of these focus on relaxometry-based tuning of T1 and T2 or on simultaneous modulation of fat fraction and R2* (via iron content) [12,14,21,24,47]. Zhao et al. [24], for example presented a phantom design that allows simultaneous modulation of fat fraction, R2* and T1 to mimic the complex signal behavior of diffuse liver pathologies (fat, iron, fibrosis). However, as noted by Keenan et al. [2], it has not yet been possible to create a material that simultaneously represents a specific T1, a specific T2 and a specific ADC value in the same voxel.

A major challenge in multi-parametric phantom development is the interdependence of parameter-modifying agents [4]. The preparation of a material with specific T1, T2, and ADC values requires at least three different components with different chemical properties: a T1 modifier, a T2 modifier, and an ADC modifier. However, a substance intended to adjust one MR property often influences others, making independent parameter control challenging. For example, agents used to modify the diffusion properties usually also affect the relaxation times of materials used in phantoms [13,67]. Similarly, relaxation modifiers do not act exclusively on T1 or T2 but influence both [12]. In addition, ensuring compatibility between the selected components is critical, i.e., there is little or no interaction between them and their individual effects remain intact in the presence of the other substances. Undesired interactions, as seen between $GdCl_3$ and agarose, lead to unexpected shifts in target values [4,89]. In summary,

a suitable triple must be chemically compatible while allowing independent adjustment of a wide range of relaxation times and ADC values.

In this context, Gd-DTPA, agarose and soy lecithin were found to be promising candidates. The combination of Gd-DTPA and agarose has already been established as a suitable pair for independent adjustment of T1 and T2 [4,89]. In addition, soy lecithin has recently been identified as a promising ADC modifier that, when combined with agarose, allows for largely independent control of ADC and T2 (see *Publication 2*).

Publication 4 was therefore motivated by the question of whether these three substances remain effective when combined into a single mixture and whether they allow simultaneous and independent adjustment of T1, T2, and ADC. This work presents a step-by-step protocol (recipe) for the preparation of hydrogels with independently adjustable T1, T2 and ADC values at 3T using soy lecithin, agarose and Gd-DTPA. The resulting gels were checked for reproducibility and temporal stability.

# Summary of publications: Results and Discussion

This chapter provides a summary for each of the 4 publications listed above which are covered in the thesis.
Each summary is followed by a brief description of author contributions.

## Publication 1

*Reproduced and summarized from:*
*Fritz, V., Martirosian, P., Machann, J., Daniels, R., Schick, F. (2022)*
*A comparison of emulsifiers for the formation of oil-in-water emulsions: stability of the emulsions within 9 h after production and MR signal properties.*
*Magnetic Resonance Materials in Physics, Biology and Medicine.*
*DOI: https://doi.org/10.1007/s10334-021-00970-9*


In this publication, three emulsifiers (polysorbate 60, sodium dodecyl sulfate (SDS), and soy lecithin) were systematically evaluated for their suitability in the preparation of emulsions used as fat-water phantoms in MRI. In addition to the ability to stabilize oil-in-water emulsions, the work focused primarily on potential influences or confounding factors caused by the emulsifiers, either by contributing additional spectral signals or by affecting the relaxation and diffusion properties of the aqueous phase.

To test the stabilizing ability of the emulsifiers, peanut-oil-based emulsions with fat contents ranging from 10% to 50% were prepared using ultrasonic homogenization. Stability was assessed after 3 and 9 hours of storage using T1 mapping and visual control. Due to the pronounced difference in T1 relaxation times between water and fat, emulsion breakdown, i.e. separation into distinct phases, can be visualized as a spatial T1 variation along the axis of gravity. It was found that emulsions stabilized with either polysorbate 60 or soy lecithin were significantly more stable than emulsions prepared with SDS (Figure 5). Both

polysorbate 60- and soy lecithin-based emulsions remained stable and homogeneous across all fat fractions tested. No creaming was observed within the first 9 hours. In contrast, SDS based emulsions showed significant instability, with visible creaming and partial phase separation after only a few hours of storage. The low stability was attributed to the formulation and method of preparation used in this study, which included peanut oil and ultrasonic homogenization. Other research groups, for example, Bernard et al. [46], reported very stable fat-water phantoms using SDS. However, they have used carrageenan as an additional stabilizer and soyabean oil instead of peanut oil.

Possible signal contributions and confounding effects of the emulsifiers themselves were investigated in aqueous solutions containing different concentrations (0, 1, 2, 3, 4, 5% wt.%) of each emulsifier (without the addition of fat). These aqueous solutions were analyzed by $^1$H-MRS, relaxometry and DWI. Spectroscopic analysis revealed several signals for polysorbate 60 and SDS (Figure 6b-c). Especially the resonances at 1.3 ppm and 0.9 ppm, which are usually seen in triglycerides, are considered to be critical with regard to fat quantification. These signals can be assigned to methylene- $(-CH_2-)_n$ and terminal methyl protons ($-CH_3$) [90] and coincide with the signals of triglycerides in peanut oil (Figure 6a). Soy lecithin, on the other hand, remained invisible in our spectroscopic examinations with TE = 10 ms. Lecithins are phospholipids consisting of a hydrophilic head group and two hydrophobic hydrocarbon chains ($C_mH_n$) [72]. One possible explanation for MR invisibility is the micellar structure of lecithin: In aqueous solution, lecithin forms so-called bilayers, similar to those of phospholipids in the cell membranes of animal cells [50]. Due to the restricted mobility within such bilayer structures, the lipids have a very short transverse relaxation time ($T2 \sim 10^{-2}$ ms) and are therefore invisible for $^1$H-MRS measurements with TE values in the range of a few milliseconds [91].

Relaxometry and DWI measurements also showed completely different effects of polysorbate 60 and SDS on the one hand and soy lecithin on the other. While polysorbate 60 and SDS had little to no effect on the relaxation times and the ADC value of water, soy lecithin caused a relatively strong decrease in relaxation times ($r_{1lecithin} = 0.11\ s^{-1}(wt.\%)^{-1}$ and $r_{2lecithin} = 0.57\ s^{-1}(wt.\%)^{-1}$) and the ADC value with increasing concentration.

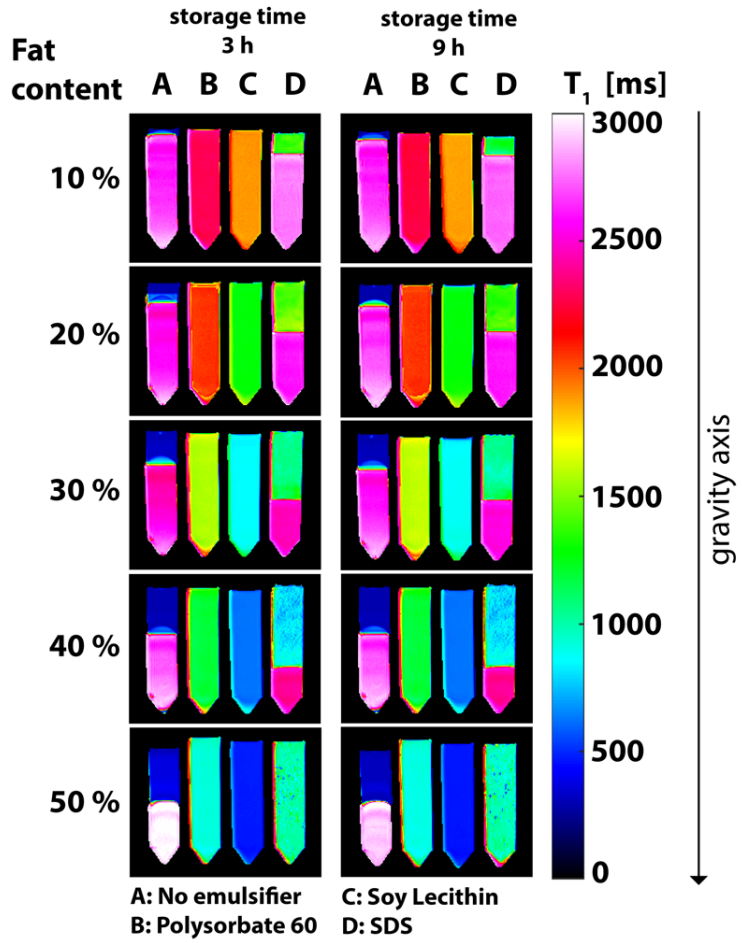


*Figure 5. T1-maps of oil-in-water emulsions with different emulsifiers (A: no emulsifier, B: polysorbate 60, C: soy lecithin, D: SDS) and with increasing fat content (from 10% to 50%) from top to bottom. Measurements were carried out after storage times of approx. 3 h and 9 h, respectively. The presented T1 values were obtained by monoexponential fitting and correspond to the T1 values of the oil/water mixture. Reprinted from [43], licensed under CC BY 4.0.*

In particular, the influence on diffusivity was remarkable: Even small amounts of soy lecithin considerably reduced the mobility of water molecules (Figure 7). ADC values ranged from $2.2 \cdot 10^{-3}$ mm$^2$/s for pure water to $0.92 \cdot 10^{-3}$ mm$^2$/s for the solution with 5 wt.% of soy lecithin. This significant decrease in ADC values and the fact that soy lecithin shows no detectable signals in the $^1$H spectrum make this substance particularly interesting for the construction of DWI phantoms – the motivation for Publication 2.

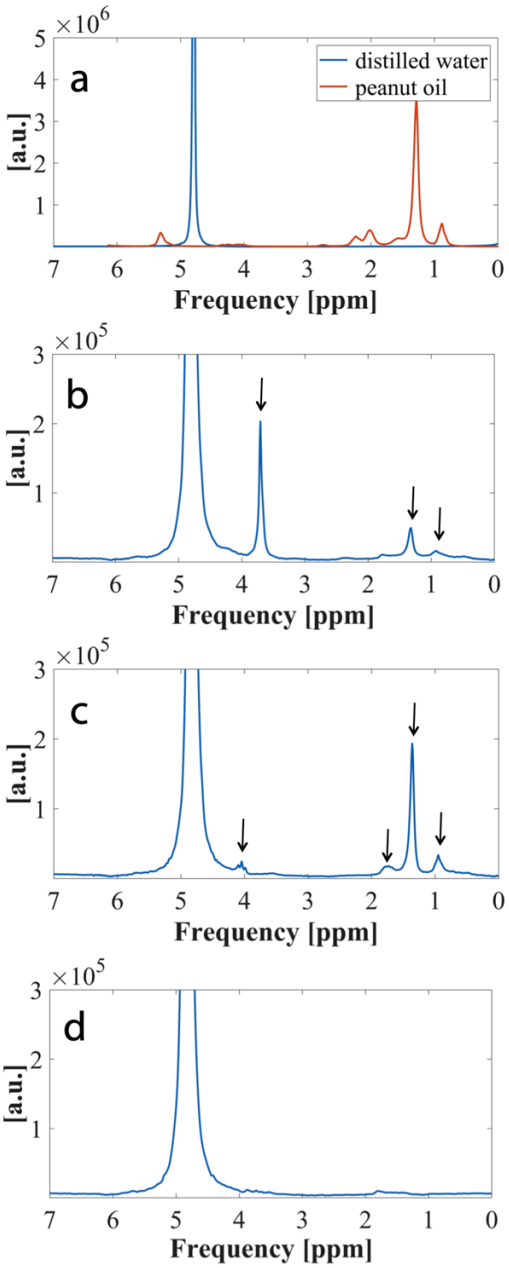


*Figure 6. $^{1}$H-MR spectra of (a) peanut oil in red color and distilled water in blue color; plotted on the same axes to illustrate their distinct chemical shifts (b) aqueous solution of polysorbate (3 wt.%) (c) aqueous solution of SDS (3 wt.%) (d) aqueous solution of lecithin (3 wt.%). Arrows indicate resonances of emulsifiers. Adapted from [43], licensed under CC BY 4.0.*

In conclusion, this study underscored the critical importance of carefully selecting emulsifiers for fat-water phantoms, given that different types lead to varied MR properties of the final test material. Soy lecithin was suggested as the preferred emulsifier for use in MRI fat-water phantoms (among the tested). Soy lecithin is non-hazardous, inexpensive and easy to handle. Use of soy lecithin as emulsifier not only provides a high stabilizing ability but also remains invisible in MRI experiments. The latter is of great importance when simulating MR properties of tissues by emulsions: additional signals are undesired and cause inaccuracies or even systematic errors in quantitative measurements.

However, while this study primarily focused on characterizing the intrinsic influence of emulsifiers on the MR properties of fat-water phantoms, it did not assess whether the resulting emulsions accurately reproduced the intended fat fractions. In this regard, further work by Machann et al. [92] (not included in this thesis) confirmed that the measured proton density fat fractions in lecithin-based emulsions were in good accordance with targeted fat fractions, thereby validating their reliability for use as test objects.

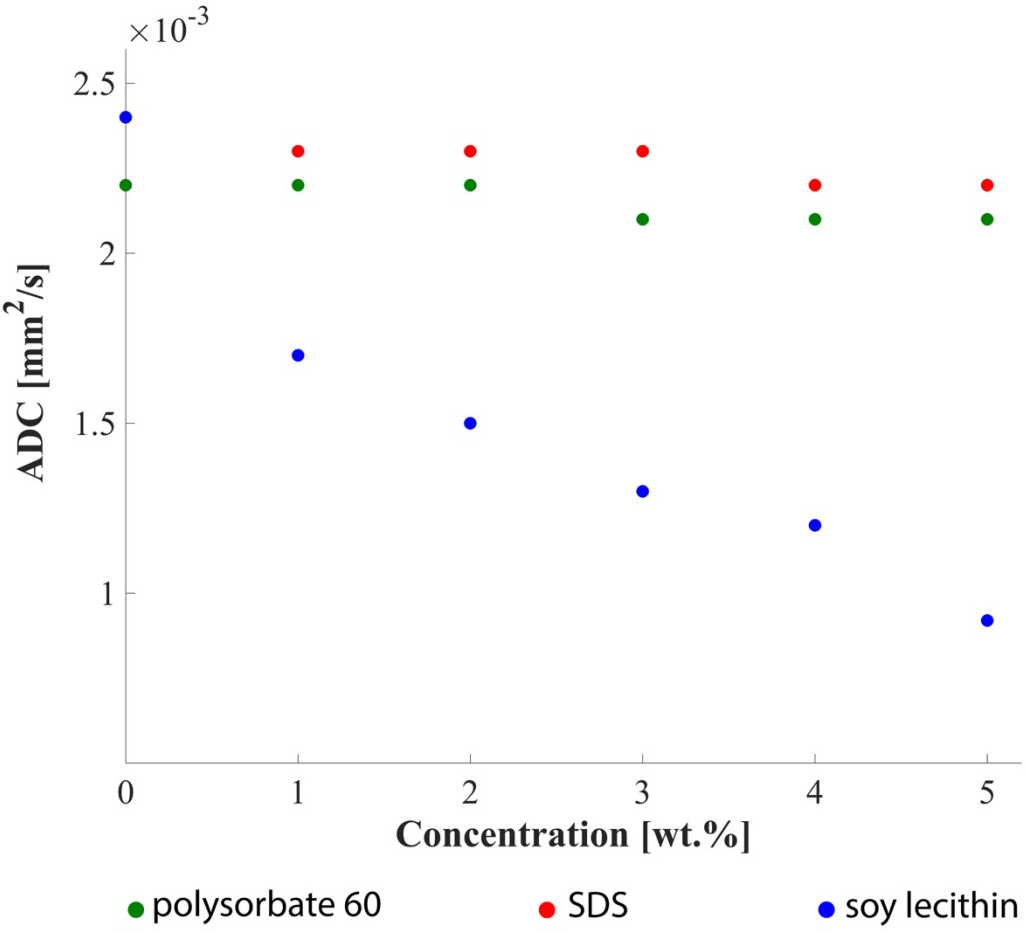


*Figure 7. ADC values of water as a function of emulsifier concentration for polysorbate 60 (green), SDS (red) and soy lecithin (blue). Adapted from [43], licensed under CC BY 4.0.*

**Statement of Contributions**

| | |
|---|---|
| Victor Fritz | Corresponding and first author, conception and study design, material preparation, data collection and analysis, writing of the manuscript. |
| Petros Martirosian | Advice and support in data acquisition and analysis, proofreading of the manuscript. |
| Jürgen Machann | Advice and support in data acquisition and analysis, proofreading of the manuscript. |
| Rolf Daniels | Provision of laboratory materials and assistance with emulsion preparation, proofreading of the manuscript. |
| Fritz Schick | Supervision, conception and study design, critical discussion, writing and proofreading of the manuscript. |

## Publication 2

*Reproduced and summarized from:*
*Fritz, V., Martirosian, P., Machann, J., Thorwarth, D., Schick, F. (2023)*
*Soy lecithin: A beneficial substance for adjusting the ADC in aqueous solutions to the values of biological tissues.*
*Magnetic Resonance in Medicine (MRM).*
*DOI: https://doi.org/10.1002/mrm.29543*


This work is a direct continuation of Publication 1 and addresses the question of whether soy lecithin is a suitable substance for the construction of test materials with predefined ADC values. Soy lecithin is a phospholipid that, due to its amphiphilic nature, forms self-assembled aggregates, so called micelles, in aqueous solution [50]. These molecular constructs are well suited to act as barriers and impede the diffusion of water protons, analogous to cellular structures in biological tissues. In Publication 1 it was found that dissolving small quantities of soy lecithin in aqueous solution resulted in a significant reduction in ADC values while remaining invisible in $^{1}$H-MRS experiments. In this sense, soy lecithin appears to be a promising inexpensive substance for use in diffusion phantoms that overcomes the problems of previously proposed diffusion modifying substances. Previously proposed substances such as sucrose, polyethylene glycol (PEG), or polyvinylpyrrolidone (PVP) often require high concentrations, strongly influence relaxation times and/or lead to unwanted MR signals (see *Introduction and Objectives; Test materials for DWI*).

The performance of soy lecithin was therefore assessed for the useable range of adjustable ADC values, the degree of non-Gaussian diffusion, simultaneous effects on relaxation times, and spectral signal properties. In addition, a series of measurements tested whether T2 of the aqueous soy lecithin solutions can be controlled independently of the ADC value by adding agar as a T2 modifier. For this purpose, aqueous soy lecithin solutions of different concentrations (0, 0.5, 1, 2, 3, 4, 5, 6, 7, 8, 9, 10% w/v) and soy lecithin-agar gels were prepared and examined using diffusion-weighted imaging, relaxometry and MRS. All measurements were performed on a 3 Tesla clinical scanner at 18.5°±0.5°C.

A biexponential relationship was observed between soy lecithin concentration and ADC values (Figure 8, Table 1). ADC values ranged from $2.02 \cdot 10^{-3}$ $mm^2/s$ (for pure water) to $0.48 \cdot 10^{-3}$ $mm^2/s$ (for 10% w/v) and thus cover almost the entire physiological range of values reported on biological tissue [93-95]. To the best of our knowledge, no substance has yet been described in the literature that influences the ADC value of water to a comparable extent as soy lecithin. Even small amounts of soy lecithin considerably restrict the diffusion of the water protons: The ADC of water is reduced by 20% at a concentration of only 0.5% (w/v). Previously proposed substances (sucrose, PVP or PEG) require five to ten times the concentration to simulate the same range of ADC values [13,67,71].

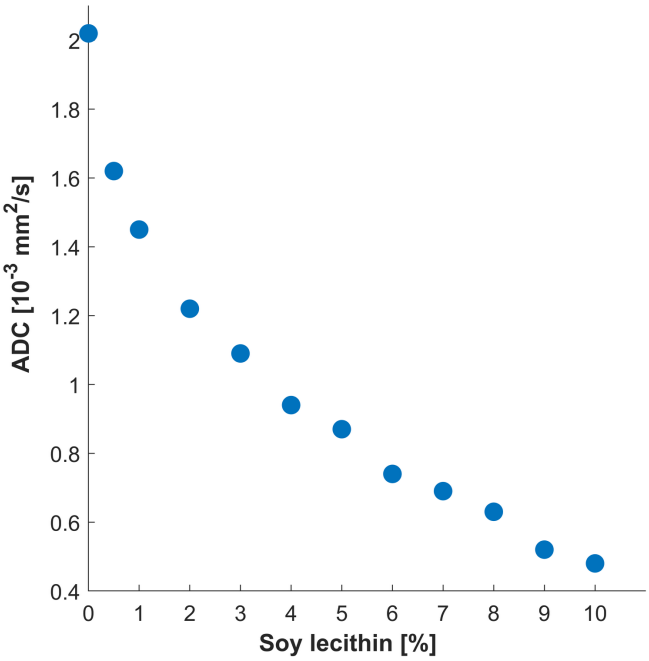


*Figure 8. ADC values of the aqueous soy lecithin solutions as a function of the soy lecithin concentration (w/v). Reprinted from [64], licensed under CC BY 4.0.*

*Table 1. ADC, T1 and T2 values of aqueous soy lecithin solutions as a function of soy lecithin concentration. Adapted from [64], licensed under CC BY 4.0.*

| Concentration [% w/v] | ADC [$10^{-3}$ $mm^2/s$] | T1 [ms] | T2 [ms] |
|---|---|---|---|
| 0 | 2.02 ± 0.02 | 2685 ± 67 | 2013 ± 41 |
| 0,5 | 1.59 ± 0.02 | 2286 ± 70 | 1089 ± 28 |
| 1 | 1.42 ± 0.02 | 1993 ± 65 | 792 ± 37 |
| 2 | 1.22 ± 0.01 | 1618 ± 48 | 506 ± 34 |
| 3 | 1.08 ± 0.01 | 1359 ± 35 | 375 ± 23 |
| 4 | 0.94 ± 0.01 | 1170 ± 23 | 293 ± 9 |
| 5 | 0.86 ± 0.01 | 1030 ± 18 | 242 ± 6 |
| 6 | 0.73 ± 0.02 | 929 ± 13 | 207 ± 5 |
| 7 | 0.68 ± 0.02 | 843 ± 8 | 183 ± 3 |
| 8 | 0.61 ± 0.02 | 778 ± 6 | 164 ± 2 |
| 9 | 0.52 ± 0.03 | 717 ± 4 | 148 ± 1 |
| 10 | 0.48 ± 0.02 | 668 ± 4 | 133 ± 2 |

Diffusion kurtosis measurements revealed that the water diffusion within aqueous soy lecithin solutions (slightly) deviates from the Gaussian nature at high b-values above 1000 s/$mm^2$ (Figure 9a). The mean kurtosis value ranged from 0 for pure water to ~ 0.5 for the solution with the highest concentration (Figure 9b). This suggested that soy lecithin in aqueous solution is a promising substance that could mimic not only ADC values but also, in contrast to sucrose, the restricted diffusion of water in biological tissues.

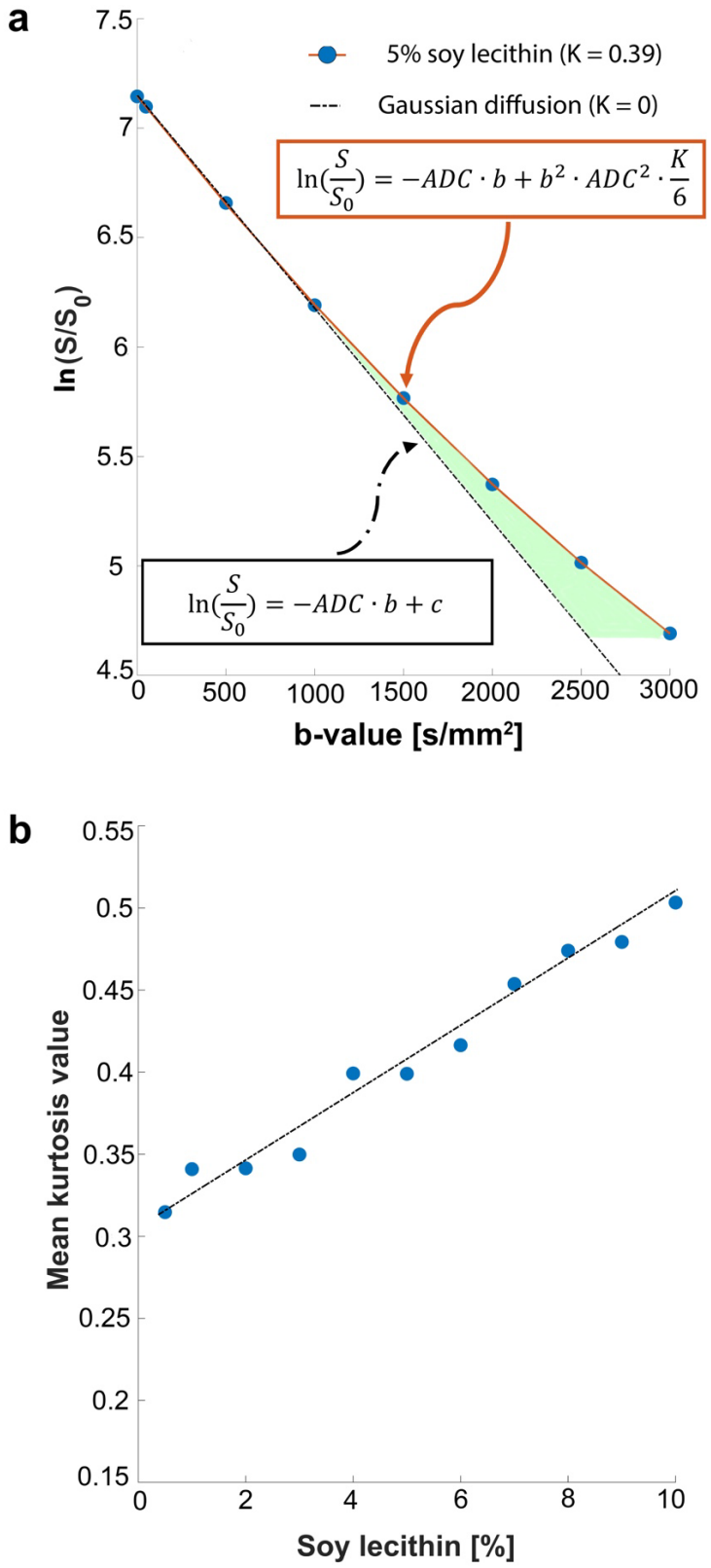


*Figure 9. (a) Signal decay as a function of b-value for a 5% (w/v) soy lecithin solution. The dashed-dotted line represents the linear signal decay for free or Gaussian water proton diffusion observed*

*in pure liquids without barriers. (b) Mean kurtosis value K of the aqueous soy lecithin solutions as a function of the soy lecithin concentration. Adapted from [64], licensed under CC BY 4.0.*

Another remarkable result of this study was that soy lecithin, even at the highest concentration, did not contribute any $^{1}H$ signal to the spectrum recorded at a (relatively) short echo time of 20 ms. This is particularly advantageous as solute signals could have undesirable effects and cause inaccuracies or even systematic errors in quantitative ADC measurements. For example, PEG, which has a dominant signal at about 3.7 ppm, caused problems and distortions in the determination of the ADC value in PEG-based diffusion phantoms [67].

Like other ADC modifying substances, soy lecithin causes a reduction in T1 and T2 (Table 1). T1 times ranged from 2685 ms (0% w/v) to 668 ms (10% w/v) and remained within biologically relevant ranges. T2 ranged from 2013 ms (0% w/v) to 133 ms (10% w/v), still well above the T2 of almost all parenchymal tissues [75]. This seems to be another advantage of soy lecithin, as it offers the possibility to adjust the apparent diffusion coefficient and the T2 relaxation time largely independently. As shown in Figure 10, the ADC value could be controlled by the concentration of soy lecithin, while the T2 values could be adjusted to the desired values by adding agar. The addition of agar to the aqueous soy lecithin solutions resulted in a large decrease in T2 with no significant effect on the ADC.

Overall, soy lecithin proves to be a substance that reliably meets the critical criteria defined by Tofts et al. [65] for diffusion test materials, thereby expanding the range of available diffusion modifiers. It provides several advantages over previously proposed substances, especially a wide range of adjustable ADC values, lacking additional $^{1}H$-signals, and the possibility to adjust ADC and T2 values (by adding agar) almost independently of each other.

However, open questions remain. The temperature dependence of the aqueous soy lecithin solutions has not been investigated. However, knowledge of temperature dependence is very important, especially when the test solutions are used in multicenter studies where temperature varies from site to site and over time. Therefore, temperature calibration curves as described by Wagner et al. [96] for PVP phantoms are needed to make the application of soy lecithin-based diffusion phantoms more practical. Furthermore, the underlying mechanism of the observed effective restriction of water mobility remains unclear. An independent

physical characterization using techniques such as dynamic light scattering (DLS), small-angle X-ray scattering (SAXS), or cryogenic transmission electron microscopy (cryo-TEM) could provide deeper insights into the morphology and size distribution of the formed aggregates [73,97,98], thereby improving the understanding of the diffusion effects and MR signal behavior. Initial DLS measurements (see *Publication 4*) revealed that the aggregates were between 250 nm and 350 nm in size at soy lecithin concentrations of up to 0.5% (w/v).

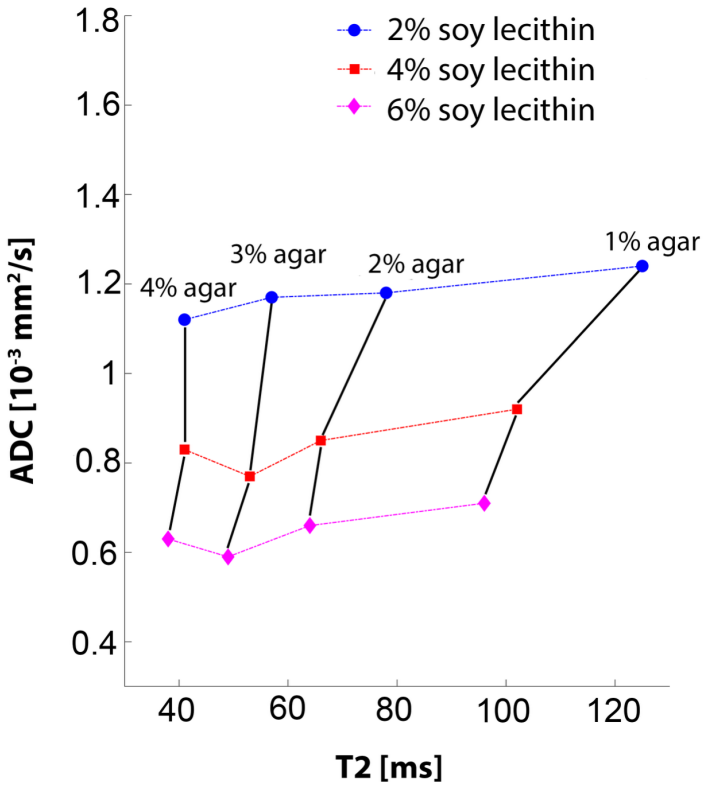


*Figure 10. Variation of the ADC and T2 values of the soy lecithin-agar gels depending on the agar and soy lecithin concentration. Adapted from [64], licensed under CC BY 4.0.*

**Statement of Contributions**

| | |
|---|---|
| Victor Fritz | Corresponding and first author, conception and study design, material preparation, data collection and analysis, writing of the manuscript. |
| Petros Martirosian | Advice and support in data acquisition and analysis, proofreading of the manuscript. |
| Jürgen Machann | Advice and support in data acquisition and analysis, proofreading of the manuscript. |
| Daniela Thorwarth | Supervision, critical discussion, proofreading of the manuscript. |
| Fritz Schick | Supervision, conception and study design, critical discussion, writing and proofreading of the manuscript. |

# Publication 3

*Reproduced and summarized from:*
*Fritz, V., Eisele, S., Martirosian, P., Machann, J., Schick, F. (2024)*
*A straightforward procedure to build a non-toxic relaxometry phantom with desired T1 and T2 times at 3T.*
*Magnetic Resonance Materials in Physics, Biology and Medicine (MAGMA).*
*DOI: https://doi.org/10.1007/s10334-024-01166-7*


Publication 3 was motivated by the need for flexible and non-toxic relaxometry phantoms capable of simulating tissue-like T1 and T2 relaxation times at 3 Tesla. Traditional phantoms often rely on paramagnetic salts to modify relaxation times, but these substances are quite toxic, can alter magnetic susceptibility, and pose challenges in handling and disposal (see *Introduction and Objectives; Test materials for Relaxometry*). Given the growing interest in accessible and safe quantitative MRI phantoms, this work investigated an alternative approach using soy lecithin, an inexpensive and biologically harmless substance. As shown in Publications 1 and 2**,** soy lecithin is promising substance that alter the relaxation- and diffusion properties of water, making it ideal for phantom manufacturing.

The main objective of this work was to prepare and evaluate soy lecithin-agar gels as a phantom material for the construction of non-toxic relaxometry phantoms with tissue-like relaxation times. In the first part of this work, the compatibility of soy lecithin and agar was systematically investigated. The goal was to verify whether the individual T1- and T2-modifying effects (relaxivities) of both substances remain stable even when mixed – a prerequisite for independent adjustment of T1 and T2. For this purpose, relaxivities ($r_1$, $r_2$) of soy lecithin were measured in the presence of different concentrations of agar (0% – 4% w/v), while the relaxivities of agar were measured in the presence of different concentrations of soy lecithin (0% – 4% w/v). The results showed that both substances are compatible and retain their effect even when mixed. The relaxivities ($r_1$, $r_2$) hardly changed in the presence of the other substance. Mean relaxivities were $r_{1,lecithin} = 0.116\ s^{-1}(\%\ w/v)^{-1}$, $r_{1,agar} = 0.033\ s^{-1}(\%\ w/v)^{-1}$, $r_{2,lecithin} = 0.71\ s^{-1}(\%w/v)^{-1}$, and $r_{2,agar} = 5.78\ s^{-1}(\%\ w/v)^{-1}$.

Using the calculated relaxivities, simple equations were derived to calculate the appropriate concentrations of soy lecithin and agar to achieve the desired relaxation times:

$$C_{Agar} = \frac{180}{T2\ [ms]} - \frac{1100}{T1\ [ms]} + 0.28 \tag{12}$$

$$C_{Lecithin} = \frac{8930}{T1\ [ms]} - \frac{51}{T2\ [ms]} - 3 \tag{13}$$

To validate this approach, test phantoms mimicking the relaxation times of various tissues (gray and white matter, kidney cortex and medulla, spleen, muscle, liver) were prepared and examined using T1 and T2 mapping as well as a 3D T1-weighted sequence with high spatial resolution. Phantoms were tested for correspondence between measurements and calculated relaxation times, reproducibility, spatial homogeneity, and temporal stability. For this, all phantoms were prepared three times, independently on different days and examined on the day of preparation and four weeks after preparation. Possible mold growth was monitored by visual inspection of the samples during the 4-week study period. The preparation process is shown in Figure 11.

Table 2 provides an overview of the concentrations of soy lecithin and agar used, as well as the targeted and measured relaxation times. Except for the liver phantom, all phantoms were successfully and reproducibly produced. Good agreement was found between the targeted and measured values. The percentage deviations from the targeted relaxation times were less than 3% for T1 and less than 6.5% for T2. The liver phantom showed a significantly higher deviation (32.5% in T2), likely due to increased viscosity and inhomogeneity caused by high concentrations of soy lecithin (6.78% w/v) and agar (3.21% w/v), which also resulted in visible air bubble entrapment.

A significant drawback was found in the temporal stability of the phantoms. After four weeks of storage (at room temperature), mold growth and also changes in relaxation times were detected in almost all samples (Figure 12). In contrast, phantoms using paramagnetic salts for T1 or T2 modification remain stable for a

long time without significant changes in relaxation times [4,11,12]. This feature is very important when phantoms are employed for reproducibility measurements in multicenter studies where measurements are carried out over several weeks or even months. This instability is attributed to the biological nature of the ingredients, particularly agar, which serves as a perfect nutrient medium for microorganisms [99]. Although, preservatives could improve stability, most effective agents are quite toxic, which militates against their use as it is contrary to the motivation of this study (production of relaxometry phantoms without toxic or questionable substances).

In conclusion, soy lecithin-agar gels provide a promising, non-toxic phantom material for the construction of relaxometry phantoms. Soy lecithin-agar gels are inexpensive, easy to prepare, and allow independent adjustment of T1 and T2 without marked susceptibility effects. With the presented manufacturing process, the relaxation times of many tissue types can be mimicked. They are well suited for proof-of-concept experiments and protocol development. However, for long-term or multicenter applications, challenges related to biostability, and temperature dependence have to be considered. Future work must focus on identifying effective preservation strategies, such as incorporating antimicrobial agents, optimizing storage conditions, or employing sterilization methods like UV treatment.

Despite these limitations, this study significantly expands the range of accessible phantom materials in MRI research and represents an important step toward safer and more flexible phantom design.

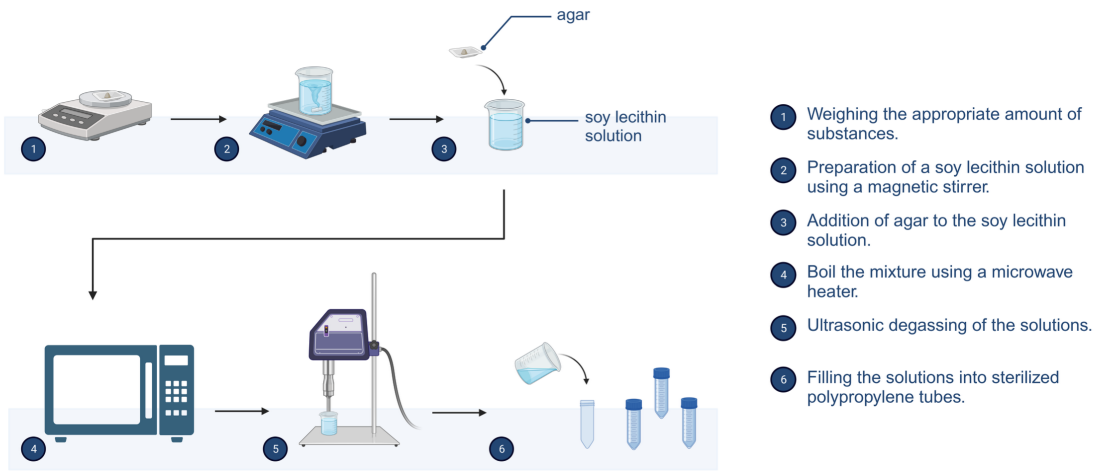


*Figure 11. Schematic representation of the manufacturing process of the soy lecithin-agar gels. Created in BioRender. https://BioRender.com/i1yh1an. Reprinted from [83], licensed under CC BY 4.0.*

*Table 2. Overview of the concentrations of soy lecithin and agar used and the targeted and measured T1 and T2 times of the test phantoms. The mean value and the standard deviation over the three measured phantom batches are shown. Adapted from [83], licensed under CC BY 4.0.*

| | T1 [ms] | | T2 [ms] | | Soy lecithin | Agar |
|---|---|---|---|---|---|---|
| | Target | Measured | Target | Measured | [% w/v] | [% w/v] |
| **Gray matter** | 1820 | 1850 ± 12 | 99 | 93 ± 3 | 1.39 | 1.49 |
| **White matter** | 1084 | 1093 ± 4 | 69 | 66 ± 2 | 4.50 | 1.87 |
| **Kidney cortex** | 1142 | 1159 ± 10 | 76 | 72 ± 2 | 4.15 | 1.69 |
| **Kidney medulla** | 1545 | 1539 ± 17 | 81 | 75 ± 3 | 2.15 | 1.79 |
| **Spleen** | 1328 | 1318 ± 23 | 61 | 58 ± 1 | 2.89 | 2.40 |
| **Muscle** | 1295 | 1262 ± 16 | 34 | 34 ± 1 | 2.40 | 4.72 |
| **Liver** | 812 | 834 ± 16 | 42 | 56 ± 6 | 6.78 | 3.21 |

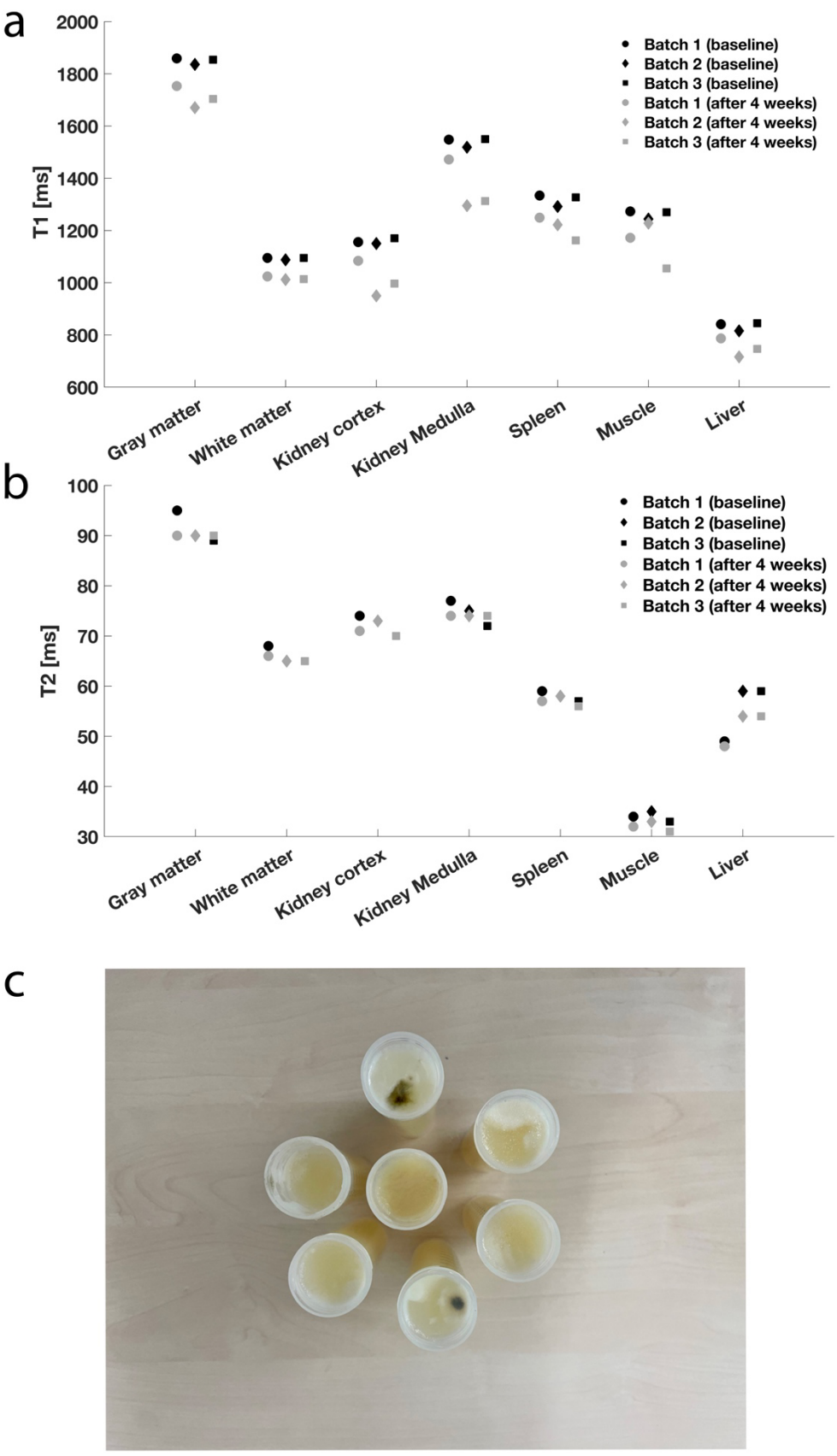


*Figure 12. To evaluate the temporal stability of the test phantoms, T1 and T2 measurements were repeated after four weeks under the same conditions. (a) Comparison of T1 times measured at*

*baseline and after four weeks. (b) Comparison of T2 times measured at baseline and after four weeks. (c) Photograph of the test phantoms (batch 1) after a storage period of four weeks – mold growth is clearly visible on some phantoms. Reprinted and adapted from [83], licensed under CC BY 4.0.*

**Statement of Contributions**

| | |
|---|---|
| Victor Fritz | Corresponding and first author, conception and study design, material preparation, data collection and analysis, writing of the manuscript. |
| Sabine Eisele | Help with phantom preparation and data collection. |
| Petros Martirosian | Advice and support in data acquisition and analysis, proofreading of the manuscript. |
| Jürgen Machann | Advice and support in data acquisition and analysis, proofreading of the manuscript. |
| Fritz Schick | Supervision, conception and study design, critical discussion, writing and proofreading of the manuscript. |

## Publication 4

*Reproduced and summarized from:*
*Fritz, V., Schick, F. (2026)*
*Recipe for hydrogels with tunable relaxation and diffusion properties for use as MRI test materials.*
*Magnetic Resonance in Medicine (MRM).*
*DOI: https://doi.org/10.1002/mrm.70120*


The aim of Publication 4 was to develop and evaluate a preparation protocol (recipe) for hydrogels with specific relaxation times and ADC values to be used as tissue-like test materials for MRI experiments at 3 Tesla. To date, no instructions have been described for test materials that allow simultaneous and independent adjustment of the important MRI parameters T1, T2 and ADC [2]. Most existing materials for test phantoms are designed to mimic only one or two of these MRI parameters, while the other(s) are not controlled (see *Introduction and Objectives; Test materials mimicking multiple MR properties*).

The presented approach is based on a three-component system of Gd-DTPA, agarose and soy lecithin in aqueous solution. The goal was to create gels with well-defined and physiologically relevant combinations of T1, T2 and ADC by adjusting the concentrations of these three substances. The modifiers were selected based on their known effects on MRI parameters and their expected compatibility in mixed systems.

First, the relaxation and diffusion modifying properties of the individual substances were characterized and their compatibility in combination was confirmed. For this purpose, 47 test solutions with different concentrations of each substance were prepared, measured, and analyzed. The preparation of the samples is shown in Figure 13. The relaxation and diffusion properties of the samples were quantified using relaxometry and DWI on a clinical 3 Tesla MRI scanner at 20° Celsius.

Based on these preliminary experiments, empirical relationships (Eqs. 14-16) between the substance concentrations and target values were established:

$$ADC\ [10^{-3}] = 0.36 \cdot e^{-2.79 \cdot C_{lec}} + 1.60 \cdot e^{-0.13 \cdot C_{lec}} \quad (14)$$

$$R1 = R1_w + r_{1,Gd} \cdot C_{Gd} + r_{1,lec} \cdot C_{lec} \quad (15)$$

$$R2 = R2_w + r_{2,Gd} \cdot C_{Gd} + r_{2,lec} \cdot C_{lec} + r_{2,a} \cdot C_a \quad (16)$$

R1 and R2 are the relaxation rates ($1/T_{1,2}$) of the gels, $R1_w$ and $R2_w$ are the relaxation rate of pure water, $C_{Gd}$ is the concentration of Gd-DTPA in mM, $C_{lec}$ and $C_a$ are the concentrations of soy lecithin and agarose in % (w/v), and $r_1$ and $r_2$ are the longitudinal- and transverse relaxivities of each substance.

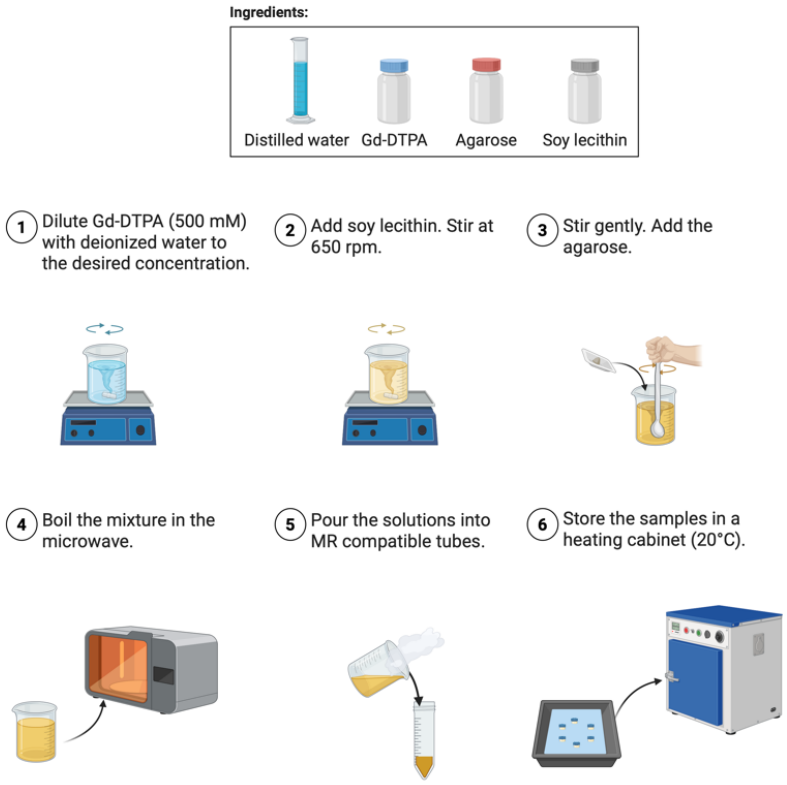


*Figure 13. Scheme of the hydrogel preparation process. Created in BioRender. https://BioRender.com/k1h8vah. Reprinted from [87], licensed under CC BY 4.0.*

Since the ADC value depends only on the soy lecithin concentration, the T1 value on the concentrations of soy lecithin and Gd-DTPA, and the T2 value on the concentrations of soy lecithin, Gd-DTPA, and agarose, the determination of the component concentrations follows a three-step procedure: (1) the soy lecithin concentration is determined based on the target ADC value using Eq. 14 to achieve the desired diffusion characteristics, (2) with the soy lecithin concentration determined, the Gd-DTPA concentration is calculated to achieve the target T1 relaxation time using Eq. 15, and (3) finally, the agarose concentration is determined using the calculated soy lecithin and Gd-DTPA concentrations along with the target T2 relaxation time using Eq. 16.

Figure 14 provides an overview of the achievable combinations of T1, T2, and ADC values, demonstrating the extent of the parameter space accessible using this approach. The properties (T1, T2, ADC) of most known tissue classes could be well approximated, only the gray matter of the brain was slightly outside the selectable range.

To validate this approach, test phantoms with hydrogels mimicking the diffusion- and relaxation properties of different tissues (pancreas, white matter, fibroglandular tissue, liver, prostate) were prepared according to the presented protocol. These were tested for accuracy (in terms of deviations from targeted values), reproducibility, and temporal stability. All hydrogels provided a reasonable agreement between measured and intended values: Deviations were less than 8% for T1, less than 7.5% for T2, and less than 11.5% for ADC (Table 3). In addition, the preparation of the gels showed a high degree of reproducibility, as evidenced by the relatively low standard deviations observed across the three batches (Table 3), underscoring the robustness and accuracy of the preparation protocol. Temporal stability was also acceptable: as shown in Figure 15, the ADC values and relaxation times of the hydrogel-filled tubes in the phantoms did not change significantly during the 12-week storage period.

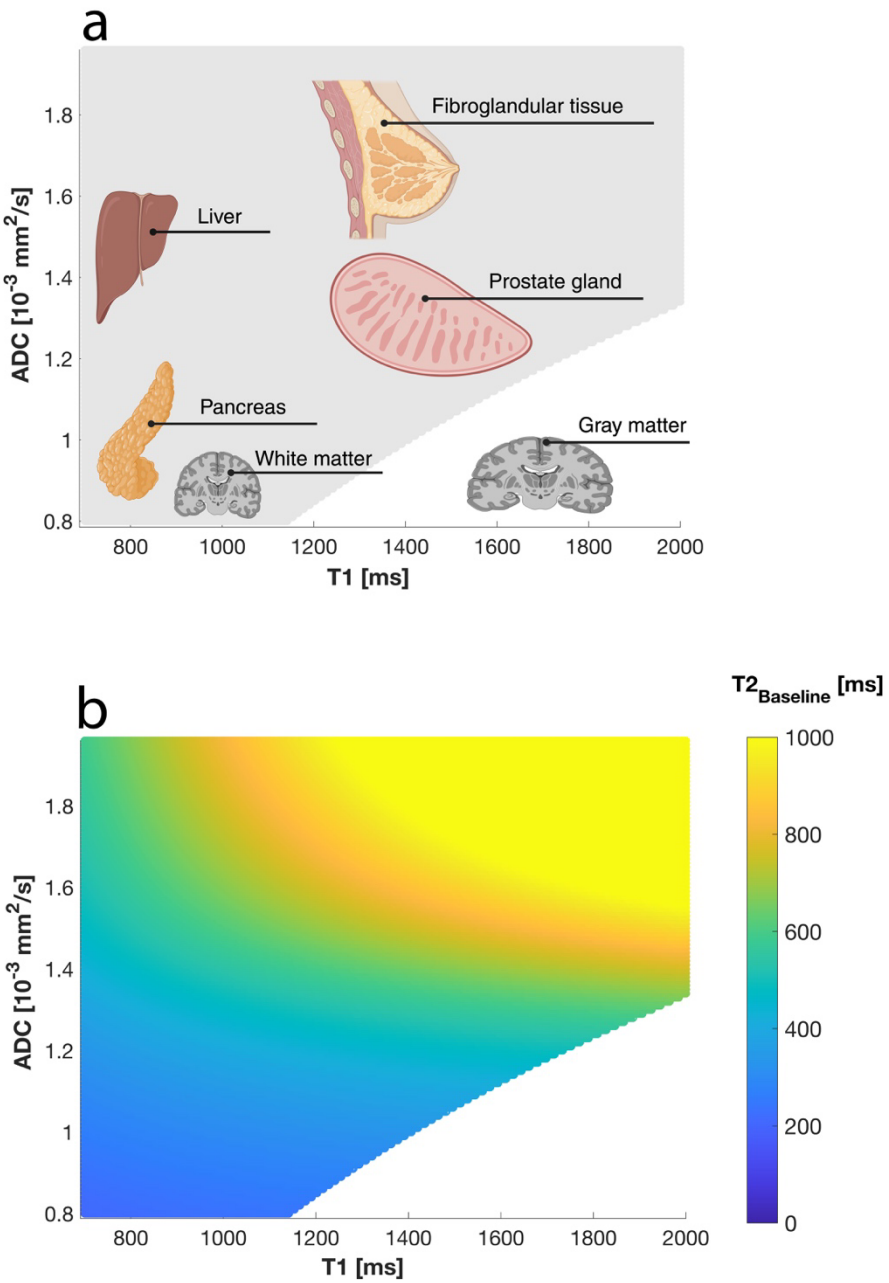


*Figure 14. (a) Achievable combinations of ADC and T1 (gray area) using the proposed recipe. Achievable values cover most human tissues such as liver, prostate and white matter. Only tissues with low ADC values but long T1 times (e.g., gray matter) are not included in the accessible range. (b) Baseline T2 values as a function of selected ADC and T1 values before addition of agarose. For all combinations of ADC and T1 considered, the baseline values remained above 200 ms, providing sufficient flexibility for further adjustment to physiologically relevant T2 values by adding agarose. Created in BioRender. https://BioRender.com/yu9nc7d. Reprinted from [87], licensed under CC BY 4.0.*

*Table 3. Target and measured values for T1, T2, and ADC, presented as mean and standard deviation across the three prepared phantom batches. Adapted from [87], licensed under CC BY 4.0.*

| | T1 [ms] | | T2 [ms] | | ADC [$mm^2/s$] | |
|---|---|---|---|---|---|---|
| | **Target** | **Measured** | **Target** | **Measured** | **Target** | **Measured** |
| **Pancreas** | 725 | 757 ± 16 | 43 | 43 ± 1 | 0.98 | 0.87 ± 0.01 |
| **White matter** | 1084 | 1143 ± 3 | 69 | 66 ± 1 | 0.84 | 0.83 ± 0.04 |
| **Fibroglandular** | 1444 | 1396 ± 13 | 54 | 50 ± 1 | 1.75 | 1.75 ± 0.02 |
| **Liver** | 812 | 809 ± 14 | 42 | 41 ± 1 | 1.40 | 1.43 ± 0.03 |
| **Prostate** | 1597 | 1721 ± 28 | 80 | 80 ± 2 | 1.25 | 1.23 ± 0.02 |

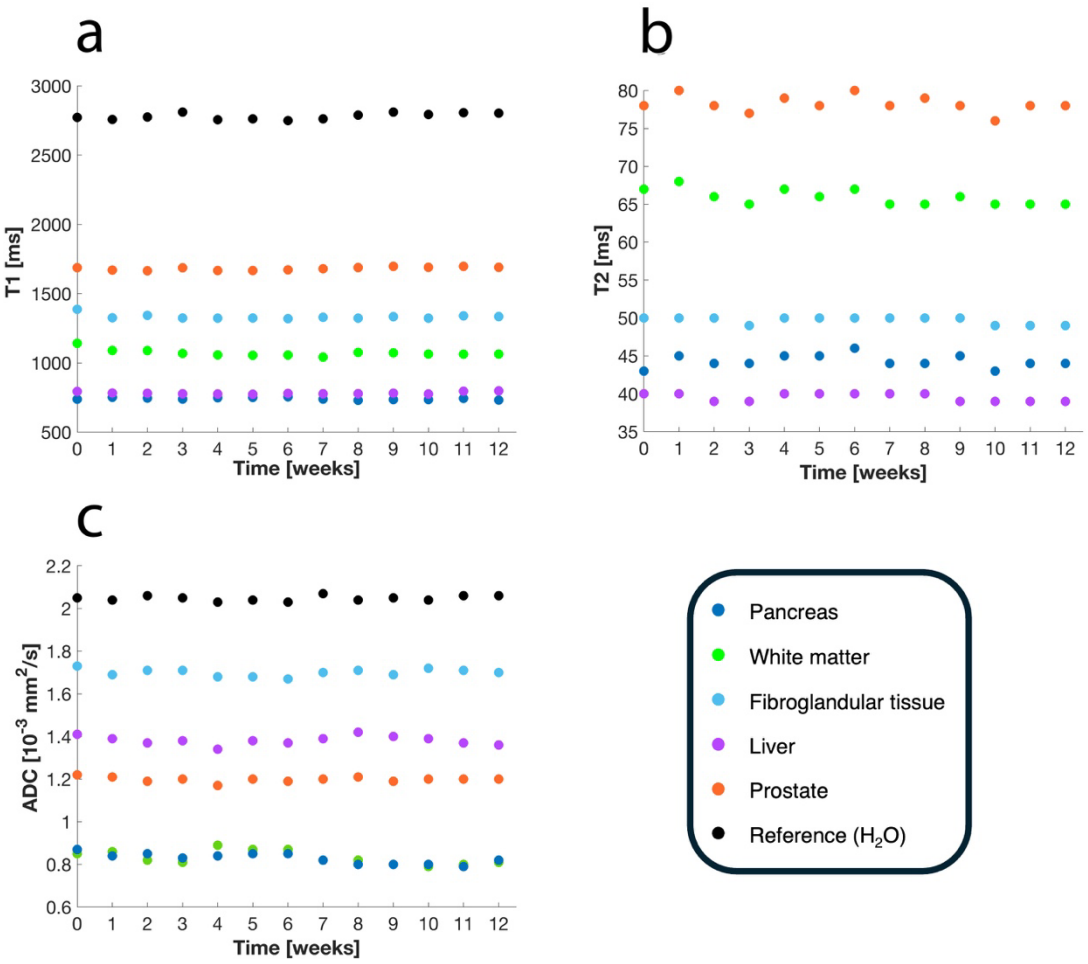


*Figure 15. Temporal stability of the prepared hydrogels (Batch 1) with respect to T1 (a), T2 (b) and ADC (c). Reprinted from [87], licensed under CC BY 4.0.*

In summary, Publication 4 provides a structured and reproducible method for the preparation of hydrogels with independently adjustable T1, T2, and ADC values at 3 Tesla using soy lecithin, agarose and Gd-DTPA. The gels are easy to prepare, inexpensive, and show an acceptable temporal stability of at least three months, making them suitable as reference materials for MRI research. Compared to phantom designs that consider only one or two quantitative MRI parameters, the presented approach allows a more comprehensive validation and optimization of MRI sequences by better reflecting the diverse properties of biological tissues. The combination of adjustable relaxation times and ADC values in a single phantom material is of great value in the development and validation of not only standard but also multi-parametric MRI (e.g. MR fingerprinting [100]) for the simultaneous acquisition of relaxation and diffusion metrics.

However, some limitations remain and must be considered: The presented work focused on developing a formulation that enables relaxation times and ADC to be adjusted largely independently. The range considered includes ADC values from 0.8 to 2 [$10^{-3}$] $mm^2/s$, T1 values from 700 to 2000 ms, and T2 values from 100 to 40 ms. While this covers a broad spectrum of clinically relevant tissue properties, full independence of parameters could not be achieved across the entire range. In particular, the interplay between ADC and T1 proved challenging, since soy lecithin affects both parameters simultaneously. As a result, tissue types characterized by relatively low ADC but long T1 values, such as gray matter [75,93,101], could not be accurately mimicked with the proposed formulation.

In addition, the presented design does not account for temperature and field-dependence. In this study, all measurements were performed at a temperature of 20°C and a field strength of 3 Tesla. Further measurements at different temperatures and field strengths are needed to determine calibration factors and adapt the manufacturing protocol (Eqs. 14-16) to different scanning conditions. Also, an assessment of their long-term stability (beyond three months) is currently ongoing to determine their suitability for extended use in multi-center and longitudinal studies.

**Statement of Contributions**

| | |
|---|---|
| Victor Fritz | Corresponding and first author, conception and study design, material preparation, data collection and analysis, writing of the manuscript. |
| Fritz Schick | Supervision, conception and study design, critical discussion, writing and proofreading of the manuscript. |

# References

1. Keenan KE, Ainslie M, Barker AJ et al. (2018) Quantitative magnetic resonance imaging phantoms: A review and the need for a system phantom. Magn Reson Med 79 (1):48-61.

2. Keenan KE, Jordanova KV, Ogier SE et al. (2024) Phantoms for Quantitative Body MRI: a review and discussion of the phantom value. Magma 37 (4):535-549.

3. Stupic KF, Ainslie M, Boss MA et al. (2021) A standard system phantom for magnetic resonance imaging. Magn Reson Med 86 (3):1194-1211.

4. Tofts PS (2003) QA: Quality Assurance, Accuracy, Precision and Phantoms. In: Tofts PS (ed) Quantitative MRI of the Brain. John Wiley & Sons, Chichester, England, pp 55-81.

5. Cheng HL, Stikov N, Ghugre NR, Wright GA (2012) Practical medical applications of quantitative MR relaxometry. J Magn Reson Imaging 36 (4):805-824.

6. Padhani AR, Liu G, Koh DM et al. (2009) Diffusion-weighted magnetic resonance imaging as a cancer biomarker: consensus and recommendations. Neoplasia 11 (2):102-125.

7. Reeder SB, Sirlin CB (2010) Quantification of liver fat with magnetic resonance imaging. Magn Reson Imaging Clin N Am 18 (3):337-357, ix.

8. Taouli B, Chouli M, Martin AJ, Qayyum A, Coakley FV, Vilgrain V (2008) Chronic hepatitis: role of diffusion-weighted imaging and diffusion tensor imaging for the diagnosis of liver fibrosis and inflammation. J Magn Reson Imaging 28 (1):89-95.

9. Mitchell MD, Kundel HL, Axel L, Joseph PM (1986) Agarose as a tissue equivalent phantom material for NMR imaging. Magn Reson Imaging 4 (3):263-266.

10. Kraft KA, Fatouros PP, Clarke GD, Kishore PR (1987) An MRI phantom material for quantitative relaxometry. Magn Reson Med 5 (6):555-562.

11. Christoffersson JO, Olsson LE, Sjöberg S (1991) Nickel-doped agarose gel phantoms in MR imaging. Acta Radiol 32 (5):426-431.

12. Tofts PS, Shuter B, Pope JM (1993) Ni-DTPA doped agarose gel--a phantom material for Gd-DTPA enhancement measurements. Magn Reson Imaging 11 (1):125-133.

13. Laubach HJ, Jakob PM, Loevblad KO et al. (1998) A phantom for diffusion-weighted imaging of acute stroke. J Magn Reson Imaging 8 (6):1349-1354.

14. Kato H, Kuroda M, Yoshimura K et al. (2005) Composition of MRI phantom equivalent to human tissues. Med Phys 32 (10):3199-3208.

15. Matsuya R, Kuroda M, Matsumoto Y et al. (2009) A new phantom using polyethylene glycol as an apparent diffusion coefficient standard for MR imaging. Int J Oncol 35 (4):893-900.

16. Pierpaoli C, Sarlls J, Nevo U, Basser P, Horkay F Polyvinylpyrrolidone (PVP) water solutions as isotropic phantoms for diffusion MRI studies. In: Proceedings of the 17th Annual Meeting of the ISMRM; Honolulu, Hawaii., Honolulu, Hawaii, 2009.

17. Hellerbach A, Schuster V, Jansen A, Sommer J (2013) MRI phantoms - are there alternatives to agar? PLoS One 8 (8):e70343.

18. Keenan KE, Wilmes LJ, Aliu SO et al. (2016) Design of a breast phantom for quantitative MRI. J Magn Reson Imaging 44 (3):610-619.

19. Bush EC, Gifford A, Coolbaugh CL, Towse TF, Damon BM, Welch EB (2018) Fat-Water Phantoms for Magnetic Resonance Imaging Validation: A Flexible and Scalable Protocol. J Vis Exp doi:10.3791/57704 (139).

20. Altermatt A, Santini F, Deligianni X et al. (2019) Design and construction of an innovative brain phantom prototype for MRI. Magn Reson Med 81 (2):1165-1171.

21. Mobini N, Malekzadeh M, Haghighatkhah H, Saligheh Rad H (2020) A hybrid (iron-fat-water) phantom for liver iron overload quantification in the presence of contaminating fat using magnetic resonance imaging. Magma 33 (3):385-392.

22. Gopalan K, Tamir JI, Arias AC, Lustig M (2021) Quantitative anatomy mimicking slice phantoms. Magn Reson Med 86 (2):1159-1166.

23. Woletz M, Roat S, Hummer A, Tik M, Windischberger C (2021) Technical Note: Human tissue-equivalent MRI phantom preparation for 3 and 7 Tesla. Med Phys 48 (8):4387-4394.

24. Zhao R, Hamilton G, Brittain JH, Reeder SB, Hernando D (2021) Design and evaluation of quantitative MRI phantoms to mimic the simultaneous presence of fat, iron, and fibrosis in the liver. Magn Reson Med 85 (2):734-747.

25. Brown RW, Cheng Y-CN, Haacke EM, Thompson MR, Venkatesan R (2014) Magnetic Resonance Imaging: Physical Principles and Sequence Design. 2nd edn. John Wiley & Sons, Hoboken, New Jersey

26. Levitt MH (2001) Spin Dynamics: Basics of Nuclear Magnetic Resonance. John Wiley & Sons, Chichester, England

27. Semmler W, Brix G, Kolem H et al. (2002) Grundlagen der MRT und MRS. In: Reiser M, Semmler W (eds) Magnetresonanztomographie. Springer, Berlin, pp 3-132.

28. Bloch F (1946) Nuclear Induction. Physical Review 70 (7-8):460-474.

29. Dixon WT (1984) Simple proton spectroscopic imaging. Radiology 153 (1):189-194.

30. Schick F, Forster J, Machann J, Huppert P, Claussen CD (1997) Highly selective water and fat imaging applying multislice sequences without sensitivity to B1 field inhomogeneities. Magn Reson Med 38 (2):269-274.

31. Schick F (1998) Simultaneous highly selective MR water and fat imaging using a simple new type of spectral-spatial excitation. Magn Reson Med 40 (2):194-202.

32. Friebolin H (1999) Ein- und zweidimensionale NMR-Spektroskopie: Eine Einführung. 3rd edn. Wiley-VCH, Weinheim

33. Bley TA, Wieben O, François CJ, Brittain JH, Reeder SB (2010) Fat and water magnetic resonance imaging. J Magn Reson Imaging 31 (1):4-18.

34. Schick F (2017) Fat and water selective MRI. Z Med Phys 27 (1):1-3.

35. Reeder SB, Cruite I, Hamilton G, Sirlin CB (2011) Quantitative Assessment of Liver Fat with Magnetic Resonance Imaging and Spectroscopy. J Magn Reson Imaging 34 (4):729-749.

36. Thomsen C, Becker U, Winkler K, Christoffersen P, Jensen M, Henriksen O (1994) Quantification of liver fat using magnetic resonance spectroscopy. Magn Reson Imaging 12 (3):487-495.

37. Machann J, Stefan N, Schick F (2008) (1)H MR spectroscopy of skeletal muscle, liver and bone marrow. Eur J Radiol 67 (2):275-284.

38. Ma J (2008) Dixon techniques for water and fat imaging. J Magn Reson Imaging 28 (3):543-558.

39. Yeung HN, Kormos DW (1986) Separation of true fat and water images by correcting magnetic field inhomogeneity in situ. Radiology 159 (3):783-786.

40. Glover GH (1991) Multipoint Dixon technique for water and fat proton and susceptibility imaging. J Magn Reson Imaging 1 (5):521-530.

41. Glover GH, Schneider E (1991) Three-point Dixon technique for true water/fat decomposition with B0 inhomogeneity correction. Magn Reson Med 18 (2):371-383.

42. Reeder SB, Pineda AR, Wen Z et al. (2005) Iterative decomposition of water and fat with echo asymmetry and least-squares estimation (IDEAL): application with fast spin-echo imaging. Magn Reson Med 54 (3):636-644.

43. Fritz V, Martirosian P, Machann J, Daniels R, Schick F (2022) A comparison of emulsifiers for the formation of oil-in-water emulsions: stability of the emulsions within 9 h after production and MR signal properties. Magma 35 (3):401-410.

44. Poon CS, Szumowski J, Plewes DB, Ashby P, Henkelman RM (1989) Fat/water quantitation and differential relaxation time measurement using chemical shift imaging technique. Magn Reson Imaging 7 (4):369-382.

45. Merritt S, Gulsen G, Chiou G et al. (2003) Comparison of water and lipid content measurements using diffuse optical spectroscopy and MRI in emulsion phantoms. Technol Cancer Res Treat 2 (6):563-569.

46. Bernard CP, Liney GP, Manton DJ, Turnbull LW, Langton CM (2008) Comparison of fat quantification methods: a phantom study at 3.0T. J Magn Reson Imaging 27 (1):192-197.

47. Hines CD, Yu H, Shimakawa A, McKenzie CA, Brittain JH, Reeder SB (2009) T1 independent, T2* corrected MRI with accurate spectral modeling for quantification of fat: validation in a fat-water-SPIO phantom. J Magn Reson Imaging 30 (5):1215-1222.

48. Fukuzawa K, Hayashi T, Takahashi J et al. (2017) Evaluation of six-point modified dixon and magnetic resonance spectroscopy for fat quantification: a fat-water-iron phantom study. Radiol Phys Technol 10 (3):349-358.

49. Hayashi T, Fukuzawa K, Kondo H et al. (2017) Influence of Gd-EOB-DTPA on proton density fat fraction using the six-echo Dixon method in 3 Tesla magnetic resonance imaging. Radiol Phys Technol 10 (4):483-488.

50. Tadros TF (2013) Emulsion Formation, Stability, and Rheology. In: Tadros TF (ed) Emulsion Formation and Stability. Wiley-VCH, pp 1-75.

51. Tipirneni-Sajja A, Brasher S, Shrestha U, Johnson H, Morin C, Satapathy SK (2023) Quantitative MRI of diffuse liver diseases: techniques and tissue-mimicking phantoms. Magma 36 (4):529-551.

52. Yu H, Shimakawa A, McKenzie CA, Brodsky E, Brittain JH, Reeder SB (2008) Multiecho water-fat separation and simultaneous R2* estimation with multifrequency fat spectrum modeling. Magn Reson Med 60 (5):1122-1134.

53. Fortier V, Levesque IR (2022) Longitudinal relaxation in fat-water mixtures and its dependence on fat content at 3 T. NMR Biomed 35 (2):e4629.

54. Hu HH, Chen HS, Hernando D (2024) Linearity and bias of proton density fat fraction across the full dynamic range of 0-100%: a multiplatform, multivendor phantom study using 1.5T and 3T MRI at two sites. Magma 37 (4):551-563.

55. Israelachvili JN (2011) 19 - Thermodynamic Principles of Self-Assembly. In: Israelachvili JN (ed) Intermolecular and Surface Forces. 3rd edn. Academic Press, San Diego, CA, pp 503-534.

56. Le Bihan D, Johansen-Berg H (2012) Diffusion MRI at 25: exploring brain tissue structure and function. Neuroimage 61 (2):324-341.

57. Le Bihan D, Iima M (2015) Diffusion Magnetic Resonance Imaging: What Water Tells Us about Biological Tissues. PLoS Biol 13 (7):e1002203.

58. Einstein A (1905) Über die von der molekularkinetischen Theorie der Wärme geforderte Bewegung von in ruhenden Flüssigkeiten suspendierten Teilchen. Annalen der Physik 322 (8):549-560.

59. Stejskal EO, Tanner JE (1965) Spin Diffusion Measurements: Spin Echoes in the Presence of a Time-Dependent Field Gradient. The Journal of Chemical Physics 42 (1):288-292.

60. Jensen JH, Helpern JA, Ramani A, Lu H, Kaczynski K (2005) Diffusional kurtosis imaging: the quantification of non-gaussian water diffusion by means of magnetic resonance imaging. Magn Reson Med 53 (6):1432-1440.

61. Jensen JH, Helpern JA (2010) MRI quantification of non-Gaussian water diffusion by kurtosis analysis. NMR Biomed 23 (7):698-710.

62. Portakal ZG, Shermer S, Jenkins C et al. (2018) Design and characterization of tissue-mimicking gel phantoms for diffusion kurtosis imaging. Med Phys 45 (6):2476-2485.

63. Malyarenko DI, Swanson SD, Konar AS et al. (2019) Multicenter Repeatability Study of a Novel Quantitative Diffusion Kurtosis Imaging Phantom. Tomography 5 (1):36-43.

64. Fritz V, Martirosian P, Machann J, Thorwarth D, Schick F (2023) Soy lecithin: A beneficial substance for adjusting the ADC in aqueous solutions to the values of biological tissues. Magn Reson Med 89 (4):1674-1683.

65. Tofts PS, Lloyd D, Clark CA et al. (2000) Test liquids for quantitative MRI measurements of self-diffusion coefficient in vivo. Magn Reson Med 43 (3):368-374.

66. Lavdas I, Behan KC, Papadaki A, McRobbie DW, Aboagye EO (2013) A phantom for diffusion-weighted MRI (DW-MRI). J Magn Reson Imaging 38 (1):173-179.

67. Gatidis S, Schmidt H, Martirosian P, Schwenzer NF (2014) Development of an MRI phantom for diffusion-weighted imaging with independent adjustment of apparent diffusion coefficient values and T2 relaxation times. Magn Reson Med 72 (2):459-463.

68. Amouzandeh G, Chenevert TL, Swanson SD, Ross BD, Malyarenko DI (2022) Technical note: Temperature and concentration dependence of water diffusion in polyvinylpyrrolidone solutions. Med Phys 49 (5):3325-3332.

69. Ozaki K, Nakada M, Kunisu M et al. (2024) Hydrogen-bonded structure of hydrated water in polyvinyl pyrrolidone aqueous solution investigated by X-ray absorption and emission spectroscopy. Journal of Molecular Liquids 403:124822.

70. Harris JM (1992) Introduction to Biotechnical and Biomedical Applications of Poly(Ethylene Glycol). In: Harris JM (ed) Poly(Ethylene Glycol) Chemistry: Biotechnical and Biomedical Applications. Springer, Boston, MA, pp 1-14.

71. Wang X, Reeder SB, Hernando D (2017) An acetone-based phantom for quantitative diffusion MRI. J Magn Reson Imaging 46 (6):1683-1692.

72. Fritsche O (2021) Cytologie: Der Aufbau von Zellen im Überblick. In: Boenigk J (ed) Boenigk, Biologie. Springer Spektrum, Berlin, pp 37-56.

73. Mkam Tsengam IK, Omarova M, Kelley EG et al. (2022) Transformation of Lipid Vesicles into Micelles by Adding Nonionic Surfactants: Elucidating the Structural Pathway and the Intermediate Structures. J Phys Chem B 126 (11):2208-2216.

74. Hanley L, Ghazani SM, Marangoni AG (2024) Giant multilamellar and large unilamellar lecithin vesicles for the encapsulation and oral delivery of cannabinoids. Food Chemistry 433:137291.

75. Bojorquez JZ, Bricq S, Acquitter C, Brunotte F, Walker PM, Lalande A (2017) What are normal relaxation times of tissues at 3 T? Magn Reson Imaging 35:69-80.

76. Bottomley PA, Foster TH, Argersinger RE, Pfeifer LM (1984) A review of normal tissue hydrogen NMR relaxation times and relaxation mechanisms from

1-100 MHz: dependence on tissue type, NMR frequency, temperature, species, excision, and age. Med Phys 11 (4):425-448.

77. Stikov N, Boudreau M, Levesque IR, Tardif CL, Barral JK, Pike GB (2015) On the accuracy of T1 mapping: searching for common ground. Magn Reson Med 73 (2):514-522.

78. Barral JK, Gudmundson E, Stikov N, Etezadi-Amoli M, Stoica P, Nishimura DG (2010) A robust methodology for in vivo T1 mapping. Magn Reson Med 64 (4):1057-1067.

79. Crawley AP, Henkelman RM (1987) Errors in T2 estimation using multislice multiple-echo imaging. Magn Reson Med 4 (1):34-47.

80. Hennig J (1991) Echoes—how to generate, recognize, use or avoid them in MR-imaging sequences. Part I: Fundamental and not so fundamental properties of spin echoes. Concepts in Magnetic Resonance 3 (3):125-143.

81. Poon CS, Henkelman RM (1992) Practical T2 quantitation for clinical applications. J Magn Reson Imaging 2 (5):541-553.

82. Fransson A, Ericsson A, Sperber GO (1993) Dependence on T1 of the echo amplitudes from multiple spin-echo sequences with equidistant echoes: simulation studies. Magn Reson Imaging 11 (2):197-205.

83. Fritz V, Eisele S, Martirosian P, Machann J, Schick F (2024) A straightforward procedure to build a non-toxic relaxometry phantom with desired T1 and T2 times at 3T. Magma 37 (5):899-907.

84. Bloembergen N, Morgan LO (1961) Proton Relaxation Times in Paramagnetic Solutions. Effects of Electron Spin Relaxation. The Journal of Chemical Physics 34 (3):842-850.

85. Erdevig HE, Russek SE, Carnicka S, Stupic KF, Keenan KE (2017) Accuracy of magnetic resonance based susceptibility measurements. AIP Advances 7 (5).

86. Sękowska A, Majchrowicz D, Sabisz A et al. (2020) Nanodiamond phantoms mimicking human liver: perspective to calibration of T1 relaxation time in magnetic resonance imaging. Scientific Reports 10 (1):6446.

87. Fritz V, Schick F (2026) Recipe for Hydrogels With Tunable Relaxation and Diffusion Properties for Use as MRI Test Materials. Magn Reson Med 95 (3):1823-1832.

88. Deichmann R, Adolf H, Kuchenbrod E, Nöth U, Schwarzbauer C, Haase A (1995) Compensation of diffusion effects in T2 measurements. Magn Reson Med 33 (1):113-115.

89. Walker P, Lerski RA, Mathur-De Vré R, Binet J, Yane F (1988) Preparation of agarose gels as reference substances for NMR relaxation time measurement. EEC Concerted Action Program. Magn Reson Imaging 6 (2):215-222.

90. Kamba M, Meshitsuka S, Iriguchi N, Koda M, Kimura K, Ogawa T (2000) Measurement of relative fat content by proton magnetic resonance spectroscopy using a clinical imager. J Magn Reson Imaging 11 (3):330-335.

91. Delikatny EJ, Chawla S, Leung DJ, Poptani H (2011) MR-visible lipids and the tumor microenvironment. NMR Biomed 24 (6):592-611.

92. Machann J, Hasenbalg M, Dienes J et al. (2022) Short-Term Variability of Proton Density Fat Fraction in Pancreas and Liver Assessed by Multiecho Chemical-Shift Encoding-Based MRI at 3 T. J Magn Reson Imaging 56 (4):1018-1026.

93. Helenius J, Soinne L, Perkiö J et al. (2002) Diffusion-weighted MR imaging in normal human brains in various age groups. AJNR Am J Neuroradiol 23 (2):194-199.

94. Yoshikawa T, Kawamitsu H, Mitchell DG et al. (2006) ADC measurement of abdominal organs and lesions using parallel imaging technique. AJR Am J Roentgenol 187 (6):1521-1530.

95. Kim BR, Song JS, Choi EJ, Hwang SB, Hwang HP (2018) Diffusion-Weighted Imaging of Upper Abdominal Organs Acquired with Multiple B-Value Combinations: Value of Normalization Using Spleen as the Reference Organ. Korean J Radiol 19 (3):389-396.

96. Wagner F, Laun FB, Kuder TA et al. (2017) Temperature and concentration calibration of aqueous polyvinylpyrrolidone (PVP) solutions for isotropic diffusion MRI phantoms. PLOS ONE 12 (6):e0179276.

97. Sutherland E, Mercer SM, Everist M, Leaist DG (2009) Diffusion in Solutions of Micelles. What Does Dynamic Light Scattering Measure? Journal of Chemical & Engineering Data 54 (2):272-278.

98. Ivanović MT, Hermann MR, Wójcik M, Pérez J, Hub JS (2020) Small-Angle X-ray Scattering Curves of Detergent Micelles: Effects of Asymmetry, Shape Fluctuations, Disorder, and Atomic Details. The Journal of Physical Chemistry Letters 11 (3):945-951.

99. Sandle T (2019) Chapter 7 - Selection and Application of Culture Media. In: Sandle T (ed) Biocontamination Control for Pharmaceuticals and Healthcare. Academic Press, London, UK, pp 103-123.

100. Ma D, Gulani V, Seiberlich N et al. (2013) Magnetic resonance fingerprinting. Nature 495 (7440):187-192.

101. Sener RN (2001) Diffusion MRI: apparent diffusion coefficient (ADC) values in the normal brain and a classification of brain disorders based on ADC values. Comput Med Imaging Graph 25 (4):299-326.

# Appended Publications

## Publication 1

*Fritz, V., Martirosian, P., Machann, J., Daniels, R., Schick, F. (2022)*
*A comparison of emulsifiers for the formation of oil-in-water emulsions: stability of the emulsions within 9 h after production and MR signal properties.*
*Magnetic Resonance Materials in Physics, Biology and Medicine.*
*DOI: https://doi.org/10.1007/s10334-021-00970-9*

Magnetic Resonance Materials in Physics, Biology and Medicine
https://doi.org/10.1007/s10334-021-00970-9

RESEARCH ARTICLE

# A comparison of emulsifiers for the formation of oil-in-water emulsions: stability of the emulsions within 9 h after production and MR signal properties

Victor Fritz[1] · Petros Martirosian[1] · Jürgen Machann[1,2,3] · Rolf Daniels[4] · Fritz Schick[1,2]

Received: 24 June 2021 / Revised: 12 October 2021 / Accepted: 13 October 2021


## Abstract

**Objective** To provide a basis for the selection of suitable emulsifiers in oil-in-water emulsions used as tissue analogs for MRI experiments. Three different emulsifiers were investigated with regard to their ability to stabilize tissue-like oil-in-water emulsions. Furthermore, MR signal properties of the emulsifiers themselves and influences on relaxation times and ADC values of the aqueous phase were investigated.

**Materials and methods** Polysorbate 60, sodium dodecyl sulfate (SDS) and soy lecithin were used as emulsifiers. MR characteristics of emulsifiers were assessed in aqueous solutions and their function as a stabilizer was examined in oil-in-water emulsions of varying fat content (10, 20, 30, 40, 50%). Stability and homogeneity of the oil-in-water emulsions were evaluated with a delay of 3 h and 9 h after preparation using $T_1$ mapping and visual control. Signal properties of the emulsifiers were investigated by $^1$H-MRS in aqueous emulsifier solutions. Relaxometry and diffusion weighted MRI (DWI) were performed to investigate the effect of various emulsifier concentrations on relaxation times ($T_1$ and $T_2$) and ADC values of aqueous solutions.

**Results** Emulsions stabilized by polysorbate 60 or soy lecithin were stable and homogeneous across all tested fat fractions. In contrast, emulsions with SDS showed a significantly lower stability and homogeneity. Recorded $T_1$ maps revealed marked creaming of oil droplets in almost all of the emulsions with SDS. The spectral analysis showed several additional signals for polysorbate and SDS. However, lecithin remained invisible in $^1$H-MRS. Relaxometry and DWI revealed different influences of the emulsifiers on water: Polysorbate and SDS showed only minor effects on relaxation times and ADC values of aqueous solutions, whereas lecithin showed a strong decrease in both relaxation times ($r_{1,\text{lecithin}} = 0.11$ wt.%$^{-1}$ s$^{-1}$, $r_{2,\text{lecithin}} = 0.57$ wt.%$^{-1}$ s$^{-1}$) and ADC value ($\Delta(\text{ADC})_{\text{lecithin}} = -0.18 \times 10^{-3}$ mm$^2$/s·wt.%) with increasing concentration.

**Conclusion** Lecithin is suggested as the preferred emulsifier of oil-in-water emulsions in MRI as it shows a high stabilizing ability and remains invisible in MRI experiments. In addition, lecithin is suitable as an alternative means of adjusting relaxation times and ADC values of water.

**Keywords** Oil-in-water emulsions · Fat water MRI · Emulsifiers · Relaxometry · DWI

✉ Victor Fritz
victor.fritz@med.uni-tuebingen.de

1 Section on Experimental Radiology, Department of Diagnostic and Interventional Radiology, University of Tuebingen, Tuebingen, Germany

2 Institute for Diabetes Research and Metabolic Diseases of the Helmholtz Centre Munich at the University of Tuebingen, Tuebingen, Germany

3 German Center for Diabetes Research (DZD), Neuherberg, Germany

4 Institute of Pharmaceutical Technology, University of Tuebingen, Tuebingen, Germany

## Introduction

Magnetic resonance imaging (MRI) provides a powerful non-invasive tool that enables the quantitative determination of various tissue properties, such as fat content, relaxation times and diffusivity. In recent years, huge efforts have been made to develop and optimize new imaging techniques with high contrast between different types of tissue. Furthermore, there is a clear tendency to use MRI for quantitative tissue characterization. The results of MRI examinations regarding relaxation properties, fat content of tissues (especially liver and pancreas, but also musculature) should be as consistent

Published online: 26 October 2021

as possible in examinations on different MRI systems from different manufacturers. Only then are absolute values and results of follow-up examinations of patients on different MRI systems comparable. Reliable measurement phantoms are therefore indispensable for testing MRI equipment, and their composition and production have become an important area of research [1–4].

The main components of biological tissues are water and fat, which make emulsions particularly suitable for simulation of in vivo conditions. Emulsions are disperse systems consisting of at least two immiscible liquids, such as water and oil [5, 6]. They combine both, the properties of water and those of fat, and thus provide an excellent material for phantoms that simulate a variety of tissues in MRI, but also for studying changes in relaxation times and diffusivity of water and fat in the mixture.

Unfortunately, emulsions are thermodynamically unstable by nature. Due to the hydrophobic nature of lipids and the resulting high interfacial tension, emulsions are short-lived and tend to separate in a pure water and a pure oil phase immediately after preparation. To produce a stable or at least long-lived emulsion, a third component, namely an emulsifier, has to be added. Emulsifiers are surface active agents ("surfactants") that facilitate the formation of an emulsion and assist in their stabilization. This is due to their amphiphilic molecular structure. They consist of both, a hydrophilic head group and at least one non-hydrophilic hydrocarbon chain tail. Another fundamental characteristic of surfactants is the formation of aggregates, so-called micelles, in aqueous solution [7]. Micelles are complex structures that are formed due to the hydrophobic effect. Depending on the molecular structure of the emulsifier molecules, various shapes of micelles, such as spherical, cylindrical, bilayers, occur as depicted in Fig. 1.

A large number of surfactants (e.g., polysorbates, sodium dodecyl sulfate, soy lecithin) are utilized for industrial production of cosmetics, food, pharmaceuticals, and many other goods. Nevertheless, those substances are usually not present in human tissues and their MR signals might lead to undesired effects. Micellization of emulsifier molecules may influence the state of water and thus also MR parameters, such as relaxation times and diffusivity.

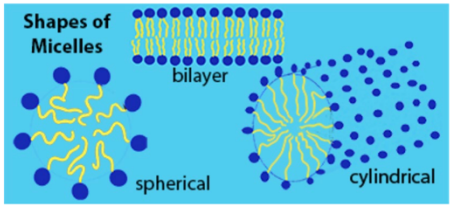


**Fig. 1** Schematic representation of different shapes of micelles in aqueous solutions (inspired by [7])

For a reliable simulation of tissue, it is essential that the emulsifiers used for stabilization have either none or precisely calculable effects on the MR measurements. Therefore, the influences that originate from the used emulsifiers should be well known prior to the measurements. Consequently, when selecting a suitable emulsifier, its MR signal properties and effects on MR properties of the solvent, e.g., relaxation times and diffusivity, should be taken into account.

Up till now, many MR scientists have already used oil-in-water (o/w) emulsions for validation and comparison of various water or fat MRI-based quantification methods [8–14], but also to study changes in the MR signal of water in the presence of fat and vice versa [15]. In MR technology, there are a number of different approaches for determining the fat content in tissue. In principle, a distinction is made between the very sensitive volume-selective $^{1}$H spectroscopy and imaging-based methods. Different sequences have been proposed and used as imaging techniques, mostly based on the different chemical shift of water and fat resonances. Currently, the so-called Dixon technique is mainly used to determine the fat content in tissue in clinical and experimental investigations. Different types of emulsifiers and thickeners have been used to stabilize the emulsions. However, to the best of our knowledge, the potential impact of surfactants on various MR parameters has not yet been systematically investigated.

The overall purpose of this work was to test common approaches and to derive a recommendation for the selection of a suitable emulsifier for use in MRI fat–water phantoms. For this, three different common emulsifiers were chosen and tested with regard to the following criteria: (1) Their ability to stabilize oil-in-water emulsions with the preparation method (ultrasound emulsification) presented in this study, (2) whether and which signal properties the emulsifiers show by themselves and (3) what influences they have on MR parameters, such as relaxation times and diffusivity of the aqueous phase. For these purposes, the emulsifiers were examined both as an additive in o/w emulsions and individually in aqueous solutions (without the presence of fat).

To assess the stabilizing ability of the emulsifiers, o/w emulsions of varying fat/water content (10/90, 20/80, 30/70, 40/60, 50/50%) were prepared and examined using $T_1$ mapping. Due to the different relaxation properties of water and fat, $T_1$ mapping provides a valuable tool for monitoring of phase separation or creaming occurring in emulsions. There are already some publications that have shown that MRI is a promising tool for assessing the stability and homogeneity of emulsions [16, 17].

For determination of signal properties of the emulsifiers, aqueous emulsifier solutions were investigated in proton-MR

spectroscopy ($^1$H-MRS) experiments. Effects of various emulsifier concentrations on relaxation times and apparent diffusion coefficient (ADC) values of aqueous emulsifier solutions were investigated by relaxometry ($T_1$ and $T_2$ mapping) and diffusion weighted MRI.

## Materials and methods

### Data acquisition and analysis

Imaging and spectroscopy were performed on a clinical-, whole-body 3.0 T MR system (MAGNETOM Prisma$^{fit}$, Siemens Healthineers, Erlangen, Germany) using a 20-channel head coil. All data were collected at room temperature (22 °C) and processed offline with MATLAB software (MathWorks, Natick, MA).

### Choice of emulsifiers

Polysorbate 60 (Kolliphor® PS 60, BASF, Ludwigshafen, Germany), sodium dodecyl sulfate (SDS, Carl Roth, Karlsruhe, Germany) and soy lecithin (Carl Roth, Karlsruhe, Germany) were used as emulsifiers and trialed individually. The cost of each emulsifier is around 20–30 euros per 250 g.

Polysorbate 60 is a non-ionic surfactant and emulsifier derived from polyethoxylated sorbitan and stearic acid (polyoxyethylene (20) sorbitan monostearate). Polysorbates are widely used as a solubilizer and emulsifier in pharmaceuticals and food. It shows excellent emulsifying properties and low toxicity.

Sodium dodecyl sulfate (SDS) is an anionic surfactant, consisting of a hydrocarbon chain with a sulfate anion at its end and a sodium cation ($C_{12}H_{25}NaO_4S$). SDS is mainly used in detergents and cosmetics.

Lecithins are phospholipids and form the group of emulsifiers most commonly used in the food industry. Lecithins are naturally occurring emulsifiers and the building block of biological membranes in animal and plant cells. They consist of fatty acids (two hydrocarbon chains), phosphoric acid, glycerol and choline.

### Preparation of oil-in-water emulsions

For testing the emulsifiers, oil-in-water emulsions of varying fat/water content (10/90, 20/80, 30/70, 40/60, 50/50%) were prepared in volumes of 50 ml. Emulsions without any additives were prepared additionally. Peanut oil was used as dispersed phase because of its nuclear magnetic resonance spectrum which is similar to that of triglycerides in human adipose tissues [18]. The aqueous phase was first prepared by completely dissolving the emulsifiers in distilled water. The weight fraction of the emulsifier was fixed at 10% with respect to the oil phase for each emulsion ($m_{emulsifier}/m_{oil} = 0.1$). To increase solubility, the aqueous phase was heated up to 30–40 °C using a water bath.

Coarse emulsions ("premixes") were prepared by adding the peanut oil into the aqueous phase under gentle stirring. These premixes were emulsified by ultra-sonication using UP200Ht with S26d14 sonotrode (Hielscher Ultrasonics, Teltow, Germany). Ultrasonic emulsification is very common, as it offers short preparation times, easy handling and resulting stable and fine emulsions [19]. The sonication time was 90–120 s with an output of 70 W. First, the premixes for each emulsifier and each fat fraction were prepared and then all samples were emulsified by ultra-sonication. The total preparation time for all 20 emulsions was approx. 4 h. All emulsions were stored in CELLSTAR polypropylene tubes (Greiner Bio-One, Frickenhausen, Germany) at room temperature until analysis. Figure 2 shows a photograph of the emulsions with a fat content of 30%.

### Stability analysis of emulsions

MR examinations were carried out approximately 3 h and 9 h after preparation of the emulsions. Since emulsions are hardly completely stable for several weeks or months, it was important for us to test the stability of the emulsions in the practical range of a few hours after production. The components water and oil show pronounced $T_1$ differences and thus the decomposition of the emulsion leads to a dispersion of measured $T_1$ values obtained by mono-exponential fitting along the gravity axis. Thus, spatially resolved $T_1$ mapping was applied for estimation of the temporal–spatial stability of the emulsions. The $T_1$ maps were calculated based on signal amplitudes from inversion recovery measurements by an IR-TSE sequence with seven different TIs ranging from 25 to 8000 ms. TR and TE were set to 10,000 ms and 9.9 ms, respectively. A three-parameter model was used for pixelwise mono-exponential fitting of the measured signal

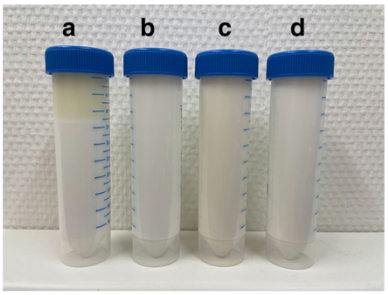


**Fig. 2** Photograph of emulsions with a fat content of 30% immediately after their preparation. Different emulsifiers were used for stabilization (**a**: no emulsifier, **b**: polysorbate 60, **c**: soy lecithin, **d**: SDS)

intensities. It should be mentioned that quantitative $T_1$ values obtained by mono-exponential fitting are neither correct for water nor for fat, but for the fat/water mixture. Resulting $T_1$ values were only used as sensitive markers to assess the stability of the emulsions. In addition to the MR examinations, all emulsions were visually controlled over a storage time of a maximum of 48 h.

### Spectroscopic characterization of the emulsifiers

To determine whether the emulsifiers themselves lead to detectable MR signals, an aqueous emulsifier solution (3 wt.%) of each emulsifier was spectrally analyzed. MR spectra were recorded using a Stimulated Echo Acquisition Mode (STEAM) sequence with TR of 10,000 ms and TE of 10 ms. For each spectrum, 8 acquisitions were taken from a $10 \times 10 \times 10$ mm cubic volume in the center of the sample. Reference spectra of distilled water and peanut oil were recorded to identify possible emulsifier signals in emulsions. Post-processing of spectra, such as apodization, and baseline and phase correction, were performed using jMRUI software (http://www.jmrui.eu) [20, 21].

### Influence of the emulsifier concentration on the relaxation times of the aqueous phase

Relaxometric measurements were performed to investigate whether and to what extent the presence of emulsifiers might modify the relaxation times of the aqueous phase. For this purpose, $T_1$ and $T_2$ mapping sequences were applied on aqueous emulsifier solutions of concentrations with 0, 1, 2, 3, 4, and 5 wt.% (without the presence of fat). The solutions were stored in CELLSTAR tubes and fixed in a cylindrical phantom as shown in Fig. 3a.

Quantitative $T_1$ mapping was performed using the same scanning protocol as for the stability analysis described above. Quantitative $T_2$ maps were acquired using a Carr-Purcell-Meiboom-Gill (CPMG) spin-echo pulse sequence with non-selective refocusing pulses. TR was 6000 ms and images with 32 different TEs ranging from 50 to 1600 ms (increment: 50 ms) were recorded. For $T_1$ and $T_2$ measurements, the selected slice orientation was coronal as shown in Fig. 3b, c.

$T_1$ and $T_2$ maps were calculated pixel by pixel and representative relaxation times for the solutions were determined from regions of interest (ROIs) within each sample. Following this, measured relaxation times ($T_1$, $T_2$) and relaxation rates ($R_1 = 1/T_1$, $R_2 = 1/T_2$) were plotted as a function of emulsifier concentration. From the slope of the straight line functions in these plots, relaxivities $r_1 = \Delta R_1$ and $r_2 = \Delta R_2$ were derived for each emulsifier.

### Influence of the emulsifier concentration on the diffusivity of the aqueous phase

Emulsifier effects on diffusivity of water were measured as a function of the emulsifier concentration. The same samples were used as for the relaxation time measurements.

Diffusion-weighted imaging (DWI) was performed using a readout-segmented echo planar imaging sequence in 3-scan-trace mode with monopolar diffusion gradients, four different b values (0, 50, 500, 1000), and coronal slice orientation. TR and TE were set to 5000 ms and 51 ms, respectively. For polysorbate and SDS, DWI data were acquired with an additional inversion recovery magnetization preparation ($TI_{poly} = 240$ ms, $TI_{SDS} = 300$ ms) to avoid interfering signal components caused by the emulsifiers. ADC maps were calculated from the acquisitions with multiple $b$ values using a log-linear fitting of the signal intensities. In analogy to the relaxation time measurements, ADC values were determined in a ROI within each sample and plotted as a function of the emulsifier concentration.

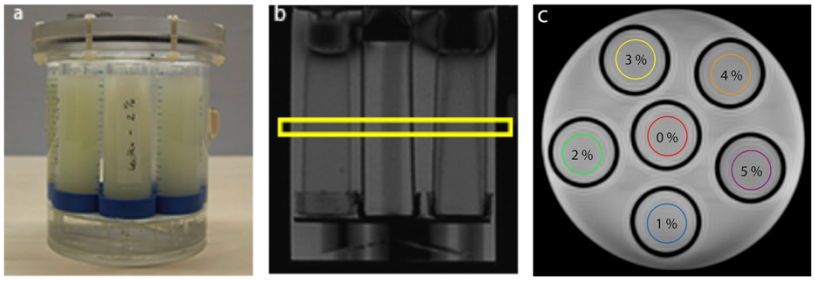


**Fig. 3** (**a**) Photograph of the cylindrical MR phantom with CELLSTAR tubes containing emulsifier solutions of varying concentrations. The surroundings of the tubes in the phantom were filled with water to reduce susceptibility effects at the walls of the tubes. (**b**) Localizer image with selected slice for $T_1$ and $T_2$ mapping. (**c**) Localizer image to illustrate the arrangement of the aqueous emulsifier solutions in the cylindrical MR phantom

## Results

### Stability analysis

$T_1$ mapping provided high sensitivity to segregation processes in the samples. Figure 4 displays the $T_1$ maps of the oil-in-water emulsions for the three emulsifiers, regarding samples with increasing fat content from top to bottom. Hardly any differences were found between a storage time of 3 h and a storage time of 9 h.

As expected, emulsions without any additives (column: A) did not mix and tended to separate into a pure water (higher $T_1$) and pure oil phase (lower $T_1$) immediately after preparation. Results could be used as a benchmark for a stability assessment of emulsions prepared with polysorbate 60, SDS and lecithin.

Emulsions prepared with Polysorbate 60 (column: B) and soy lecithin (column: C) show a spatially very homogeneous $T_1$ distributions over the entire samples, regardless of fat content and storage time. Thus, all emulsions stabilized by polysorbate or lecithin were stable and homogeneous, and none of those showed marked decomposition or creaming within the first 9 h. An interesting finding was a distinct difference between $T_1$ values of emulsions with the same composition of water and oil, but different emulsifiers: Emulsions with Polysorbate 60 (column: B) showed clearly longer $T_1$ values than those with soy lecithin (column: C).

In contrast to the successful stabilization of emulsions in columns B and C, emulsions using SDS as emulsifier (column: D) showed a significantly lower stability and homogeneity. With the exception of the sample with a fat content of 50%, emulsions with SDS had a separation into two distinct phases, indicated by areas with different $T_1$ in the map. The phase separation was caused by the gravitational creaming of oil droplets. This means that the oil droplets individually rose to the top of the containers (so-called "creaming"), which obviously results in two distinct phases, an upper oil-rich phase (lower $T_1$) and a lower water-rich phase (higher $T_1$) within the emulsions. However, a complete separation or a break into a pure water and pure oil phase, as in the case of the emulsions in column A, was not observed in any of the emulsions with SDS. Emulsions with a fat content of 50% were the most stable and homogeneous for SDS. No creaming was observed. But even those does not appear (by means of visual control) as homogeneous compared to those emulsions prepared with polysorbate or lecithin.

After a storage time of 48 h, at least a slight creaming was visible to the eye in almost all of the emulsions.

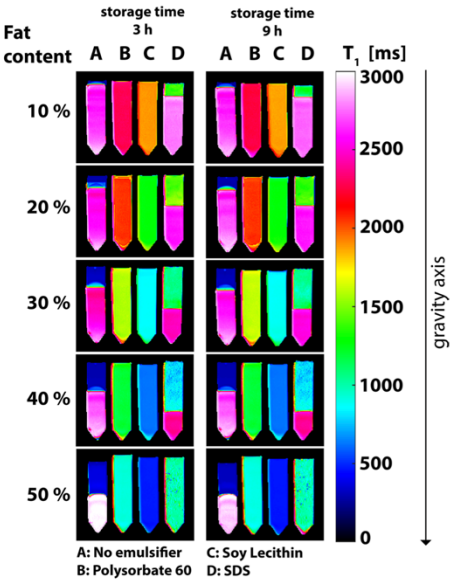


**Fig. 4** $T_1$ maps of oil-in-water emulsions with different emulsifiers (**A**: no emulsifier, **B**: polysorbate 60, **C**: soy lecithin, **D**: SDS) and with increasing fat content (from 10% to 50%) from top to bottom. Measurements were carried out after storage times of approx. 3 h and 9 h, respectively. The presented $T_1$ values were obtained by mono-exponential fitting and correspond to the $T_1$ values of the oil/water mixture

### Spectroscopic characterization of the emulsifiers

The results of the spectroscopic examinations of aqueous solution of the emulsifiers are presented in Fig. 5. Several signals (besides those of water and lipids) could be observed for polysorbate and SDS (indicated by arrows in Fig. 5b, c). Both show resonances at 1.3 ppm and 0.9 ppm. These signals can be assigned to methylene- $(-CH_2-)_n$ and terminal methyl protons $(-CH_3)$ and coincide with the signals of triglycerides in peanut oil (Fig. 5a).

Polysorbate leads to another dominant signal contribution at 3.7 ppm (Fig. 5b). For SDS, two further resonances of relatively low amplitudes were detected at 1.7 ppm and 4.2 ppm (Fig. 5c). For lecithin, no additional signals could be observed (Fig. 5d).

### Influence of the emulsifier concentration on the relaxation times of the aqueous phase

Measured relaxation times ($T_1$, $T_2$) and the relaxation rates ($R_1$, $R_2$) of aqueous solutions are presented in Fig. 6a-d as a function of the concentration for all three emulsifiers investigated. Depending on the type of emulsifier, different influences on the relaxation times and rates were identified.

Lecithin (blue data points) showed a strong decrease in $T_1$ and $T_2$ with increasing concentration. There was a linear relationship between the relaxation rates ($R_1$, $R_2$)

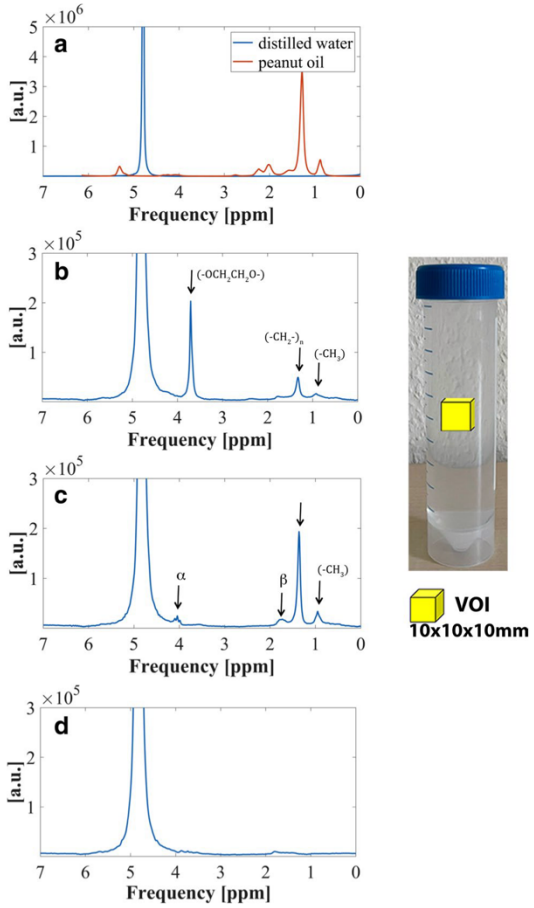


**Fig. 5** $^{1}$H-MR spectra of (**a**) peanut oil in red color and distilled water in blue color (**b**) aqueous solution of polysorbate (3 wt.%) (**c**) aqueous solution of SDS (3 wt.%) (d) aqueous solution of lecithin (3 wt.%). Arrows indicate resonances of emulsifiers. The Voxel of interest (VOI) was positioned in the center of the samples

and the concentration of dissolved lecithin. The longitudinal and transversal relaxivities were determined to be $r_{1lecithin} = 0.11$ wt.%$^{-1}$ s$^{-1}$ ($R^2 = 0.99$) and $r_{2lecithin} = 0.57$ wt.%$^{-1}$ s$^{-1}$ ($R^2 = 0.99$).

In contrast, polysorbate and SDS (green and red data points) only resulted in slight shortening of $T_1$ with increasing concentration. The longitudinal relaxivities were $r_{1polysorbate} = 0.01$ wt.%$^{-1}$ s$^{-1}$ ($R^2 = 0.97$) for polysorbate and $r_{1SDS} = 0.005$ wt.%$^{-1}$ s$^{-1}$ ($R^2 = 0.98$) for SDS. The transverse relaxation time did not show any clear dependence on the emulsifier concentration at all.

## Influence of the emulsifier concentration on the diffusivity of the aqueous phase

ADC maps of aqueous emulsifier solutions are shown in Fig. 7, with the arrangement of the sample tubes regarding their concentration depicted in Fig. 7f. ADC maps derived from original images recorded without an additional inversion pulse show chemical shift artifacts in solutions with polysorbate and SDS (arrows in Figs. 7a, b). These effects originate from relatively strong signals of these emulsifiers at 3.7 ppm in polysorbate and 1.3 ppm in SDS (see spectral analysis). No artifacts were present when using an adapted inversion recovery preparation for nulling the frequency shifted signal contributions (Figs. 7d, e).

For all aqueous solutions with emulsifiers, the ADC value of water decreased nearly linearly with increasing emulsifier concentration (Fig. 8), with the ADC reduction being most pronounced for lecithin [$\Delta(ADC)_{lecithin} = -0.18 \times 10^{-3}$ mm$^2$/s·wt.% ($R^2 = 0.95$)]. Significantly weaker effects on ADC values were found for polysorbate and SDS with $\Delta(ADC)_{polysorbate} = -0.035 \times 10^{-3}$ mm$^2$/s·wt.% ($R^2 = 0.94$) and $\Delta(ADC)_{SDS} = -0.02 \times 10^{-3}$ mm$^2$/s·wt.% ($R^2 = 0.99$), respectively.

## Discussion and conclusion

The presented work checked the suitability of three different emulsifiers for the production of emulsions for tissue-like and/or sequence calibration phantoms. The stabilizing ability of the emulsifiers was evaluated in emulsions with an oil content up to of 50%. Furthermore, influences of the emulsifiers on the spectrum of detectable MR signals and on relaxation and diffusion properties of water in which the emulsifiers are dissolved were investigated. Reproducibility was not tested systematically, but most phantom procedures were carried out several times with very similar results.

Stability of emulsions could be achieved using polysorbate 60 or soy lecithin as stabilizers. Both emulsifiers showed a high stabilizing ability with the ultrasound preparation method. No creaming was observed within the first 9 h. Emulsions with SDS were found to be the ones with the lowest stability in this study. Already after a storage time of 3 h, recorded $T_1$ maps (and visual inspection) revealed marked creaming of oil droplets in almost all of the emulsions with SDS. Since the rate of creaming is directly proportional to the square of the droplet size, it can be assumed that the droplet size achieved in the preparation process was significantly larger than that in emulsions stabilized by polysorbate or lecithin. Exact creaming rates can be determined by further measurements at earlier points in time, which was not done in our study. However, decomposition in our preparation scheme was much too fast for SDS. A

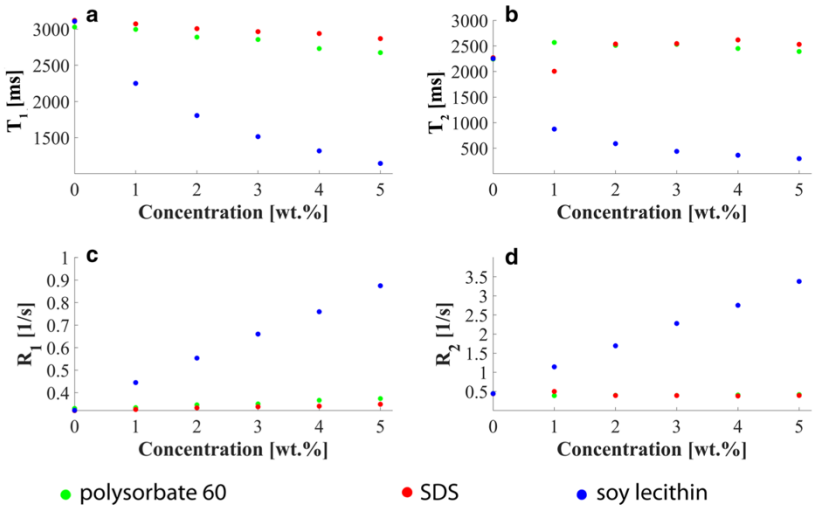


**Fig. 6** Dependence of relaxation properties on concentration of emulsifiers in distilled water: (**a**) $T_1$ relaxation times, (**b**) $T_2$ relaxation times (**c**) $R_1$ relaxation rates and (**d**) $R_2$ relaxation rates of aqueous solutions as a function of emulsifier concentration for polysorbate (green), SDS (red) and lecithin (blue)

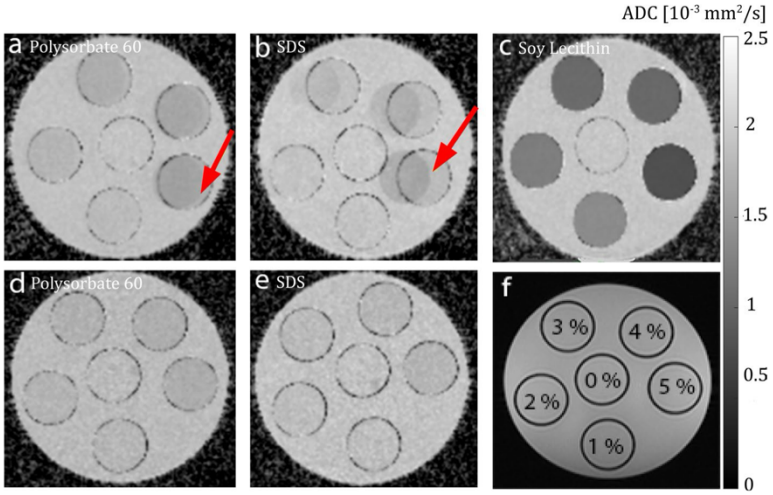


**Fig. 7** ADC maps of aqueous emulsifier solutions. The solutions were stored in CELLSTAR tubes and fixed in a cylindrical MR phantom. A central slice through the phantom is shown. (**a**–**c**) ADC maps obtained without additional inversion recovery preparation to suppress signal components caused by the emulsifiers (**a**: polysorbate, **b**: SDS, c: lecithin). Red arrows indicate chemical shift artifacts caused by the emulsifiers. (**d**–**e**) ADC maps acquired using an additional inversion recovery preparation for suppression of signal contributions from the emulsifiers themselves (**d**: polysorbate, **e**: SDS). (**f**) The arrangement of the samples with different emulsifier concentration in the MR phantom is depicted

reason for rapid decomposition seems to be the preparation process itself, since other research groups, for example, Bernard et al. [8], reported very stable fat–water phantoms using SDS. However, they added carrageenan as a gelling agent, which additionally increases the stability of the samples. Another reason could be the selection of the lipid phase. The mentioned group used soya oil instead of peanut oil, which has a different fatty acid composition and could lead to a modified effect of the emulsifier. For these reasons, SDS was included in the rest of the study.

Spectroscopic measurements of aqueous solutions with emulsifiers showed additional signals for polysorbate at 0.9 ppm, 1.3 ppm, and 3.7 ppm and for SDS at 0.9 ppm, 1.3 ppm, 1.7 ppm, and 4.2 ppm. Similar results were reported in previous spectrometer studies [22, 23]. Especially the resonances at 1.3 ppm and 0.9 ppm, which are

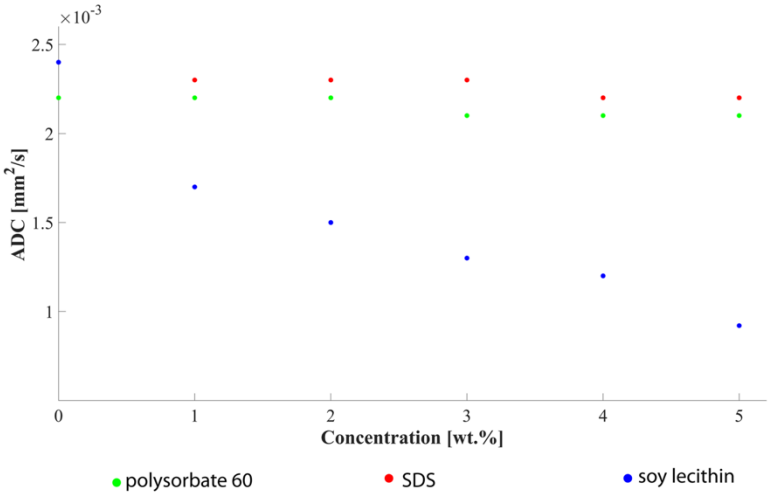


**Fig. 8** ADC values of water as a function of emulsifier concentration for polysorbate (green), SDS (red) and lecithin (blue)

usually seen in triglycerides, are considered to be critical with regard to fat quantification. Other resonances located at 3.7 ppm for polysorbate and at 1.7 ppm and 4.2 ppm for SDS do not coincide with relevant fat signals, but influences of these signals on quantitative MR imaging cannot be ruled out and require further investigations. Even though the molecular structure of lecithin suggests signals in the $^{1}$H-MR spectrum, lecithin remained invisible in our spectroscopic examinations with TE = 10 ms. Lecithins are phospholipids consisting of a hydrophilic head group and two hydrophobic hydrocarbon chains ($C_mH_n$). One possible explanation for MR invisibility is the micellar structure of lecithin: In aqueous solution, lecithin forms so-called bilayers (shown in Fig. 1), similar to those of phospholipids in the cell membranes of animal cells. Due to the restricted mobility within such bilayer structures, the lipids have a very short relaxation time ($T_2 \sim 10^{-2}$ ms) and are therefore invisible for $^{1}$H-MRS measurements with TE values in the range of a few milliseconds [24, 25].

Relaxometric measurements of the aqueous solutions revealed partly considerable effects of emulsifiers on relaxation properties of water. However, for polysorbate and SDS, influences on relaxation times $T_1$ and especially $T_2$ were only minor. In both cases, the addition of the emulsifier led to a slight decrease in $T_1$ for higher concentrations ($r_{1\text{polysorbate}} = 0.01$ wt.%$^{-1}$ s$^{-1}$, $r_{1\text{SDS}} = 0.005$ wt.%$^{-1}$ s$^{-1}$). A meaningful evaluation for transverse relaxivity $r_2$ was not possible for polysorbate and SDS, as neither a steady decrease nor a steady increase in $T_2$ was observed along the concentration axis. The samples with lecithin showed a completely different behavior: a comparatively strong decline in $T_1$ and $T_2$ was observed with increasing concentration, with relaxivities of $r_{1\text{lecithin}} = 0.11$ wt.%$^{-1}$ s$^{-1}$ and $r_{2\text{lecithin}} = 0.57$ wt.%$^{-1}$ s$^{-1}$. This interesting finding implies that lecithin might also provide an alternative agent for modification of relaxation times. Commonly, paramagnetic additives as Gd compounds or nickel or manganese ions, but also to some extend polysaccharides as agar or agarose are utilized as $T_2$ and $T_1$ modifiers [3, 26–28]. Unfortunately, these substances are partially toxic or require high temperature to be solved.

DWI experiments investigated potential restrictions of the mobility of water molecules by emulsifiers in aqueous solution. For all three emulsifiers, the ADC value of water in the solutions decreased with increasing concentration of the emulsifier. The probable cause for the decrease is the restriction of the water diffusivity by aggregates of emulsifier molecules. In aqueous solution, emulsifier molecules form their own organizational forms, the micelles, which represent barriers for the water molecules and restrict their mobility. With an increasing concentration of emulsifier molecules, the number of micelles and associated impairment of diffusivity increases. The greatest effect per amount of emulsifier was observed for lecithin with a decrease in the ADC value of $\Delta(\text{ADC})_{\text{lecithin}} = -0.18 \cdot 10^{-3}$ mm$^2$/s per percent emulsifier by weight. This distinct decrease in the measured ADC values and the fact that lecithin does not show any detectable signals in $^{1}$H spectra or artifacts in MR images makes this substance particularly interesting for the construction of novel DWI phantoms. Polysorbate and SDS, on the other hand, showed significantly less influence on water diffusion properties at the same concentrations. For the latter, chemical shift artifacts in the diffusion images and ADC maps proved to be disruptive. Obvious chemical shift artifacts can be traced back to the signal components of the emulsifiers and are therefore consistent with the results from the spectral analysis.

In conclusion, lecithin is suggested as the preferred emulsifier for use in MRI, especially when common ultrasound

emulsification is applied. Lecithin is non-hazardous, inexpensive and easy to handle. Use of lecithin as emulsifier not only provides a high stabilizing ability but also remains invisible in MRI experiments. The latter is of great importance when simulating MR properties of tissues by emulsions: additional signals are undesired and cause inaccuracies or even systematic errors in quantitative measurements. Besides its function as a stabilizer for o/w emulsions in fat–water phantoms, lecithin may provide an attractive agent for modifying $T_1$ and $T_2$ values or for adjusting diffusion properties. These features seem particularly interesting for matching relaxation times and/or ADC values to those of human tissues.

**Acknowledgements** This work was supported and funded by the German Research Foundation (DFG) under Grants SCHI 498/14-1 (Package No. 997/1).

**Author contributions** All authors contributed to the study conception and design. Material preparation, data collection and analysis were performed by [FV]. [MP] and [MJ] assisted with the MR measurements and analysis of data. [DR] provided laboratory materials and supported the planning and production of the emulsions. [SF] conceived and supervised the project. The first draft of the manuscript was written by [FV] in consultation with [SF]. All authors commented on previous versions of the manuscript and approved the final version for submission.

**Funding** Open Access funding enabled and organized by Projekt DEAL.



## References

1. Bush EC, Gifford A, Coolbaugh CL, Towse TF, Damon BM, Welch EB (2018) Fat-water phantoms for magnetic resonance imaging validation: a flexible and scalable protocol. J Vis Exp (139).
2. Gatidis S, Schmidt H, Martirosian P, Schwenzer NF (2014) Development of an MRI phantom for diffusion-weighted imaging with independent adjustment of apparent diffusion coefficient values and T2 relaxation times. Magn Reson Med 72(2):459–463
3. Kato H, Kuroda M, Yoshimura K, Yoshida A, Hanamoto K, Kawasaki S, Shibuya K, Kanazawa S (2005) Composition of MRI phantom equivalent to human tissues. Med Phys 32(10):3199–3208
4. Mobini N, Malekzadeh M, Haghighatkhah H, Saligheh Rad H (2020) A hybrid (iron-fat-water) phantom for liver iron overload quantification in the presence of contaminating fat using magnetic resonance imaging. MAGMA 33(3):385–392
5. Kutz G, Daniels R, Trommer H (2011) Emulsionen: entwicklung, herstellung. Editio Cantor Verlag
6. Tadros TF (2013) Emulsion formation and stability. Wiley-VCH
7. Israelachvili JN (2011) Intermolecular and surface forces, 3rd edn. Academic Press
8. Bernard CP, Liney GP, Manton DJ, Turnbull LW, Langton CM (2008) Comparison of fat quantification methods: a phantom study at 3.0T. J Magn Reson Imaging 27(1):192–197
9. Fukuzawa K, Hayashi T, Takahashi J, Yoshihara C, Tano M, Kotoku J, Saitoh S (2017) Evaluation of six-point modified dixon and magnetic resonance spectroscopy for fat quantification: a fat-water-iron phantom study. Radiol Phys Technol 10(3):349–358
10. Hayashi T, Fukuzawa K, Kondo H, Onodera H, Toyotaka S, Tojo R, Yano S, Tano M, Miyati T, Kotoku J, Okamoto T, Toyoda K, Oba H (2017) Influence of Gd-EOB-DTPA on proton density fat fraction using the six-echo Dixon method in 3 Tesla magnetic resonance imaging. Radiol Phys Technol 10(4):483–488
11. Hines CD, Yu H, Shimakawa A, McKenzie CA, Brittain JH, Reeder SB (2009) T1 independent, T2* corrected MRI with accurate spectral modeling for quantification of fat: validation in a fat-water-SPIO phantom. J Magn Reson Imaging 30(5):1215–1222
12. Leporq B, Lambert SA, Ronot M, Boucenna I, Colinart P, Cauchy F, Vilgrain V, Paradis V, Van Beers BE (2016) Hepatic fat fraction and visceral adipose tissue fatty acid composition in mice: quantification with 70T MRI. Magn Reson Med 76(2):510–518
13. Merritt S, Gulsen G, Chiou G, Chu Y, Deng C, Cerussi AE, Durkin AJ, Tromberg BJ, Nalcioglu O (2003) Comparison of water and lipid content measurements using diffuse optical spectroscopy and MRI in emulsion phantoms. Technol Cancer Res Treat 2(6):563–569
14. Poon CS, Szumowski J, Plewes DB, Ashby P, Henkelman RM (1989) Fat/water quantitation and differential relaxation time measurement using chemical shift imaging technique. Magn Reson Imaging 7(4):369–382
15. Hu HH, Nayak KS (2010) Change in the proton T1 of fat and water in mixture. Magn Reson Med 63(2):494–501
16. Onuki Y, Horita A, Kuribayashi H, Okuno Y, Obata Y, Takayama K (2014) Non-destructive monitoring of creaming of oil-in-water emulsion-based formulations using magnetic resonance imaging. Drug Dev Ind Pharm 40(7):937–943
17. Onuki Y, Kida C, Funatani C, Hayashi Y, Takayama K (2016) MRI as a promising tool for evaluation of the stability of cosmetic emulsions. Int J Cosmet Sci 38(3):272–278
18. Yu H, Shimakawa A, McKenzie CA, Brodsky E, Brittain JH, Reeder SB (2008) Multiecho water-fat separation and simultaneous R2* estimation with multifrequency fat spectrum modeling. Magn Reson Med 60(5):1122–1134
19. Abismail B, Canselier JP, Wilhelm AM, Delmas H, Gourdon C (1999) Emulsification by ultrasound: drop size distribution and stability. Ultra Sonochem 6(1):75–83
20. Naressi A, Couturier C, Devos JM, Janssen M, Mangeat C, de Beer R, Graveron-Demilly D (2001) Java-based graphical user interface for the MRUI quantitation package. MAGMA 12(2–3):141–152
21. Stefan D, Cesare FD, Andrasescu A, Popa E, Lazariev A, Vescovo E, Strbak O, Williams S, Starcuk Z, Cabanas M, van Ormondt D, Graveron-Demilly D (2009) Quantitation of magnetic resonance spectroscopy signals: the jMRUI software package. Measure Sci Technol 20(10):104035
22. Idiyatullin BZ, Potarikina KS, Zuev YF, Zueva OS, Usyarov OG (2013) Association of sodium dodecyl sulfate in aqueous solutions according to chemical shifts in 1H NMR spectra. Colloid J 75(5):532–537
23. Vu Dang H, Gray AI, Watson D, Bates CD, Scholes P, Eccleston GM (2006) Composition analysis of two batches of polysorbate 60 using MS and NMR techniques. J Pharm Biomed Anal 40(5):1155–1165

24. Delikatny EJ, Chawla S, Leung DJ, Poptani H (2011) MR-visible lipids and the tumor microenvironment. NMR Biomed 24(6):592–611
25. Hakumaki JM, Kauppinen RA (2000) 1H NMR visible lipids in the life and death of cells. Trends Biochem Sci 25(8):357–362
26. Christoffersson JO, Olsson LE, Sjöberg S (1991) Nickel-doped agarose gel phantoms in MR imaging. Acta Radiol 32(5):426–431
27. Hellerbach A, Schuster V, Jansen A, Sommer J (2013) MRI phantoms - are there alternatives to agar? PLoS ONE 8(8):e70343–e70343
28. Mitchell MD, Kundel HL, Axel L, Joseph PM (1986) Agarose as a tissue equivalent phantom material for NMR imaging. Magn Reson Imaging 4(3):263–266

# Publication 2

*Fritz, V., Martirosian, P., Machann, J., Thorwarth, D., Schick, F. (2023)*
*Soy lecithin: A beneficial substance for adjusting the ADC in aqueous solutions to the values of biological tissues.*
*Magnetic Resonance in Medicine.*
*DOI: https://doi.org/10.1002/mrm.29543*

Received: 29 July 2022 | Revised: 31 October 2022 | Accepted: 11 November 2022

DOI: 10.1002/mrm.29543

RESEARCH ARTICLE

Magnetic Resonance in Medicine

# Soy lecithin: A beneficial substance for adjusting the ADC in aqueous solutions to the values of biological tissues

**Victor Fritz**[1] | **Petros Martirosian**[1] | **Jürgen Machann**[1,2,3] | **Daniela Thorwarth**[4] | **Fritz Schick**[1,5]

[1]Section on Experimental Radiology, Department of Diagnostic and Interventional Radiology, University of Tübingen, Tübingen, Germany

[2]Institute for Diabetes Research and Metabolic Diseases of the Helmholtz Centre Munich at the University of Tübingen, Tübingen, Germany

[3]German Center for Diabetes Research (DZD), Neuherberg, Germany

[4]Section for Biomedical Physics, Department of Radiation Oncology, University of Tübingen, Tübingen, Germany

[5]Cluster of Excellence iFIT (EXC 2180) "Image Guided and Functionally Instructed Tumor Therapies", University of Tübingen, Tübingen, Germany

**Correspondence**
Victor Fritz, Section on Experimental Radiology, Department of Diagnostic and Interventional Radiology, University of Tübingen, Hoppe-Seyler-Str. 3, 72076 Tübingen, Germany.
Email: victor.fritz@med.uni-tuebingen.de

**Funding information**
German Research Foundation (DFG), Grant/Award Numbers: SCHI 498/14-1, TH 1528/6-1(PAK 997/1)

**Purpose:** To test soy lecithin as a substance added to water for the construction of MRI phantoms with tissue-like diffusion coefficients. The performance of soy lecithin was assessed for the useable range of adjustable ADC values, the degree of non-Gaussian diffusion, simultaneous effects on relaxation times, and spectral signal properties.

**Methods:** Aqueous soy lecithin solutions of different concentrations (0%, 0.5%, 1%, 2%, 3% …, 10%) and soy lecithin–agar gels were prepared and examined on a 3 Tesla clinical scanner at 18.5° ± 0.5°C. Echoplanar sequences ($b$ values: 0–1000/3000 s/mm$^2$) were applied for ADC measurements. Quantitative relaxometry and MRS were performed for assessment of $T_1$, $T_2$, and detectable spectral components.

**Results:** The presence of soy lecithin significantly restricts the diffusion of water molecules and mimics the nearly Gaussian nature of diffusion observed in tissue (for $b$ values <1000 s/mm$^2$). ADC values ranged from $2.02 \times 10^{-3}$ mm$^2$/s to $0.48 \times 10^{-3}$ mm$^2$/s and cover the entire physiological range reported on biological tissue. Measured $T_1/T_2$ values of pure lecithin solutions varied from 2685/2013 to 668/133 ms with increasing concentration. No characteristic signals of soy lecithin were observed in the MR spectrum. The addition of agar to the soy lecithin solutions allowed $T_2$ values to be well adjusted to typical values found in parenchymal tissue without affecting the soy lecithin–controlled ADC value.

**Conclusion:** Soy lecithin is a promising substance for the construction of diffusion phantoms with tissue-like ADC values. It provides several advantages over previously proposed substances, in particular a wide range of adjustable ADC values, the lack of additional $^1$H-signals, and the possibility to adjust ADC and $T_2$ values (by adding agar) almost independently of each other.

**KEYWORDS**
ADC, diffusion phantom, DWI, relaxometry, soy lecithin

## 1 | INTRODUCTION

The ADC of water molecules as determined by DWI plays a crucial role in the diagnosis and assessment of a variety of tissue disorders, including cerebral infarctions, malignant lesions, and tissue fibrosis.[1–3] In oncology, the ADC is considered a promising biomarker for monitoring treatment response. It has been shown that the ADC value increases with a decrease of tumor cell density caused by the application of radiation therapy.[4–10] For a reliable use of ADC values as biomarkers, it is essential that measurements of ADC values of tissues are accurate and as consistent as possible.

Because accuracy and precision of measured ADC values are difficult to verify in patients, the construction of phantoms containing materials with known reference values is of great value to check the performance of imaging techniques and MRI systems. At best, ADC values of test materials can be adjusted flexibly and cover the entire range of values found in biological tissue (~2–0.5 [$10^{-3}$ $mm^2/s$]). In addition to a wide range of adjustable ADC values, DWI phantoms should mimic other intrinsic tissue properties, such as $T_2$ relaxation times, but also limited diffusion kurtosis, as these properties have been shown to significantly affect the quantification of ADC values in biological tissue.[11,12] Although not explicitly stated as problematic in the literature, it is desirable that $T_1$ relaxation times of the DWI tissue-mimicking phantoms also reflect in vivo conditions.

Several DWI phantoms simulating predefined ADC values have already been presented.[13–17] They are mainly based on sucrose, polyethylene glycol, or polyvinylpyrrolidone, with the ADC value being controlled by the concentration of the solute or the measurement temperature. However, as already discussed in the literature,[15,17] all these substances bring with them different problems and disadvantages, such as a limited range of ADC values, strong reduction in $T_2$ relaxation time, and/or additional MR signal components with multiple spectral peaks. In addition, a relatively large amount of the respective substance is often required to significantly reduce the ADC of the solvent.

For this reason, we searched for a substance that solves the aforementioned problems with the materials proposed thus far for diffusion phantoms: in short, the ADC-modifying substance should essentially fulfill 4 criteria: (1) coverage of the full range of ADC values found in biological tissue, (2) mimicking the approximate Gaussian nature of water diffusion in tissue for $b$ values <1000 $s/mm^2$, (3) a relatively small effect on the $T_2$ relaxation time so that the ADC and $T_2$ values can be adjusted independently by adding a $T_2$ modifier, and (4) a $^1H$ spectrum without undesired lines from the added substance because interfering signals can lead to artifacts and inaccuracies in quantitative measurements. As mentioned above, it is also desirable that the $T_1$ relaxation times are within the range of values found in biological tissue.

Recently, soy lecithin, a naturally occurring emulsifier that is mainly used in the food industry, has been identified as an attractive agent for the preparation of tissue-like MRI fat–water phantoms.[18,19] In former experiments, it was found that dissolving small quantities of soy lecithin in aqueous solution does not lead to visible signals in spectra with a relatively short TE of 10 ms.[18]

Soy lecithin molecules are a class of phospholipids that, due to their amphiphilic nature, form self-assembled aggregates, so-called micelles, in aqueous solution. Depending on the concentration, temperature, and ionic environment, different shapes of aggregates such as bilayers or liposomes can form (Figure 1).[20,21] These molecular constructs are well suited to act as barriers and impede diffusion of water protons, analogous to cellular structures in biological tissues. With this background, soy lecithin seems to be a promising inexpensive (20–30 euros per 250 grams) substance for use in diffusion MRI phantoms that might meet the criteria mentioned above.

The aim of this work was to systematically investigate the MR-related properties of aqueous solutions with soy lecithin. The effects on the ADC and on the relaxation times ($T_1$ and $T_2$) of water were systematically investigated using different concentrations (0%–10%) of soy lecithin. The grade of non-Gaussian diffusion was determined using diffusion kurtosis imaging. To see if soy lecithin remains "MR invisible" at higher concentrations or leads to detectable additional spectral signals at proton resonance frequencies, the highest concentrated solution (10%) was also examined by $^1H$ MRS. In addition, signals of a 10% soy lecithin solution in deuterium oxide ($D_2O$) and pure $D_2O$ were recorded and compared using a gradient echo sequence with short TE in order to exclude possible signal contributions from soy lecithin at the water resonance frequency. Series of measurements tested whether $T_2$ of the aqueous soy lecithin solutions can be controlled independently of the ADC value by adding agar as a $T_2$ modifier.

## 2 | METHODS

### 2.1 | Sample preparation and measurement setup

Twelve tubes with aqueous solutions of soy lecithin (Carl Roth, Karlsruhe, Germany) were prepared in volumes of 50 mL. The concentration of dissolved soy lecithin varied from 0% to a maximum of 10% (0%, 0.5%, 1%, 2%, 3% …,

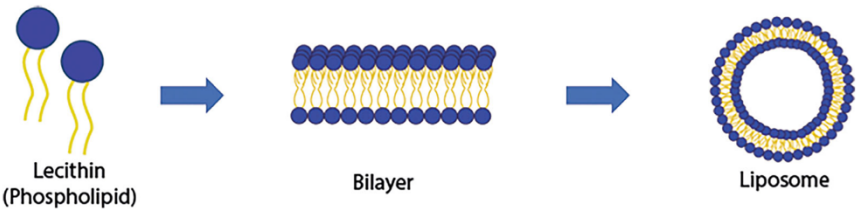


**FIGURE 1** Schematic representation of micellization of lecithin molecules in aqueous solution. Depending on concentration, temperature, and ionic environment, different types of aggregates form (e.g., bilayer, liposomes)[20,21]

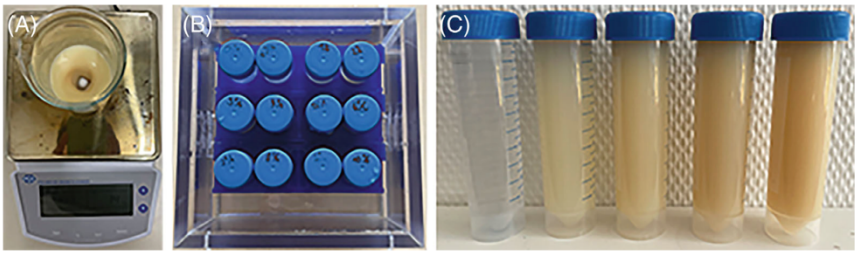


**FIGURE 2** Sample photos of (A) the preparation process of the aqueous soy lecithin solutions. The solutions were prepared by dissolving soy lecithin in distilled water using a 125 mL glass beaker and magnetic stirring. (B) The MRI phantom with 12 CELLSTAR tubes (Greiner Bio-One, Frickenhausen, Germany) containing aqueous soy lecithin solutions of different concentrations. The surroundings of the tubes were filled with water to reduce susceptibility effects at the wall of the tubes. (C) Soy lecithin solutions with different concentrations (from left to right: 0%, 2%, 4%, 6%, 8%)

10%) with respect to the solvent. The solutions were prepared by dissolving soy lecithin in distilled water using a 125 mL glass beaker and magnetic stirring (PCE-MSR 300, PCE Instruments, Meschede, Germany) at 650 revolutions per minute for 20 min at room temperature (Figure 2A). All samples were prepared under the same conditions.

Furthermore, a series of soy lecithin–agar gels was prepared to investigate whether $T_2$ of the aqueous soy lecithin solutions can be controlled independently of the ADC value by the addition of agar. The effects of adding agar on ADC and $T_1$ values of the aqueous soy lecithin solutions were also monitored. For this purpose, the concentration of agar was varied (1%, 2%, 3%, 4%), whereas the concentration of soy lecithin was kept constant. Series of measurements were performed for 3 different fixed concentrations of soy lecithin of 2%, 4%, and 6%. Because agar requires high temperature to be solved, the soy lecithin and agar portions were first dissolved separately and then mixed. The aqueous soy lecithin solutions were prepared as described above. The agar solution was prepared by completely dissolving the appropriate amount of agar (Agar powdered, AppliChem Panreac, Darmstadt, Germany) in distilled water using a microwave heater. The agar solution was then cooled, and once the temperature of the solution dropped below 70°C, the aqueous soy lecithin solution was added with gentle stirring to obtain a homogeneous mixture.

After preparation, all samples were stored in sterilized CELLSTAR polypropylene tubes (Greiner Bio-One, Frickenhausen, Germany) and fixed in a square MRI phantom for measurement (Figure 2B,C). The surroundings of the tubes were filled with water in order to reduce susceptibility effects at the wall of the tubes.

To avoid temperature bias, all samples were stored overnight in the scanner room prior to measurements to ensure all samples were at the same measurement temperature. The temperature was measured with an alcohol thermometer in the water around the tubes before each measurement ($18.5 \pm 0.5$°C).

## 2.2 | Data acquisition and analysis

Imaging and spectroscopy were performed on a clinical, whole-body 3.0 Tesla MR system (Magnetom Prisma$^{fit}$, Siemens Healthcare, Erlangen, Germany) using an 18-channel body array coil. All measurements were performed 3 times, and all data were processed offline using in-house developed software (MatLab R2020b, MathWorks, Natick, MA).

DWI was performed using a readout-segmented spin-echo EPI sequence with a pair of monopolar diffusion sensitizing gradients and 4 different $b$ values (0, 50, 500, 1000 s/mm$^2$). TR and TE were set to 5000 and 48 ms, respectively. Other parameters include FOV = 200 × 200 mm, matrix size = 128 × 128, slice thickness = 5 mm, number of slices = 10, slice in coronal plane, bandwidth = 751 Hz/px, GRAPPA factor = 2, fat suppression = fat sat. standard, number of readout segments = 7, $\delta$ = 6.9 ms, and $\Delta$ = 21.7 ms. Noise-corrected ADC maps were calculated from the acquisitions with multiple $b$ values using a log-linear fitting of the signal intensities: $\ln(S/S_0) = -ADC \cdot b + c$.

Diffusion kurtosis imaging was performed using the same DWI sequence type as described above. In contrast to the former measurements, 8 $b$ values 0, 50, 500, 1000, 1500, 2000, 2500, 3000 s/mm$^2$ were chosen, and the following modified parameters were applied: TE = 56 ms, $\delta$ = 10.9 ms, and $\Delta$ = 25.7 ms. The natural logarithm of the signal intensities ($S/S_0$) was plotted as a function of $b$ value and compared with a linear signal decay observed with free or Gaussian diffusion in pure liquids. The mean kurtosis value $K$ was calculated in each solution by pixel-wise fitting the signal intensities as a function of $b$ value using the following diffusion kurtosis model: $\ln(S/S_0) = -\mathrm{ADC} \cdot b + b^2 \cdot \mathrm{ADC}^2 \cdot K/6 + c$. All 8 $b$ values were used for the fitting procedure.

Measurements of $T_1$ were performed using a turbo spin-echo-based inversion-recovery pulse sequence with 9 different logarithmically equally spaced TIs (25–6400 ms). TR and TE were set to 10,000 ms and 9.9 ms, respectively. One slice was recorded in the coronal plane, which was positioned at the center of the samples. $T_1$ maps were calculated using a 3-parameter model for pixelwise mono-exponential fitting of the measured signal intensities: $S = S_0 \cdot [1 - a \cdot \exp(-T_I/T_1) + \exp(-TR/T_1)]$.

Relaxation times $T_2$ were assessed in the same slice using a Carr-Purcell-Meiboom-Gill spin-echo pulse sequence with a TR of 6000 ms and 32 TE values ranging from 50 ms to 1600 ms (increment 50 ms). Because the addition of agar leads to a strong reduction in the $T_2$ values, the measurement for the soy lecithin–agar gels was carried out with shorter TEs in the range of 10–320 ms (incr. 10 ms). $T_2$ maps were calculated by pixel-wise monoexponential fitting of the measured signal intensities using a 3-parameter model: $S = S_0 \cdot \exp(-TE/T_2) + c$. All signal values were noise-corrected before being used for the fit procedure in the specified model.

ADC, $T_1$, and $T_2$ values of each sample were determined from circular regions of interest in the calculated parametric maps. The mean and SD were determined from all measurements.

Single voxel STEAM spectra were recorded with short TE from the highest concentrated soy lecithin solution (10% in water) to check whether signals from $^1$H atoms in soy lecithin appear in the spectra, which could lead to unwanted interference in MRI experiments. Parameters for measuring a cubic volume of interest (10 × 10 × 10 mm) positioned in the center of the sample were TR 5000 ms, TE = 20 ms, bandwidth 1200 Hz, 16 acquisitions. In order to investigate possible signal contributions from soy lecithin at the water resonance frequency, signals of a 10% soy lecithin solution in $D_2O$ and pure $D_2O$ were recorded and compared using a gradient echo sequence with TE = 3 ms.

## 3 | RESULTS

DW images ($b$ = 0 s/mm$^2$, $b$ = 1000 s/mm$^2$), ADC, and relaxation time maps of the vials filled with aqueous soy lecithin solutions of different concentrations are shown in Figure 3A–3E. The vials were arranged as shown in Figure 3F. The parametric maps reveal a clear dependence of the ADC value and relaxation times on the concentration of dissolved soy lecithin in water. Chemical shift artifacts could not be observed in either the ADC or the $T_1$ and $T_2$ maps.

Table 1 summarizes the mean ADC, $T_1$, and $T_2$ values as a function of the concentration of dissolved soy lecithin. Both the ADC value and relaxation times show a decrease with increasing concentration of soy lecithin.

Even small amounts of soy lecithin considerably restrict the diffusion of the water protons (reduction of 20% at a concentration of 0.5%). The determined ADC values ranged from $2.02 \times 10^{-3}$ mm$^2$/s for pure water to $0.48 \times 10^{-3}$ mm$^2$/s for the sample with the highest concentration of dissolved soy lecithin (10%). It is striking that the ADC value and the concentration of soy lecithin show a nonlinear relationship. The change in ADC value as a function of soy lecithin concentration slightly decreases at higher concentrations (Figure 4).

Figure 5A shows the signal decay as a function of $b$ value for a 5% soy lecithin solution. The dashed–dotted line represents a linear signal decay, which is expected for free or Gaussian water proton diffusion observed in pure liquids without barriers. It is obvious that the signal decay originating from the aqueous soy lecithin solutions at high $b$ values deviates significantly from the expected values of Gaussian diffusion, indicating non-Gaussian diffusion in the aqueous soy lecithin solution. An increase of soy lecithin concentration was associated with an increase in the mean kurtosis value $K$ (Figure 5B). Values ranged from 0 for pure water to ~0.5 for the highest concentrated soy lecithin solution.

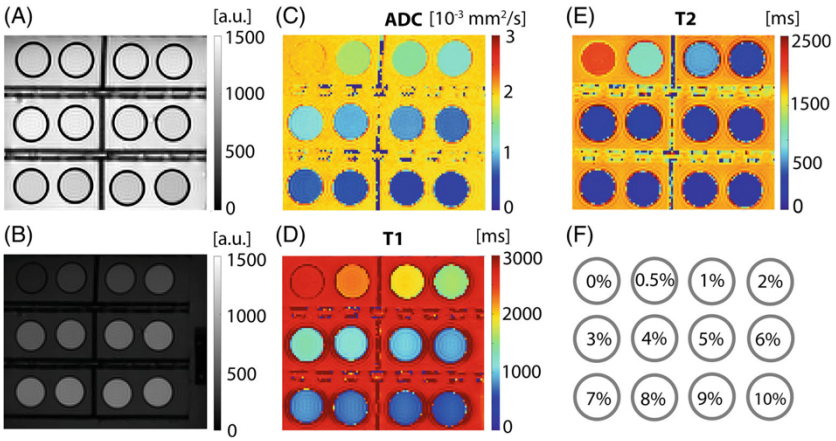


**FIGURE 3** Images and parametric maps of the aqueous soy lecithin solutions of different concentrations in an MRI phantom. (A) DW image with $b = 0$ s/mm$^2$. (B) DW image with b = 1000 s/mm$^2$. (C) Parametric map of ADC values. (D) Parametric map of $T_1$ values. (E) Parametric map of $T_2$ values. (F) Illustration of the positions of the aqueous soy lecithin solutions with different concentrations in the phantom

**TABLE 1** ADC, $T_1$, and $T_2$ values of aqueous soy lecithin solutions as a function of soy lecithin concentration.

| Concentration (%) | ADC ($10^{-3}$ mm$^2$/s) | $T_1$ (ms) | $T_2$ (ms) |
|---|---|---|---|
| 0 | 2.02 ± 0.02 | 2685 ± 67 | 2013 ± 41 |
| 0.5 | 1.59 ± 0.02 | 2286 ± 70 | 1089 ± 28 |
| 1 | 1.42 ± 0.02 | 1993 ± 65 | 792 ± 37 |
| 2 | 1.22 ± 0.01 | 1618 ± 48 | 506 ± 34 |
| 3 | 1.08 ± 0.01 | 1359 ± 35 | 375 ± 23 |
| 4 | 0.94 ± 0.01 | 1170 ± 23 | 293 ± 9 |
| 5 | 0.86 ± 0.01 | 1030 ± 18 | 242 ± 6 |
| 6 | 0.73 ± 0.02 | 929 ± 13 | 207 ± 5 |
| 7 | 0.68 ± 0.02 | 843 ± 8 | 183 ± 3 |
| 8 | 0.61 ± 0.02 | 778 ± 6 | 164 ± 2 |
| 9 | 0.52 ± 0.03 | 717 ± 4 | 148 ± 1 |
| 10 | 0.48 ± 0.02 | 668 ± 4 | 133 ± 2 |

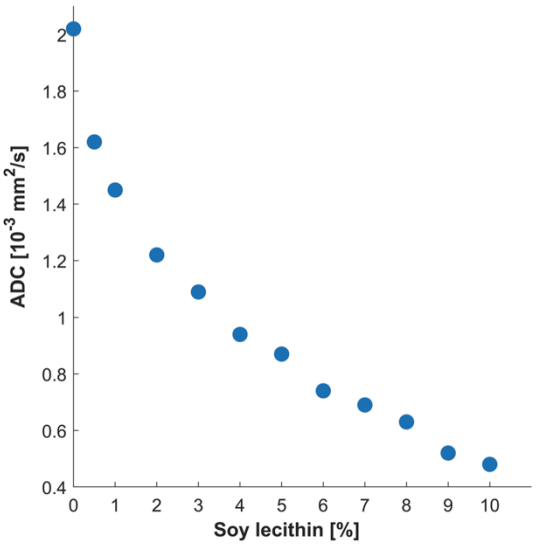


**FIGURE 4** ADC values of the aqueous soy lecithin solutions as a function of the soy lecithin concentration.

As mentioned above, changing the soy lecithin concentration not only influenced the ADC value but also the relaxation times of the aqueous solutions. Measured $T_1/T_2$ values ranged from 2685 ms/2013 ms for pure water to 668 ms/133 ms for the highest concentration of soy lecithin.

Figure 6 shows a representative $^1$H spectrum obtained from a highly concentrated (10%) aqueous soy lecithin solution, which was acquired to check for potential soy lecithin signals at higher concentrations. However, apart from the water signal at 4.75 ppm, no distinct signals could be detected in the STEAM spectrum recoded with TE = 20 ms. Only when zooming in closer, a small signal shoulder is guessed near the water signal, which, however, seems to be close to the noise level (red arrow in Figure 6).

This result agrees well with the fact that no chemical shift artifacts were observed in the ADC and relaxation time maps. Signal intensities recorded by gradient echo imaging from solutions of 10% soy lecithin dissolved in $D_2O$ confirmed the absence of direct signal contributions from soy lecithin, as signal intensities were not increased compared to results from pure $D_2O$ (99.9%).

Figure 7A–7C shows ADC and relaxation time maps of the soy lecithin–agar gels. Vials were arranged in the order of increasing agar concentrations (from left to right), whereas soy lecithin concentration increases from top to bottom (Figure 7D). The numbers in the parentheses indicate the soy lecithin or agar concentrations (soy

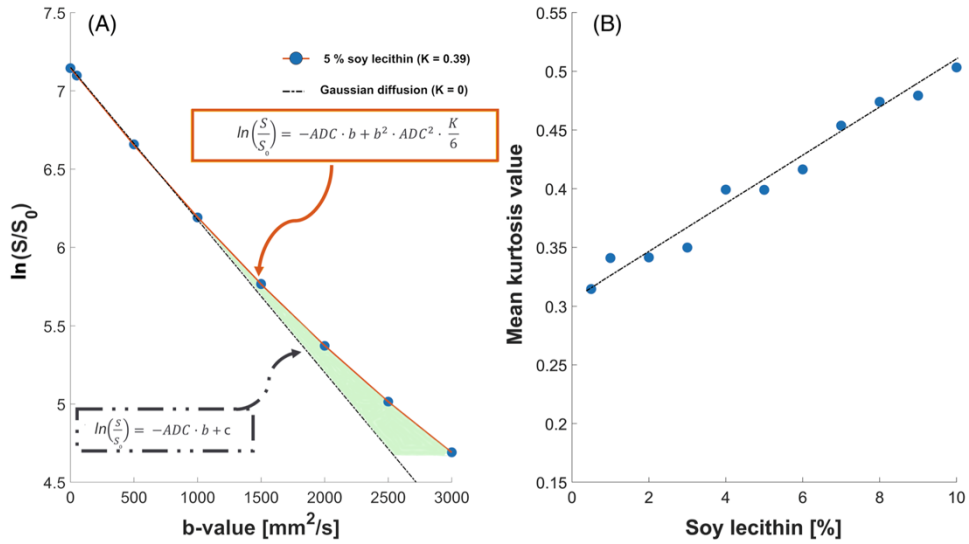


FIGURE 5 (A) Signal decay as a function of *b* value for a 5% soy lecithin solution. The dashed–dotted line represents the linear signal decay for free or Gaussian water proton diffusion observed in pure liquids without barriers. (B) Mean kurtosis value *K* of the aqueous soy lecithin solutions as a function of the soy lecithin concentration

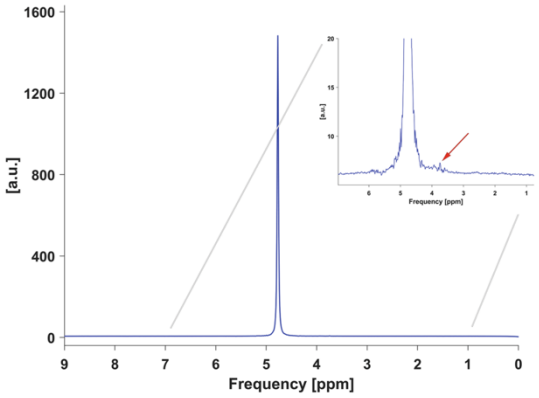


FIGURE 6 $^{1}$H spectrum obtained from a highly concentrated (10%) aqueous soy lecithin solution using single voxel STEAM spectroscopy with TE = 20 ms. Apart from the water signal at 4.75 ppm, no distinct signals could be detected. When zooming in closer, a small signal shoulder is guessed near the water signal, which, however, seems to be close to the noise level (red arrow)

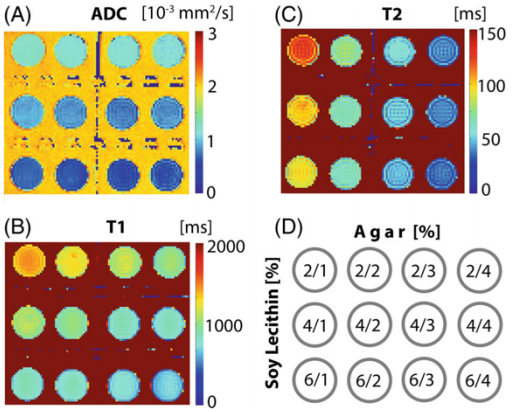


FIGURE 7 (A) Parametric map of measured ADC values as a function of agar or soy lecithin concentration. (B) Parametric map of measured $T_1$ values as a function of agar or soy lecithin concentration. (C) Parametric map of measured $T_2$ values as a function of agar or soy lecithin concentration. (D) Illustration of the positions of the soy lecithin–agar gels in the phantom. Vials were arranged in the order in which agar concentration increases from left to right and soy lecithin concentration increases from top to bottom. The numbers in the parentheses indicate the soy lecithin or agar concentration (soy lecithin/agar)

lecithin/agar). Table 2 summarizes the mean ADC, $T_1$, and $T_2$ values of the gels as a function of agar and soy lecithin concentration, respectively. The addition of agar to the aqueous soy lecithin solutions resulted in a strong decrease of the $T_2$ relaxation time (Figure 7C). The $T_2$ values of the aqueous soy lecithin solutions were reduced to a value of 38 ms by adding 4% of agar. On the other hand, the ADC value of the aqueous soy lecithin solutions was hardly affected with increasing agar concentration (Figure 7A). Comparing the $T_2$ and ADC values of the gels leads to the

**TABLE 2** ADC, $T_1$, and $T_2$ values of the soy lecithin–agar gels as a function of agar or soy lecithin concentration.

| Soy lecithin (%) | Agar (%) | | | |
|---|---|---|---|---|
| | 1 | 2 | 3 | 4 |
| 2 | | | | |
| ADC ($10^{-3}$ mm$^2$/s) | 1.24 ± 0.02 | 1.18 ± 0.03 | 1.17 ± 0.03 | 1.12 ± 0.04 |
| $T_1$ (ms) | 1456 ± 13 | 1283 ± 18 | 1165 ± 24 | 1057 ± 26 |
| $T_2$ (ms) | 125 ± 5 | 78 ± 4 | 57 ± 3 | 41 ± 4 |
| 4 | | | | |
| ADC ($10^{-3}$ mm$^2$/s) | 0.92 ± 0.03 | 0.85 ± 0.03 | 0.77 ± 0.04 | 0.83 ± 0.04 |
| $T_1$ (ms) | 1126 ± 18 | 1031 ± 10 | 881 ± 25 | 875 ± 14 |
| $T_2$ (ms) | 102 ± 3 | 66 ± 2 | 53 ± 5 | 41 ± 2 |
| 6 | | | | |
| ADC ($10^{-3}$ mm$^2$/s) | 0.71 ± 0.02 | 0.66 ± 0.04 | 0.59 ± 0.04 | 0.63 ± 0.05 |
| $T_1$ (ms) | 884 ± 14 | 877 ± 23 | 770 ± 23 | 718 ± 16 |
| $T_2$ (ms) | 96 ± 3 | 64 ± 4 | 49 ± 2 | 38 ± 2 |

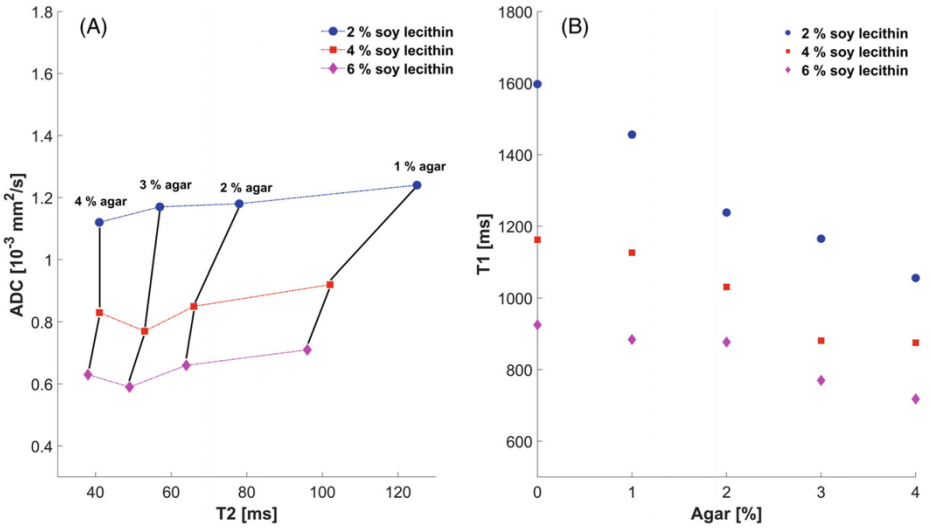


**FIGURE 8** (A) Variation of the ADC and $T_2$ values of the soy lecithin–agar gels depending on the agar and soy lecithin concentration. (B) $T_1$ values of the aqueous soy lecithin solutions are given as a function of agar concentration

conclusion that the $T_2$ value is mainly dependent on the amount of agar, whereas the ADC is mainly determined by the amount of soy lecithin (Figure 8A). With increasing concentration of agar, the influence of soy lecithin on $T_2$ becomes more and more negligible. In addition to reducing $T_2$, agar caused a slight decrease in $T_1$ of the gels with increasing concentration. On the other hand, the influence of agar on $T_1$ decreased with lecithin concentration (Figure 8B) (Table 2).

## 4 | DISCUSSION

Soy lecithin is a relatively cheap natural emulsifier that provides stable emulsions for MR experiments.[18] Because soy lecithin was found to significantly alter the ADC of water in aqueous solutions, the potential of soy lecithin to generate DWI phantoms with predefined tissue-like ADC values was evaluated in this work. To this end, series of systematic measurements were performed on aqueous soy

lecithin solutions and soy lecithin agar gels, investigating the influences on diffusion, relaxation times, and the signal components that occur.

With increasing concentration of soy lecithin in aqueous solution, the ADC value of water steadily decreased. The ADC values achieved were between $2.02 \times 10^{-3}$ mm$^2$/s and $0.48 \times 10^{-3}$ mm$^2$/s and thus cover a large range of values that includes the ADCs of most biological tissues and malignant lesions (e.g., liver, prostate, spleen, pancreas, gray and white matter).[22–24] However, it was found that the ADC decrease was not linear with soy lecithin concentration, which was also observed for polyethylene glycol.[15]

To the authors' knowledge, no substance has yet been described in the literature that influences the ADC value of water to a comparable extent as soy lecithin. Previously proposed substances such as sucrose, polyvinylpyrrolidone, or polyethylene glycol require 5 to 10 times the concentration to simulate the same range of ADC values. As reported in Wang et al.,[17] 40% sucrose is required to achieve an ADC value of $0.61 \times 10^{-3}$ mm$^2$/s, whereas only about 8% soy lecithin is required here. Soy lecithin thus enables flexible adjustment of the ADC value of water with low resource consumption. Diffusion kurtosis measurements revealed that the water diffusion within aqueous soy lecithin solutions (slightly) deviates from the Gaussian behavior ($K > 0$) at high $b$ values. This could be explained by the concentration dependent micellization of soy lecithin molecules. In aqueous solutions, amphiphilic substances such as soy lecithin form self-assembled aggregates that act as barriers and thus restrict the self-diffusion of water protons, similar to intrinsic microstructures (e.g., cell membranes) in biological tissues. As the concentration of soy lecithin increased, the number and possibly the geometry/size of aggregates changed, and with it the associated restriction of water proton diffusion. The mean kurtosis value ranged from 0 for pure water to ~0.5 for the solution with the highest concentration (10%). In the latter case, kurtosis was in the same order of magnitude as reported from biological tissue.[25,26] This finding suggests that soy lecithin in aqueous solution is a promising substance that could mimic not only ADC values but also—in contrast to sucrose—the restricted diffusion of water in biological tissues. However, the mechanism by which the aqueous soy lecithin solutions generates restricted diffusion appears to be clearly different from that of biological tissue (or tumors). In particular, the concentration-dependent micelle morphology (in terms of size and geometry) is considered critical, as diffusion changes in tumors are understood to be due to changes in cell density without changes in basic cell geometry. In addition, the micelles formed are usually mobile and few 100 nm in size,[27] whereas the cell membranes in the tissues are immobile and their size is in the order of several micrometers. Therefore, further work is needed to study micelle formation in more detail and to understand how well they actually can mimic tissue microstructure. It needs to be investigated whether and to what extent the morphology (size/geometry) of the micelles changes as a function of the soy lecithin concentration but also of the temperature. Furthermore, relative intra-liposome/extra-liposome water volumes might be a source of non-Gaussian diffusion. It is also not yet examined how the kurtosis effects in soy lecithin solution change using higher $b$ values and longer diffusion-sensitive time between dephasing and rephasing diffusion gradients (e.g., using stimulated echo sequences). In this context, another approach to mimic diffusion characteristics of tumor tissue should be mentioned, which was proposed by McHugh et al.[28] This group developed a biomimetic tumor tissue phantom using hollow polymer spheres with predefined sizes to mimic cells in tissues.

Like other ADC-modifying substances, soy lecithin causes a reduction in $T_1$ and $T_2$. The measurements indicated that the $T_1$ values of the aqueous solutions of soy lecithin were in the range of values that most biological tissues also exhibit (600–1800 ms).[29] Only solutions with low soy lecithin concentration (< 2%) presented $T_1$ values slightly above 1800 ms. However, these could be safely adjusted by adding $T_1$-active substances (e.g., gadolinium-diethylenetriamine pentaacetic acid or nickel chloride) to the soy lecithin solutions, but this was not pursued further in our experiments. Published studies have shown that the $T_1$ and $T_2$ values of aqueous solutions can be adjusted quite well independently by adding nickel chloride and agar as $T_1$ and $T_2$ modifiers, respectively.[30,31] However, possible interactions between nickel chloride and soy lecithin must then also be taken into account and investigated, which was not done in our study.

The $T_2$ values of the aqueous soy lecithin solutions ranged from 2013 to 133 ms, still well above the $T_2$ of almost all parenchymal tissues.[29] This seems to be another advantage of soy lecithin, as it offers the possibility to adjust the apparent diffusion coefficient and the $T_2$ relaxation time largely independently. As shown in this work, the ADC value can be controlled by the concentration of soy lecithin, whereas the $T_2$ values can be adjusted to the desired values by adding agar. The addition of agar to the aqueous soy lecithin solutions resulted in a large decrease in $T_2$ with no significant effect on ADC values and little effect on $T_1$. A similar approach was previously proposed by Gatidis et al.[15] This group used a mixture of polyethylene glycol (as ADC modifier) and gadobutrol (as $T_2$ modifier) to adjust ADC and $T_2$ values independently.

Another remarkable result of the present study is that soy lecithin, even at the highest concentration, did not

contribute any direct $^{1}H$ signal to the spectrum recorded at a (relatively) short TE of 20 ms. The lack of direct signals from soy lecithin was confirmed by gradient echo imaging of 10% soy lecithin dissolved in $D_2O$, where the signal intensity was equal to that of pure $D_2O$. One explanation could be that soy lecithin molecules, similar to phospholipids in the cell membranes of intact animal cells, have very limited mobility within the formed micelles, which in turn leads to an extremely short relaxation time ($T_2 < 1$ ms), making them undetectable in MRS or MRI measurements with TEs of a few milliseconds. This is particularly advantageous as solute signals could have undesirable effects and cause inaccuracies or even systematic errors in quantitative ADC measurements. For example, polyethylene glycol, which has a dominant signal at about 3.7 ppm, caused problems and distortions in the determination of the ADC value in polyethylene glycol-based DWI phantoms.[15]

However, there are also some potential limitations that should be mentioned. First, soy lecithin is a nature product; thus, unlike synthetic substances, the composition of soy lecithin may vary slightly in different product batches. This could make reproducibility difficult if different sources of soy lecithin are used. Second, because soy lecithin is an organic substance and the aqueous solutions may mold or rot after some time, a suitable fungicide and bactericide must probably be added to ensure the long-term stability of the phantoms. Third, the temperature dependence of the DW-MRI–derived parameters (ADC value, mean kurtosis) was not investigated. However, knowledge of temperature dependence is very important, especially when the phantom is used in multicenter studies in which temperature varies from site to site and over time. Therefore, temperature calibration curves as described by Wagner et al.[32] for polyvinylpyrrolidone phantoms are needed to make the application of soy lecithin–based diffusion phantoms practical. Furthermore, there might be a hysteresis effect due to a dependence of micelle composition on the temperature curve during phantom production, which has to be considered and further explored.

In summary, the systematic measurements carried out show that aqueous solutions of soy lecithin are a promising material for the construction of MRI diffusion phantoms with tissue-like diffusion coefficients. The use of soy lecithin fulfills the criteria mentioned at the beginning very well and offers several advantages over the substances used thus far. In addition, soy lecithin is nonhazardous, inexpensive, and easy to handle. However, there are still some problems regarding the influence of the manufacturing process and the durability but also the behavior when applying different DWI methods, which must be worked on and solved before using soy lecithin as a material for quantitative diffusion phantoms.

## ACKNOWLEDGMENT

This work was supported and funded by the German Research Foundation (DFG) under grants SCHI 498/14-1, TH 1528/6-1 (package no. 997/1). Open Access funding enabled and organized by Projekt DEAL.

## ORCID

*Victor Fritz* https://orcid.org/0000-0003-0601-9901
*Jürgen Machann* https://orcid.org/0000-0002-4458-5886

## REFERENCES

1. Fung SH, Roccatagliata L, Gonzalez RG, Schaefer PW. MR diffusion imaging in ischemic stroke. *Neuroimaging Clin N Am*. 2011;21:345-377. xi, 377.
2. Malayeri AA, El Khouli RH, Zaheer A, et al. Principles and applications of diffusion-weighted imaging in cancer detection, staging, and treatment follow-up. *Radiographics*. 2011;31:1773-1791.
3. Taouli B, Chouli M, Martin AJ, Qayyum A, Coakley FV, Vilgrain V. Chronic hepatitis: role of diffusion-weighted imaging and diffusion tensor imaging for the diagnosis of liver fibrosis and inflammation. *J Magn Reson Imaging*. 2008;28:89-95.
4. Padhani AR, Liu G, Koh DM, et al. Diffusion-weighted magnetic resonance imaging as a cancer biomarker: consensus and recommendations. *Neoplasia*. 2009;11:102-125.
5. Park SY, Kim CK, Park BK, et al. Early changes in apparent diffusion coefficient from diffusion-weighted MR imaging during radiotherapy for prostate cancer. *Int J Radiat Oncol Biol Phys*. 2012;83:749-755.
6. Yang Y, Cao M, Sheng K, et al. Longitudinal diffusion MRI for treatment response assessment: preliminary experience using an MRI-guided tri-cobalt 60 radiotherapy system. *Med Phys*. 2016;43:1369-1373.
7. Mahmood F, Johannesen HH, Geertsen P, Hansen RH. Repeated diffusion MRI reveals earliest time point for stratification of radiotherapy response in brain metastases. *Phys Med Biol*. 2017;62:2990-3002.
8. van Houdt PJ, Yang Y, van der Heide UA. Quantitative magnetic resonance imaging for biological image-guided adaptive radiotherapy. *Front Oncol*. 2020;10:615643.
9. Patterson DM, Padhani AR, Collins DJ. Technology insight: water diffusion MRI—a potential new biomarker of response to cancer therapy. *Nat Clin Pract Oncol*. 2008;5:220-233.
10. Leibfarth S, Winter RM, Lyng H, Zips D, Thorwarth D. Potentials and challenges of diffusion-weighted magnetic resonance imaging in radiotherapy. *Clin Transl Radiat Oncol*. 2018;13:29-37.
11. Colagrande S, Belli G, Politi LS, Mannelli L, Pasquinelli F, Villari N. The influence of diffusion- and relaxation-related factors on signal intensity: an introductive guide to magnetic resonance diffusion-weighted imaging studies. *J Comput Assist Tomogr*. 2008;32:463-474.
12. Baltzer P, Mann RM, Iima M, et al. Diffusion-weighted imaging of the breast-a consensus and mission statement from the

EUSOBI international breast diffusion-weighted imaging working group. *Eur Radiol*. 2020;30:1436-1450.
13. Laubach HJ, Jakob PM, Loevblad KO, et al. A phantom for diffusion-weighted imaging of acute stroke. *J Magn Reson Imaging*. 1998;8:1349-1354.
14. Matsuya R, Kuroda M, Matsumoto Y, et al. A new phantom using polyethylene glycol as an apparent diffusion coefficient standard for MR imaging. *Int J Oncol*. 2009;35:893-900.
15. Gatidis S, Schmidt H, Martirosian P, Schwenzer NF. Development of an MRI phantom for diffusion-weighted imaging with independent adjustment of apparent diffusion coefficient values and T2 relaxation times. *Magn Reson Med*. 2014;72:459-463.
16. Lavdas I, Behan KC, Papadaki A, McRobbie DW, Aboagye EO. A phantom for diffusion-weighted MRI (DW-MRI). *J Magn Reson Imaging*. 2013;38:173-179.
17. Wang X, Reeder SB, Hernando D. An acetone-based phantom for quantitative diffusion MRI. *J Magn Reson Imaging*. 2017;46:1683-1692.
18. Fritz V, Martirosian P, Machann J, Daniels R, Schick F. A comparison of emulsifiers for the formation of oil-in-water emulsions: stability of the emulsions within 9 h after production and MR signal properties. *MAGMA*. 2022;35:401-410.
19. Machann J, Hasenbalg M, Dienes J, et al. Short-term variability of proton density fat fraction in pancreas and liver assessed by multiecho chemical-shift encoding-based MRI at 3T. *J Magn Reson Imaging*. 2022;56:1018-1026.
20. Israelachvili JN. *Intermolecular and Surface Forces*. Elsevier; 2011:676.
21. Tadros TF. Emulsion formation, stability, and rheology. In: Tadros TF, ed. *Emulsion Formation and Stability*. Wiley-VCH; 2013:1-75.
22. Kim BR, Song JS, Choi EJ, Hwang SB, Hwang HP. Diffusion-weighted imaging of upper abdominal organs acquired with multiple b-value combinations: value of normalization using spleen as the reference organ. *Korean J Radiol*. 2018;19:389-396.
23. Yoshikawa T, Kawamitsu H, Mitchell DG, et al. ADC measurement of abdominal organs and lesions using parallel imaging technique. *AJR Am J Roentgenol*. 2006;187:1521-1530.
24. Helenius J, Soinne L, Perkiö J, et al. Diffusion-weighted MR imaging in normal human brains in various age groups. *AJNR Am J Neuroradiol*. 2002;23:194-199.
25. Malyarenko DI, Swanson SD, Konar AS, et al. Multicenter repeatability study of a novel quantitative diffusion kurtosis imaging phantom. *Tomography*. 2019;5:36-43.
26. Portakal ZG, Shermer S, Jenkins C, et al. Design and characterization of tissue-mimicking gel phantoms for diffusion kurtosis imaging. *Med Phys*. 2018;45:2476-2485.
27. Mkam Tsengam IK, Omarova M, et al. Transformation of lipid vesicles into micelles by adding nonionic surfactants: elucidating the structural pathway and the intermediate structures. *J Phys Chem B*. 2022;126:2208-2216.
28. McHugh DJ, Zhou FL, Wimpenny I, et al. A biomimetic tumor tissue phantom for validating diffusion-weighted MRI measurements. *Magn Reson Med*. 2018;80:147-158.
29. Bojorquez JZ, Bricq S, Acquitter C, Brunotte F, Walker PM, Lalande A. What are normal relaxation times of tissues at 3 T? *Magn Reson Imaging*. 2017;35:69-80.
30. Tofts PS, Shuter B, Pope JM. Ni-DTPA doped agarose gel—a phantom material for Gd-DTPA enhancement measurements. *Magn Reson Imaging*. 1993;11:125-133.
31. Christoffersson JO, Olsson LE, Sjöberg S. Nickel-doped agarose gel phantoms in MR imaging. *Acta Radiol*. 1991;32:426-431.
32. Wagner F, Laun FB, Kuder TA, et al. Temperature and concentration calibration of aqueous polyvinylpyrrolidone (PVP) solutions for isotropic diffusion MRI phantoms. *PLoS One*. 2017;12:e0179276.

**How to cite this article:** Fritz V, Martirosian P, Machann J, Thorwarth D, Schick F. Soy lecithin: A beneficial substance for adjusting the ADC in aqueous solutions to the values of biological tissues. *Magn Reson Med*. 2022;1-10. doi: 10.1002/mrm.29543

# Publication 3

*Fritz, V., Eisele, S., Martirosian, P., Machann, J., Schick, F. (2024)*
*A straightforward procedure to build a non-toxic relaxometry phantom with desired T1 and T2 times at 3T.*
*Magnetic Resonance Materials in Physics, Biology and Medicine (MAGMA).*
*DOI: https://doi.org/10.1007/s10334-024-01166-7*

Magnetic Resonance Materials in Physics, Biology and Medicine
https://doi.org/10.1007/s10334-024-01166-7

RESEARCH ARTICLE

# A straightforward procedure to build a non-toxic relaxometry phantom with desired T1 and T2 times at 3T

Victor Fritz[1,2,3] · Sabine Eisele[1] · Petros Martirosian[1] · Jürgen Machann[1,2,3] · Fritz Schick[1]

Received: 2 November 2023 / Revised: 1 May 2024 / Accepted: 3 May 2024


## Abstract

**Objective** To prepare and analyze soy-lecithin-agar gels for non-toxic relaxometry phantoms with tissue-like relaxation times at 3T.

**Methods** Phantoms mimicking the relaxation times of various tissues (gray and white matter, kidney cortex and medulla, spleen, muscle, liver) were built and tested with a clinical 3T whole-body MR scanner. Simple equations were derived to calculate the appropriate concentrations of soy lecithin and agar in aqueous solutions to achieve the desired relaxation times. Phantoms were tested for correspondence between measurements and calculated T1 and T2 values, reproducibility, spatial homogeneity, and temporal stability. T1 and T2 mapping techniques and a 3D T1-weighted sequence with high spatial resolution were applied.

**Results** Except for the liver relaxation phantom, all phantoms were successfully and reproducibly produced. Good agreement was found between the targeted and measured relaxation times. The percentage deviations from the targeted relaxation times were less than 3% for T1 and less than 6.5% for T2. In addition, the phantoms were homogeneous and had little to no air bubbles. However, the phantoms were unstable over time: after a storage period of 4 weeks, mold growth and also changes in relaxation times were detected in almost all phantoms.

**Conclusion** Soy-lecithin-agar gels are a non-toxic material for the construction of relaxometry phantoms with tissue-like relaxation times. They are easy to prepare, inexpensive and allow independent adjustment of T1 and T2. However, there is still work to be done to improve the long-term stability of the phantoms.

**Keywords** MRI Phantom · Relaxometry · T1 · T2 · 3T · Soy Lecithin

## Introduction

Phantoms serve as substitutes for biological tissue and are indispensable tools in quantitative magnetic resonance imaging (qMRI) research. Gels with known (or even adjustable) tissue-like T1 and T2 relaxation properties are useful for research, especially for developing and testing new pulse sequences and post-processing techniques [1, 2] as human volunteers are not always available for long test sessions. Since medical device-grade phantoms with desired relaxation properties are not present at all research sites, a protocol for flexible, homemade phantoms could be very useful. Ideally, the materials used to make the phantoms should be inexpensive, non-toxic, and easy to work with.

In particular, relaxometry phantoms that mimic tissue-like relaxation times attract the interest of researchers. Relaxation times T1 and T2 are intrinsic tissue properties that depend on tissue composition and microenvironment [3]. Changes in native T1 and T2 values are known as sensitive indicators of various pathologies, including cancer, cardiovascular abnormalities, and brain diseases [4]. To verify accurate and precise T1 and T2 measurements with MRI equipment, the availability of suitable test objects with predefined values is essential.

✉ Victor Fritz
victor.fritz@med.uni-tuebingen.de

1 Section of Experimental Radiology, Department of Diagnostic and Interventional Radiology, University of Tübingen, Hoppe-Seyler-Str. 3, 72076 Tübingen, Germany

2 Institute for Diabetes Research and Metabolic Diseases of the Helmholtz Centre Munich at the University of Tübingen, Tübingen, Germany

3 German Center for Diabetes Research (DZD), Neuherberg, Germany

Published online: 11 May 2024

Interestingly, there are only few approaches to the fabrication of phantoms with tissue-like relaxation times T1 and T2. Relaxometry phantoms proposed so far are typically two-component mixtures consisting of a gelling agent (e.g. agarose, agar) doped with paramagnetic salt (e.g. $MnCl_2$, $NiCl_2$, $GdCl_3$) [5–16]. Here, the paramagnetic salt generally serves as a T1-modifier and the gelling agent as a T2-modifier. Knowing the relaxivities ($r_1$,$r_2$) of each component, one can design a phantom material that has the desired relaxation times. The required concentrations of the respective substances can be calculated according to the following formulas described by Tofts et al. [8, 9]:

$$C_a = \frac{R2 - R2_w - (r_2^{(b)}/r_1^{(b)})(R1 - R1_w)}{r_2^{(a)} - (r_2^{(b)}/r_1^{(b)})r_1^{(a)}} \quad (1)$$

$$C_b = \frac{R1 - R1_w - (r_1^{(a)}/r_2^{(a)})(R2 - R2_w)}{r_1^{(b)} - (r_1^{(a)}/r_2^{(a)})r_2^{(b)}} \quad (2)$$

where $C_a$ and $C_b$ are the concentrations of component a and b, $r_1^{(a,b)}$ and $r_2^{(a,b)}$ are the relaxivities of component a and b, $R1_w$ and $R2_w$ are the relaxation rates of pure water, and R1 and R2 are the relaxation rates to be achieved.

It has been shown that those phantoms can be reproducibly produced and exhibit high temporal stability [7–9]. However, paramagnetic salts are toxic, which complicates the production, handling and disposal of these phantoms. Furthermore, the presence of paramagnetic salts can strongly affect the magnetic susceptibility of the phantom material [17]. This could lead to adverse effects, especially for gradient echo sequences, as undesirable magnetic field inhomogeneities occur depending on the geometry and composition of the phantom. Therefore, research is underway to find alternative, non-hazardous substances that can replace paramagnetic salt as a T1 modifier and allow phantoms to be produced without safety and toxicity issues [18].

In this context, Sękowska et al. [19] presented MRI phantoms based on non-toxic detonation diamond nanoparticles (DND). The phantoms composed of agar, carageen, and DND particles suspended in dimethyl sulfoxide have been shown to successfully mimic the relaxation times of liver tissue. However, the data from the study suggests that phantoms with T1 values above 950 ms cannot be fabricated, at least not with the fabrication method presented—which is a disadvantage, as many tissues (e.g. gray matter, kidney, spleen, etc.) have T1 values in the range of 1000–2000 ms and therefore cannot be covered.

Another relatively new and promising approach is the use of soy lecithin in MRI phantoms. Soy lecithin is a naturally occurring emulsifier that has recently been found to alter the relaxation times and diffusion properties of water [20, 21]. In addition, soy lecithin is inexpensive, readily available and non-toxic, making it ideal for phantom manufacturing. Therefore, it is obvious to use and test soy lecithin for the preparation of relaxometry phantoms, which was also the motivation for this work.

In the present work, soy-lecithin-agar gels were prepared and evaluated as an alternative phantom material for the construction of relaxometry phantoms with tissue-like relaxation times. Special attention was paid to an understandable presentation of the phantoms' development and fabrication process. Test phantoms mimicking the relaxation times of different tissue types were evaluated for their correctness (agreement between measured and targeted values), reproducibility and temporal stability.

## Methods

### Study design

Before phantom fabrication can begin, relaxivities $r_1$ and $r_2$ of soy lecithin and agar have to be determined (see Eqs. 1 and 2). For this purpose, pure aqueous soy lecithin solutions and pure agar gels of different concentrations (0, 1, 2, 3, 4, 5%) were prepared and examined using T1- and T2 mapping techniques.

Furthermore, it has to be ensured that the two substances are compatible and retain their effect even when mixed. A change in relaxivity as a function of the concentration of the other substance would make it impossible to apply simple Eqs. (1, 2) for determination of concentrations and thus produce correct phantoms. At least, the T1 modifier should have stable longitudinal relaxivity $r_1$ and the T2 modifier should have stable transverse relaxivity $r_2$. To verify this, relaxivities of soy-lecithin were measured in the presence of different concentrations of agar (1%, 2%, 3%, 4%), while agar-relaxivities were measured in the presence of different concentrations of soy lecithin (1%, 2%, 3%, 4%).

After the preliminary experiments, test phantoms were designed to match the relaxation times T1/T2 of different tissues: grey matter (1820 ms/99 ms [3]), white matter (1084 ms/69 ms [3]), kidney cortex (1142 ms/76 ms [22]), kidney medulla (1545 ms/81 ms [22]), spleen (1328 ms/61 ms [22]), liver (812 ms/42 ms [3]), and muscle (1295 ms/34 ms [22]). Using the previously determined relaxivities and Eqs. 1 and 2, the appropriate concentrations of soy-lecithin and agar were calculated to achieve the desired T1 and T2 values. For the relaxation rates of pure water, the values $R1_w = 2950$ ms and $R2_w = 2000$ ms were used (determined by several preliminary measurements).

The phantoms were tested for correctness (agreement between measured and target values), reproducibility and

temporal stability. For this, all phantoms were prepared three times, independently on different days and examined on the day of preparation and 4 weeks after preparation. Possible mold growth was monitored by visual inspection of the samples during the 4-week study period. In addition, the samples were checked for homogeneity and the absence of air bubbles. Air bubbles are problematic because they cause magnetic field distortions that lead to susceptibility artifacts [15].

## Preparation of the phantoms

Phantoms were prepared as follows (Fig. 1): First, the appropriate amount of soy lecithin (Carl Roth, Karlsruhe, Germany) was dissolved in demineralized water (Carl Roth, Karlsruhe, Germany) under magnetic stirring at 650 rpm for 10 min. Agar (Agar powdered pure, food grade, PanReac-AppliChem-ITW Reagents, Darmstadt, Germany) was then stirred into the soy lecithin solution and the mixture was boiled using a microwave heater until the solution was clear and homogeneous. The solutions were then filled into sterilized polypropylene tubes (50 ml, Greiner Bio-One, Frickenhausen, Germany) and cooled to room temperature for gelation. High viscosity solutions were sonicated with an ultrasonic homogenizer (Hielscher Ultrasonics, Teltow, Germany) to remove air bubbles prior to solid gel formation. Pure aqueous soy lecithin solutions and agar gels of different concentrations (0, 1, 2, 3, 4, 5%) were prepared by the same procedure without addition of the other substance.

For the measurements, the samples were fixed in water-filled MR-compatible housings (Fig. 2a–b): The measurements to determine the individual relaxivities of soy lecithin and agar as well as for the final test phantoms were performed using a cylindrical housing that can hold up to 7 tubes. In contrast, due to the large number of samples, the compatibility measurements of soy lecithin and agar were carried out using a larger square housing that can hold up to 16 phantoms.

All phantoms were stored in the scanner room for at least 6 h before measurements to ensure that the temperature of the samples could stabilize and adapt to the ambient temperature. Between measurements, the samples were stored in the dark in a laboratory cabinet at a room temperature of approx. 21 °C.

## Data acquisition and analysis

Measurements were performed on a clinical 3.0 Tesla whole-body MR scanner (MAGNETOM Prisma$^{fit}$, Siemens Healthcare, Erlangen, Germany) with a 20-channel head coil at 21 °C ± 0.5 °C.

Relaxivity measurements of soy lecithin and agar in the mixture (compatibility measurements) were performed using an 18-channel body array coil, as the square housing containing all samples did not fit into the head coil. The corresponding measurement setups are shown in Fig. 2c–d. All data were processed and analyzed offline using in-house developed software (MATLAB, MathWorks, Natick, MA).

T1 and T2 measurements were performed with the following parameters: matrix = 128 × 128, FOV = 200 × 200 mm, slice thickness = 5 mm, number of slices = 1, slice in coronal plane, positioned in the center of the samples.

T1 was measured using a single slice inversion recovery turbo spin echo pulse sequence (IR-TSE) with TR of

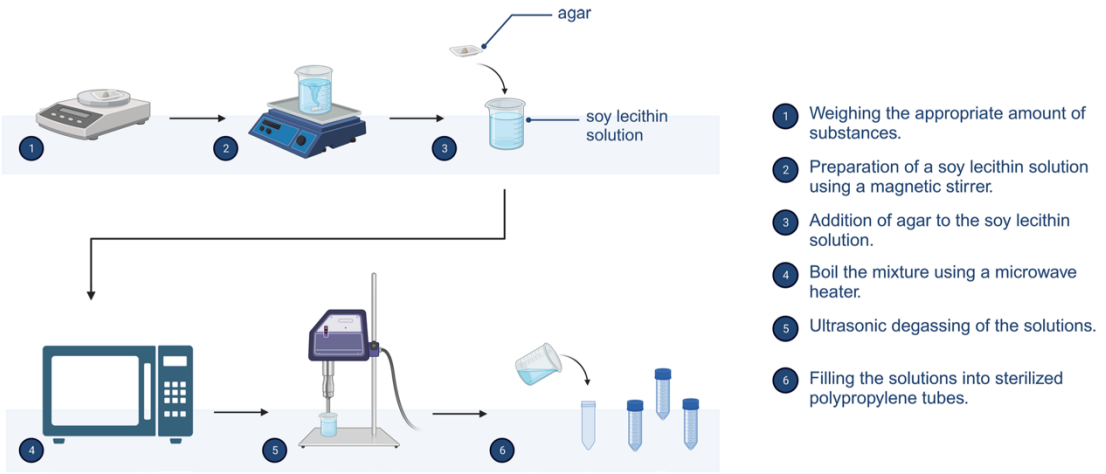


**Fig. 1** Schematic representation of the manufacturing process of the soy-lecithin-agar phantoms. Created with BioRender.com

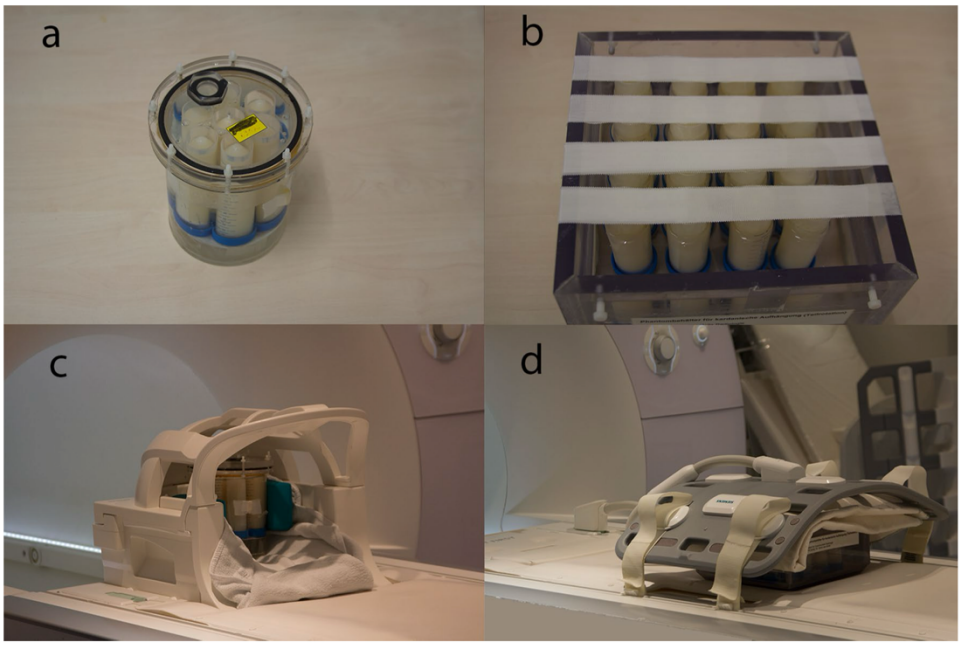


**Fig. 2** Photographs of the water-filled sample tube housings: **a** cylindrical housing with 7 sample tubes **b** larger square housing with 16 sample tubes. Photographs of the measurement setup on a clinical 3T whole-body MR scanner: **c** the cylindrical housing with 7 sample tubes was scanned using a 20-channel head coil **d** the square housing with 16 sample tubes was scanned using an 18-channel body array coil

10,000 ms and TE of 9.9 ms. Images were acquired for 9 different TIs in the range of 25–6400 ms (logarithmically equally spaced). T1 maps were calculated from the acquisitions with multiple TIs by pixel-wise monoexponential fitting of signal intensities (SI): $SI = SI_0\ (1–a\ exp(-TI/T1) + exp(-TR/T1))$ [23].

T2 was measured in the same slice using a multi-echo CPMG spin echo pulse sequence with a TR of 6000 ms and 32 TEs ranging from 10 to 320 ms (equally spaced). Since soy lecithin has a relatively small effect on T2, the T2 decay for the pure soy lecithin solutions (without agar) was sampled for longer TEs in the range of 50–1600 ms (equally spaced). T2 maps were calculated on a pixelwise basis by monoexponential fitting of the measured SI's: $SI = SI_0\ exp(-TE/T2) + c$ [22]. All signal values were noise corrected before fitting.

Relaxation times (T1, T2) and relaxation rates (R1 = 1/T1, R2 = 1/T2) of each sample were determined from circular regions of interest in the calculated parametric maps. Relaxivities were calculated from the linear regression of the relaxation rates on the concentration of the substance: $R1,2 = r_{1,2} \cdot [\text{concentration}] + c$. The slope of the line represents the relaxivity $r_{1,2}$.

A 3D T1-weighted gradient echo sequence (VIBE) with high spatial resolution was applied to examine the phantoms for homogeneity and the absence of air bubbles. Acquisition parameters include: TR = 6.3 ms, TE = 2.46 ms, FOV = 256 × 256, spatial resolution = 0.5 × 0.5x0.5 mm, number of slices = 10, coronal planes.

## Results and discussion

First, the relaxation rates R1 and R2 of pure aqueous soy lecithin solutions and pure agar gels were measured at concentrations up to 5%. For both soy lecithin and agar, the relaxation rates showed a linear correlation with concentration (Fig. 3). Relaxivities $r_1$ and $r_2$ calculated using a linear fit gave $r_{1,lecithin} = 0.112\ s^{-1}{\cdot}wt.\%^{-1}$ ($R^2 = 0.99$), $r_{1,agar} = 0.039\ s^{-1}{\cdot}wt.\%^{-1}$ ($R^2 = 0.99$), $r_{2,lecithin} = 0.68\ s^{-1}{\cdot}wt.\%^{-1}$ ($R^2 = 0.99$), and $r_{2,agar} = 5.71\ s^{-1}{\cdot}wt.\%^{-1}$ ($R^2 = 0.99$), which is in good agreement to previous work [20].

Secondly, soy lecithin and agar were found to retain their effect even when mixed. Table 1 lists the relaxivities of soy lecithin as a function of agar concentration.

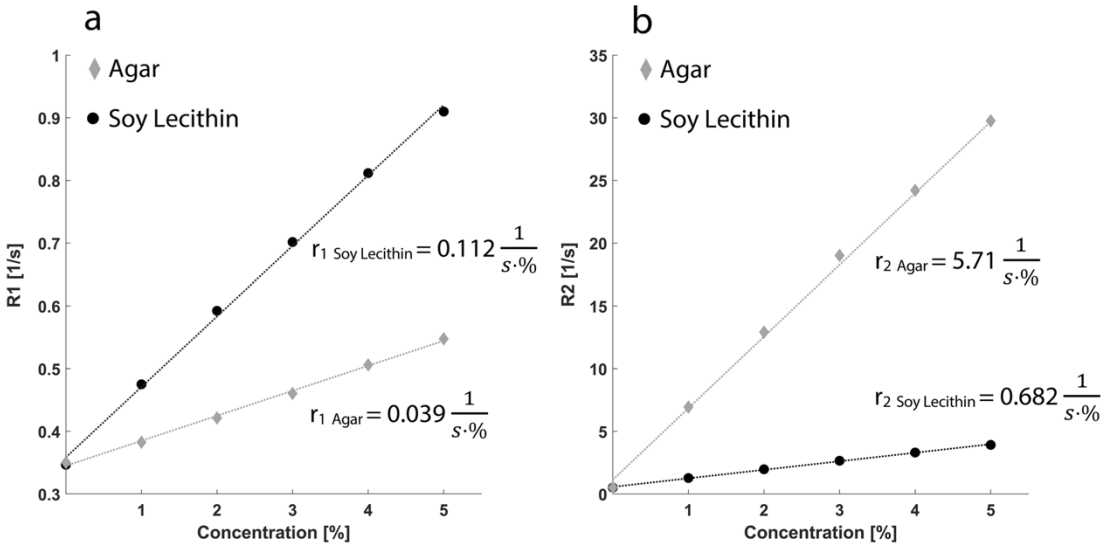


**Fig. 3** Relaxation rates R1 (**a**) and R2 (**b**) of aqueous solutions as a function of soy lecithin and agar concentration, respectively

**Table 1** Relaxivities $r_1$ and $r_2$ of soy lecithin in the presence of different agar concentrations. To measure the relaxivities of soy lecithin, the soy lecithin concentration was varied between 0%–4% (in steps of 1%) while the agar concentration was kept constant

| | Soy lecithin | | | |
|---|---|---|---|---|
| Agar [%] | $r_1$ [$s^{-1}$·wt.%$^{-1}$] | $R^2$ | $r_2$ [$s^{-1}$·wt.%$^{-1}$] | $R^2$ |
| 0 | 0.112 | 0.99 | 0.68 | 0.99 |
| 1 | 0.117 | 0.99 | 0.70 | 0.99 |
| 2 | 0.117 | 0.99 | 0.68 | 0.98 |
| 3 | 0.119 | 0.99 | 0.77 | 0.96 |
| 4 | 0.114 | 0.99 | 0.74 | 0.90 |
| Mean | 0.116 | – | 0.71 | – |

**Table 2** Relaxivities $r_1$ and $r_2$ of agar in the presence of different soy lecithin concentrations. To measure the relaxivities of agar, the agar concentration was varied between 0%–4% (in steps of 1%), while the soy lecithin concentration was kept constant

| | Agar | | | |
|---|---|---|---|---|
| Soy lecithin [%] | $r_1$ [$s^{-1}$·wt.%$^{-1}$] | $R^2$ | $r_2$ [$s^{-1}$·wt.%$^{-1}$] | $R^2$ |
| 0 | 0.039 | 0.99 | 5.71 | 0.99 |
| 1 | 0.033 | 0.95 | 5.88 | 0.99 |
| 2 | 0.032 | 0.97 | 5.60 | 0.99 |
| 3 | 0.027 | 0.98 | 5.83 | 0.99 |
| 4 | 0.033 | 0.99 | 5.87 | 0.99 |
| Mean | 0.033 | – | 5.78 | – |

It becomes clear that both, $r_1$ and $r_2$, hardly change in the presence of agar. Relaxivities showed little variation in the range of 0.112–0.119 $s^{-1}$·wt.%$^{-1}$ for $r_1$ and 0.68–0.77 $s^{-1}$·wt.%$^{-1}$ for $r_2$, respectively. Similarly, agar relaxivities remained nearly constant in the presence of soy lecithin (Table 2). Relaxivities varied between 0.027–0.039 $s^{-1}$·wt.%$^{-1}$ for $r_1$ and 5.60–5.88 $s^{-1}$·wt.%$^{-1}$ for $r_2$, respectively.

After determining the relaxivities and confirming the compatibility of soy lecithin and agar, the preparation of test phantoms mimicking organ related relaxation times was performed. For the relaxivities, the mean values $r_{1,lecithin} = 0.116$ $s^{-1}$·wt.%$^{-1}$, $r_{1,agar} = 0.033$ $s^{-1}$·wt.%$^{-1}$, $r_{2,lecithin} = 0.71$ $s^{-1}$·wt.%$^{-1}$, and $r_{2,agar} = 5.78$ $s^{-1}$·wt.%$^{-1}$ (see Table 1 and 2) were used in the following.

Substituting the calculated relaxivities into Eqs. 1 and 2 yields the following relationship between agar or soy lecithin concentration and desired relaxation times:

$$C_{Agar} = \frac{180}{T2[ms]} - \frac{1100}{T1[ms]} + 0.28 \tag{3}$$

$$C_{Lecithin} = \frac{8930}{T1[ms]} - \frac{51}{T2[ms]} - 3 \tag{4}$$

Using these equations, samples were produced with relaxation times corresponding to the T1 and T2 times published in the literature for gray and white matter, kidney cortex and medulla, spleen, muscle, and liver. Table 3 provides an overview of the concentrations of soy lecithin

**Table 3** Overview of the concentrations of soy lecithin and agar used and the targeted and measured T1 and T2 times of the test phantoms. The mean value and the standard deviation over the three measured phantom batches are shown

| | T1 [ms] | | T2 [ms] | | Soy lecithin [%] | Agar [%] |
|---|---|---|---|---|---|---|
| | Target | Measured | Target | Measured | | |
| Gray matter | 1820 | 1850 ± 12 | 99 | 93 ± 3 | 1.39 | 1.49 |
| White matter | 1084 | 1093 ± 4 | 69 | 66 ± 2 | 4.50 | 1.87 |
| Kidney cortex | 1142 | 1159 ± 10 | 76 | 72 ± 2 | 4.15 | 1.69 |
| Kidney medulla | 1545 | 1539 ± 17 | 81 | 75 ± 3 | 2.15 | 1.79 |
| Spleen | 1328 | 1318 ± 23 | 61 | 58 ± 1 | 2.89 | 2.40 |
| Muscle | 1295 | 1262 ± 16 | 34 | 34 ± 1 | 2.40 | 4.72 |
| Liver | 812 | 834 ± 16 | 42 | 56 ± 6 | 6.78 | 3.21 |

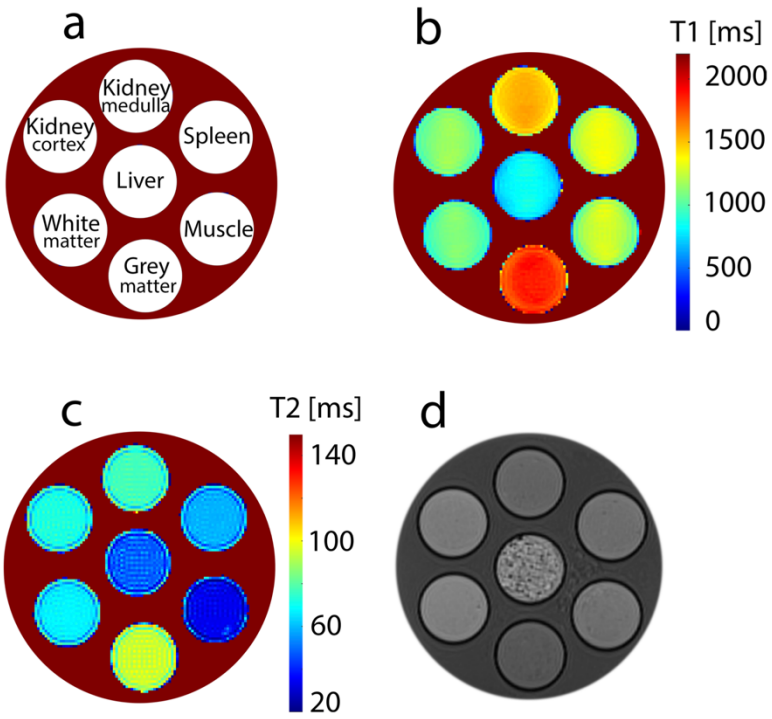


**Fig. 4** Parametric maps of test phantoms mimicking relaxation times of different tissues (grey matter, white matter, kidney cortex, kidney medulla, spleen, muscle, liver). **a** Representation of the positions of the test phantoms in the cylindrical measuring housing. **b** Parametric map of T1 times. **c** Parametric map of T2 times. **d** 3D T1-weighted image with high spatial resolution of test phantoms mimicking relaxation times of different tissues. With the exception of the liver phantom, all phantoms were homogeneous and showed little to no air bubbles. In contrast, the liver phantom had an inhomogeneous or brittle structure with many air bubbles

and agar used, as well as the targeted and measured T1- and T2 times. The corresponding T1- and T2 maps can be seen in Fig. 4a–c. Good agreement was found between the measured and targeted relaxation times. The largest deviations occurred for the liver phantom, where the percent deviation from the T1 set point was 2.7% and from the T2 set point was 32.5%. For all other phantoms, the percentage deviations from target relaxation times were less than 3% for T1 and less than 6.5% for T2, which is comparable to phantoms made with paramagnetic salts [15, 16]. In addition to the acceptable correspondence between calculated relaxation times and measured values, the reproducibility of the manufacturing process and resulting relaxation times T1 and T2 seems also sufficient for most applications, as shown by the relatively small standard deviations across the three batches (Table 3).

3D T1-weighted images with high spatial resolution showed that the samples, with the exception of the liver phantom, were quite homogeneous and contained little to no air bubbles (Fig. 4d). Only the liver phantom had an inhomogeneous or brittle structure and showed significant air bubbles. Even degassing with ultrasound could not remove those air bubbles. This can be explained by the comparatively high concentrations of soy lecithin and agar required to prepare the liver phantom (see Table 3). The combination of high soy lecithin (> 6%) and high agar (> 3%) concentration results in a very viscous mixture, which in turn favors the entrapment of air bubbles

that form during the heating process. The resulting low homogeneity of the sample could also be the reason for the relatively high deviation between measured and target T2 time (32.5%) in the liver phantom. This indicates that gels mimicking tissues that have both short T1- and T2 times (eg. Liver, myocardial tissue) are problematic, as high concentrations of agar and soy lecithin are required. Evacuation of the surroundings of highly viscous gels could help to reduce or avoid air bubbles. However, this would require additional equipment and an additional preparation step.

The temporal stability of the phantoms was evaluated after a storage period of 4 weeks. Unfortunately, the phantoms were unstable over time, which was particularly reflected in the T1 times. Across all batches, the T1 times of all phantoms decreased significantly compared to the first measurement (Fig. 5a). The changes in T2 times were not quite as pronounced, but here too most phantoms showed a deviation from the initial measurement (Fig. 5b).

One possible reason for the altered relaxation behavior of the phantoms could be biodegradation by microorganisms. Without suitable additives, agar gels provide an ideal nutrient medium for fungi and bacteria [24], which biodegrade the phantom material over time and thus also alter MR properties. This could also be observed macroscopically on some phantoms by means of mold growth (Fig. 5c).

The limited temporal stability of the soy-lecithin-agar phantoms is a major drawback compared to previously proposed phantoms using paramagnetic salts for T1 or T2 modification. Solutions with inorganic substances are stable for a long time without significant change in relaxation times [7]. This feature is very important when phantoms are employed for reproducibility measurements in multicenter studies where measurements are carried out over several weeks or even months.

To increase the biostability of soy-lecithin-agar phantoms and thus prevent microbial growth, preservatives such as fungicides and or bactericides can be used. It has been shown that the addition of these agents can maintain the stability of agar phantoms for up to 2 years [25]. However, most of the effective agents are quite toxic, which militates their use as it is contrary to the motivation of this study (production of relaxometry phantoms without toxic or questionable substances). Other preservatives such as citric acid or sodium sulfite, which are mainly used in the food industry [26], are harmless, but change the pH of the medium. Changing the pH would also be unfavorable since pH affects not only the properties of agar gels but also the micelle

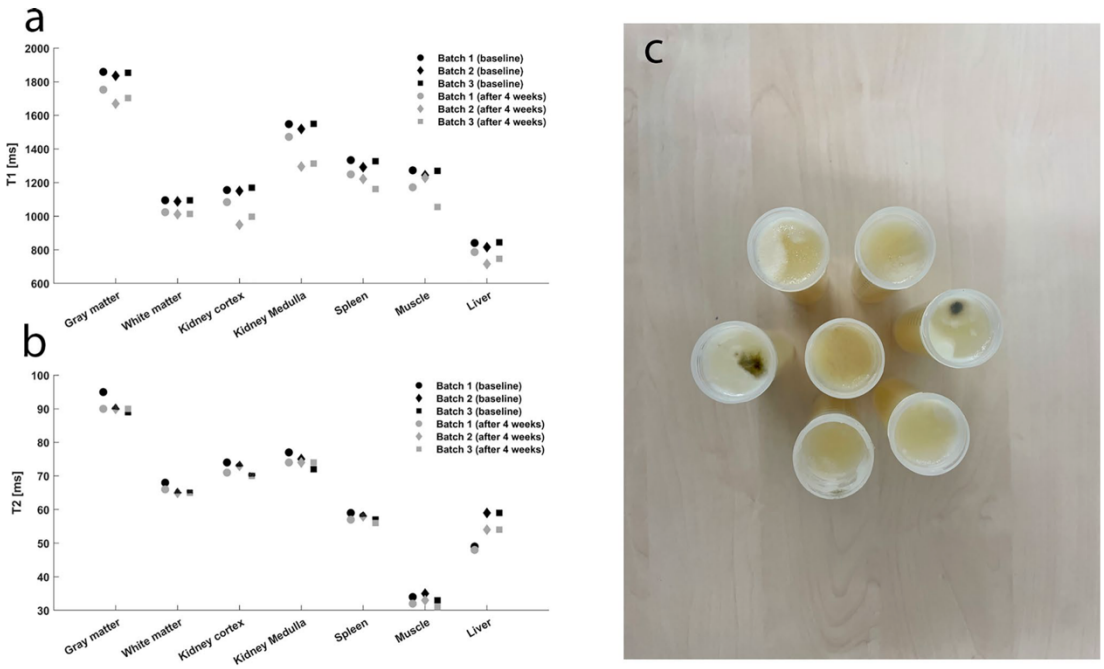


**Fig. 5** To evaluate the temporal stability of the test phantoms, T1 and T2 measurements were repeated after 4 weeks under the same conditions. **a** Comparison of T1 times measured at baseline and after 4 weeks. **b** Comparison of T2 times measured at baseline and after 4 weeks. **c** Photograph of the test phantoms (batch 1) after a storage period of 4 weeks—mold growth is clearly visible on some phantoms

formation of soy lecithin molecules [27–29]. Soy lecithin is an amphiphilic molecule that forms micelles in aqueous solutions, the number, type and shape of which depend on various environmental parameters (pH, temperature, etc.) [27, 28]. This means that a preservative that affects the pH also changes the microstructure of the phantoms and thus their MR properties. It is still a challenge to find a suitable non-toxic preservative that will ensure the stability of the phantoms without compromising the effect of soy lecithin and agar. A number of systematic measurements are needed that are beyond the scope of this work but are planned for future studies. Another potential way to increase temporal stability is sterilization of the water or autoclaving the entire gels or UV irradiation of the phantoms. In this context, sensitivity of the organic substances to heat must be considered.

The temperature dependence of relaxation properties of the proposed gels has not been investigated so far. Knowledge of the temperature dependence can be important to account for temperature-related measurement deviations in practical usage of the phantoms. Furthermore, there is unpredictable dependence of relaxation on the magnetic field strength. In this study, the soy lecithin agar phantoms were examined at a field strength of 3T only. Further studies are needed to investigate their properties at higher and lower field strengths. Effects of different approaches for relaxometry (pulse sequences and data processing) is also an interesting area of research. It is a well-documented issue that relaxation times measured with different methods can vary considerably, even in the same subjects examined with the same MRI system [23, 30]. Further work will investigate whether similar variations in the relaxation times measured with different relaxometry approaches can also be observed in the soy-lecithin-agar phantoms.

While the soy-lecithin-agar phantoms effectively mimic desired relaxation times and can serve as valuable tools for testing relaxometry methods, it is important to emphasize that they do not replicate the complexity of biological tissue. For example, they do not accurately reproduce tissue properties such as relaxation anisotropy, which is observed in highly anisotropic tissues such as white matter. Previous studies have shown that T1 and T2 relaxation times in white matter are angle-dependent due to the orientation of axon fibers in the $B_0$ magnetic field [31–34]. This anisotropic nature of relaxation times cannot be mimicked by structurally homogenous phantoms.

## Conclusion

This work shows that soy-lecithin-agar gels represents an alternative phantom material for the construction of relaxometry phantoms with tissue-like relaxation times, thus expanding the toolbox of qMRI-research. Soy-lecithin agar gels are inexpensive, easy to prepare, and allow independent adjustment of T1 and T2 without marked susceptibility effects. With the presented manufacturing process, the relaxation times of almost all tissues can be mimicked, and without the use of toxic and/or paramagnetic substances.

Nevertheless, there are still open questions regarding the long-term stability and the temperature dependence of the phantoms which will be addressed in future studies.

**Acknowledgements** This work was supported and funded by the German Research Foundation (DFG) under grants SCHI 498/14-1, TH 1528/6-1 (package no. 997/1). It was furthermore supported in part by a grant (01GI0925) from the German Federal Ministry of Education and Research (BMBF) to the German Center for Diabetes Research (DZD e.V.)

**Author contributions** All authors contributed to the study conception and design. Study design and conception, material preparation, data collection and analysis were performed by [Fritz V]. [Eisele S] helped with the planning and production of the phantoms. [Martirosian P] and [Machann J] assisted with the MR measurements and analysis of data. [Schick F] conceived and supervised the project. The first draft of the manuscript was written by [Fritz V] in consultation with [Schick F]. All authors commented on previous versions of the manuscript and approved the final version for submission.

**Funding** Open Access funding enabled and organized by Projekt DEAL.

## Declarations

**Conflict of interest** The authors declare that they have no conflict of interest.



## References

1. Keenan KE, Ainslie M, Barker AJ, Boss MA, Cecil KM, Charles C, Chenevert TL, Clarke L, Evelhoch JL, Finn P, Gembris D, Gunter JL, Hill DLG, Jack CR Jr, Jackson EF, Liu G, Russek SE, Sharma SD, Steckner M, Stupic KF, Trzasko JD, Yuan C, Zheng J (2018) Quantitative magnetic resonance imaging phantoms: A review and the need for a system phantom. Magn Reson Med 79(1):48–61
2. Stupic KF, Ainslie M, Boss MA, Charles C, Dienstfrey AM, Evelhoch JL, Finn P, Gimbutas Z, Gunter JL, Hill DLG, Jack CR, Jackson EF, Karaulanov T, Keenan KE, Liu G, Martin MN, Prasad PV, Rentz NS, Yuan C, Russek SE (2021) A standard

system phantom for magnetic resonance imaging. Magn Reson Med 86(3):1194–1211
3. Stanisz GJ, Odrobina EE, Pun J, Escaravage M, Graham SJ, Bronskill MJ, Henkelman RM (2005) T1, T2 relaxation and magnetization transfer in tissue at 3T. Magn Reson Med 54(3):507–512
4. Cheng HL, Stikov N, Ghugre NR, Wright GA (2012) Practical medical applications of quantitative MR relaxometry. J Magn Reson Imaging 36(4):805–824
5. Mitchell MD, Kundel HL, Axel L, Joseph PM (1986) Agarose as a tissue equivalent phantom material for NMR imaging. Magn Reson Imaging 4(3):263–266
6. Kraft KA, Fatouros PP, Clarke GD, Kishore PR (1987) An MRI phantom material for quantitative relaxometry. Magn Reson Med 5(6):555–562
7. Christoffersson JO, Olsson LE, Sjöberg S (1991) Nickel-doped agarose gel phantoms in MR imaging. Acta Radiol 32(5):426–431
8. Tofts PS, Shuter B, Pope JM (1993) Ni-DTPA doped agarose gel–a phantom material for Gd-DTPA enhancement measurements. Magn Reson Imaging 11(1):125–133
9. Tofts PS (2003) QA: Quality Assurance, Accuracy, Precision and Phantoms. In: Quantitative MRI of the Brain. pp 55–81. https://doi.org/10.1002/0470869526.ch3
10. Yoshimura K, Kato H, Kuroda M, Yoshida A, Hanamoto K, Tanaka A, Tsunoda M, Kanazawa S, Shibuya K, Kawasaki S, Hiraki Y (2003) Development of a tissue-equivalent MRI phantom using carrageenan gel. Magn Reson Med 50(5):1011–1017
11. Kato H, Kuroda M, Yoshimura K, Yoshida A, Hanamoto K, Kawasaki S, Shibuya K, Kanazawa S (2005) Composition of MRI phantom equivalent to human tissues. Med Phys 32(10):3199–3208
12. Hellerbach A, Schuster V, Jansen A, Sommer J (2013) MRI phantoms—are there alternatives to agar? PLoS ONE 8(8):e70343
13. Vassiliou VS, Heng EL, Gatehouse PD, Donovan J, Raphael CE, Giri S, Babu-Narayan SV, Gatzoulis MA, Pennell DJ, Prasad SK, Firmin DN (2016) Magnetic resonance imaging phantoms for quality-control of myocardial T1 and ECV mapping: specific formulation, long-term stability and variation with heart rate and temperature. J Cardiovasc Magn Reson 18(1):62
14. Altermatt A, Santini F, Deligianni X, Magon S, Sprenger T, Kappos L, Cattin P, Wuerfel J, Gaetano L (2019) Design and construction of an innovative brain phantom prototype for MRI. Magn Reson Med 81(2):1165–1171
15. Gopalan K, Tamir JI, Arias AC, Lustig M (2021) Quantitative anatomy mimicking slice phantoms. Magn Reson Med 86(2):1159–1166
16. Woletz M, Roat S, Hummer A, Tik M, Windischberger C (2021) Technical Note: Human tissue-equivalent MRI phantom preparation for 3 and 7 Tesla. Med Phys 48(8):4387–4394
17. Erdevig HE, Russek SE, Carnicka S, Stupic KF, Keenan KE (2017) Accuracy of magnetic resonance based susceptibility measurements. AIP Adv 7(5):1–6
18. Panich AM (2022) Can detonation nanodiamonds serve as MRI phantoms? MAGMA 35(3):345–347
19. Sekowska A, Majchrowicz D, Sabisz A, Ficek M, Bullo-Piontecka B, Kosowska M, Jing L, Bogdanowicz R, Szczerska M (2020) Nanodiamond phantoms mimicking human liver: perspective to calibration of T1 relaxation time in magnetic resonance imaging. Sci Rep 10(1):6446
20. Fritz V, Martirosian P, Machann J, Daniels R, Schick F (2022) A comparison of emulsifiers for the formation of oil-in-water emulsions: stability of the emulsions within 9 h after production and MR signal properties. MAGMA 35(3):401–410
21. Fritz V, Martirosian P, Machann J, Thorwarth D, Schick F (2023) Soy lecithin: A beneficial substance for adjusting the ADC in aqueous solutions to the values of biological tissues. Magn Reson Med 89(4):1674–1683
22. Bojorquez JZ, Bricq S, Acquitter C, Brunotte F, Walker PM, Lalande A (2017) What are normal relaxation times of tissues at 3 T? Magn Reson Imaging 35:69–80
23. Stikov N, Boudreau M, Levesque IR, Tardif CL, Barral JK, Pike GB (2015) On the accuracy of T1 mapping: searching for common ground. Magn Reson Med 73(2):514–522
24. Sandle T (2019) Chapter 7—Selection and Application of Culture Media. In: Sandle T (ed) Biocontamination control for pharmaceuticals and healthcare. Academic Press, pp 103–123. https://doi.org/10.1016/B978-0-12-814911-9.00007-9
25. Souza RM, Santos TQ, Oliveira DP, Souza RM, Alvarenga AV, Costa-Felix RPB (2016) Standard operating procedure to prepare agar phantoms. J Phys: Conf Ser 733(1):012044
26. García-García R, Searle SS (2016) Preservatives: Food Use. In: Caballero B, Finglas PM, Toldrá F (eds) Encyclopedia of Food and Health. Academic Press, Oxford, pp 505–509. https://doi.org/10.1016/B978-0-12-384947-2.00568-7
27. Israelachvili JN (2011) 2—Thermodynamic and Statistical Aspects of Intermolecular Forces. In: Israelachvili JN (ed) Intermolecular and Surface Forces, 3rd edn. Academic Press, San Diego, pp 23–51. https://doi.org/10.1016/B978-0-12-375182-9.10002-8
28. Tadros TF (2013) Emulsion Formation, Stability, and Rheology. In: Emulsion Formation and Stability, pp 1–75. https://doi.org/10.1002/9783527647941.ch1
29. Yu Z, Zhan J, Wang H, Zheng H, Xie J, Wang X (2020) Analysis of Influencing Factors on Viscosity of Agar Solution for Capsules. J Phys: Conf Ser 1653(1):012059
30. Matzat SJ, McWalter EJ, Kogan F, Chen W, Gold GE (2015) T2 Relaxation time quantitation differs between pulse sequences in articular cartilage. J Magn Reson Imaging 42(1):105–113
31. Schyboll F, Jaekel U, Petruccione F, Neeb H (2020) Origin of orientation-dependent R(1) (=1/T(1)) relaxation in white matter. Magn Reson Med 84(5):2713–2723
32. Kauppinen RA, Thothard J, Leskinen HPP, Pisharady PK, Manninen E, Kettunen M, Lenglet C, Gröhn OHJ, Garwood M, Nissi MJ (2023) Axon fiber orientation as the source of T(1) relaxation anisotropy in white matter: a study on corpus callosum in vivo and ex vivo. Magn Reson Med 90(2):708–721
33. Kauppinen RA, Thotland J, Pisharady PK, Lenglet C, Garwood M (2023) White matter microstructure and longitudinal relaxation time anisotropy in human brain at 3 and 7 T. NMR Biomed 36(1):e4815
34. Knight MJ, Dillon S, Jarutyte L, Kauppinen RA (2017) Magnetic resonance relaxation anisotropy: physical principles and uses in microstructure imaging. Biophys J 112(7):1517–1528

# Publication 4

*Fritz, V., Schick, F. (2026)*
*Recipe for hydrogels with tunable relaxation and diffusion properties for use as MRI test materials.*
*Magnetic Resonance in Medicine*.
DOI: https://doi.org/10.1002/mrm.70120

*Magnetic Resonance in Medicine*

WILEY | ISMRM ONE COMMUNITY FOR CLINICIANS AND SCIENTISTS

RESEARCH ARTICLE OPEN ACCESS

# Recipe for Hydrogels With Tunable Relaxation and Diffusion Properties for Use as MRI Test Materials

V. Fritz | F. Schick

Section on Experimental Radiology, Department of Diagnostic and Interventional Radiology, University of Tuebingen, Germany

**Correspondence:** V. Fritz (victor.fritz@med.uni-tuebingen.de)

**Received:** 16 April 2025 | **Revised:** 21 August 2025 | **Accepted:** 21 September 2025

**Funding:** This work was supported by Deutsche Forschungsgemeinschaft, SCHI 498/15-1 (package no. 997/2).

**Keywords:** DWI | MRI | phantoms | quantitative | relaxometry

## ABSTRACT

**Purpose:** To develop and evaluate a preparation protocol (recipe) for hydrogels with specific relaxation times and ADC values to be used as tissue-like test materials for MRI experiments at 3 Tesla.

**Methods:** Gd-DTPA, agarose, and soy lecithin were used as modulators for T1, T2, and ADC. First, systematic measurements were performed to determine the relaxation- and diffusion-modifying properties of the single substances and combinations of them. An algorithm was developed to determine the necessary concentrations of the ingredients to achieve predetermined sets of target values (T1, T2, and ADC). To validate this approach, hydrogels mimicking the relaxation and diffusion properties of different tissues (pancreas, white matter, fibroglandular tissue, liver, prostate) were prepared and evaluated. All measurements (relaxometry, diffusion-weighted imaging) were performed on a 3 Tesla clinical scanner at 20°C.

**Results:** The proposed method allowed the preparation of hydrogels with specific diffusion and relaxation properties by adjusting the concentrations of Gd-DTPA, agarose, and soy lecithin. Test phantoms containing hydrogels for simulation of various tissue types showed good agreement between targeted and measured properties, with deviations of less than 8% for T1, 7.5% for T2, and 11.5% for ADC. With the present approach, the properties (T1, T2, and ADC) of most known tissue classes could be well approximated; only the gray matter of the brain was slightly outside the selectable range. Temporal stability over 3 months was acceptable.

**Conclusion:** This work provides a relatively simple, inexpensive, and reproducible method for the preparation of hydrogels with independently adjustable T1, T2, and ADC values at 3 T.

## 1 | Introduction

Suitable tissue-mimicking materials in so-called tissue phantoms are becoming increasingly important for testing new sequences and especially in quantitative magnetic resonance imaging (MRI) [1–4]. While in vivo studies with human subjects are essential for clinical translation, early-stage validation and proof of concept are often more efficiently conducted using MRI phantoms.

Phantom materials typically consist of liquids or gels with well-defined and stable MRI properties, including relaxation times (T1, T2) or the apparent diffusion coefficient (ADC) [4]. Relaxation and diffusion properties can be modulated by adding paramagnetic substances (e.g., Gd-DTPA, CuSO4), polymers (e.g., PVP, PEG), or by adjusting the concentration of gelling agents (e.g., agarose, carrageenan) [5–14]. Despite the wide range of available phantom designs, a fundamental limitation remains:

most existing materials in phantoms were designed to mimic only a single MRI parameter (e.g., T1, T2, or ADC), while leaving the others uncontrolled, which limits their ability to replicate the complex signal characteristics seen in biological tissues [1, 15].

In vivo, tissues exhibit characteristic combinations of multiple MRI parameters, inherently linked to their structural and biochemical composition [16, 17]. For instance, healthy liver tissue at 3 Tesla is characterized by a T1 relaxation time of 800–1000 ms, a T2 relaxation time of 35–50 ms, and an ADC of ~$1 \cdot 10^{-3}$ $mm^2/s$ [18–20]. In addition, factors such as tissue perfusion, magnetization transfer, fat and iron content might play a crucial role [21]. Each of these parameters contributes to the acquired MR signal, meaning that quantitative MRI methods designed to quantify a specific parameter (e.g., T2) may be affected by others (e.g., T1 or diffusion) [22].

Very few approaches have been reported allowing the simultaneous and independent adjustment of multiple MRI parameters within a single test material. Most of these focus on relaxometry-based tuning of T1 and T2 or on simultaneous modulation of fat fraction and R2* (via iron content) [8, 15, 23–25]. However, as noted by Keenan et al. [1], it has not yet been possible to create a material that simultaneously represents a specific T1, a specific T2, and a specific ADC value in the same voxel.

A major challenge in multi-parametric phantom development is the interdependence of parameter-modifying agents [4]. The preparation of a hydrogel with specific T1, T2, and ADC values requires at least three different components with different chemical properties: a T1 modifier, a T2 modifier, and an ADC modifier. However, a substance intended to adjust one MR property often influences others, making independent parameter control challenging. For example, agents used to modify the diffusion properties usually also affect the relaxation times of materials used in phantoms [9, 26, 27]. Similarly, relaxation modifiers do not act exclusively on T1 or T2 but influence both [8]. In addition, ensuring compatibility between the selected components is critical—that is, there is little or no interaction between them and their individual effects remain intact in the presence of the other substances. Undesired interactions, as seen between $GdCl_3$ and agarose, lead to unexpected shifts in target values [4, 28]. In summary, a suitable triple must be chemically compatible while allowing independent adjustment of a wide range of relaxation times and ADC values.

In this context, Gd-DTPA, agarose, and soy lecithin were found to be promising candidates. The combination of Gd-DTPA and agarose has already been established as a suitable pair for independent adjustment of T1 and T2 [4]. In addition, soy lecithin has recently been identified as a promising ADC modifier that, when combined with agarose, allows for largely independent control of ADC and T2 [27]. This raises the question of whether these three substances (Gd-DTPA, agarose, and soy lecithin) remain effective when combined into a single mixture and whether they allow simultaneous and independent adjustment of T1, T2, and ADC—the motivation of this study. In this work, the production of hydrogels with specific diffusion and relaxation properties by adjusting the concentrations of Gd-DTPA, agarose, and soy lecithin will therefore be presented. The work is divided into three parts: First, the relaxation and diffusion-modifying properties of the single substances, as well as their compatibility in combination, were systematically investigated. Second, based on the resulting findings, a recipe for the production of a hydrogel with a desired set of properties (T1, T2, and ADC) was developed and used to build test phantoms with hydrogels mimicking the diffusion and relaxation properties of different tissues. Finally, the achieved values (T1, T2, and ADC) of the produced hydrogels were measured and compared with the intended target values. Deviations were systematically determined and the target range achievable with the selected approach was identified. In addition, the reproducibility of the preparation process and the temporal stability of the gels were tested.

## 2 | Methods

### 2.1 | Selection of Materials

Aqueous solutions were prepared in order to be able to reproduce lean tissue (without significant fat content). Known ingredients were chosen that can be mixed together and which produce hardly any additional spectral components in the $^1H$ spectrum. The following materials were used:

- Base solvent: Deionized water (Carl Roth, Karlsruhe, Germany) was used as the basis for the hydrogels.
- Gadopentetate dimeglumine (Gd-DTPA, Bayer, Leverkusen, Germany): Due to its strong paramagnetic properties, gadolinium effectively shortens T1 relaxation times and is therefore widely used as a contrast agent in MR imaging, but also to adjust T1 times in test fluids or gels [29].
- Agarose (UltraPure Agarose, Thermo Fisher Scientific, Waltham, MA, USA): Agarose is known to have a strong influence on T2 relaxation times, allowing T2 to be adjusted to tissue-like values [5, 13].
- Soy lecithin (Carl Roth, Karlsruhe, Germany): Recently, Soy lecithin was identified as a beneficial substance for adjusting the ADC in aqueous solutions to the values of biological tissues: [27, 30] It provides a wide range of adjustable ADC values, shows no additional signal components in the $^1H$ spectrum, and has a moderate effect on relaxation times. Being an amphiphilic molecule, soy lecithin is known to form different self-assembled aggregate structures in aqueous solution, such as uni- and multi-lamellar liposomal vesicles [31–33], which are assumed to be responsible for the pronounced restriction of water mobility. Using dynamic light scattering (DLS), we measured aqueous soy lecithin solutions at concentrations of 0.05%, 0.1%, 0.25%, and 0.5% wt/vol, which showed mean aggregate sizes in the range of 200 (0.05% wt/vol) to 350 nm (0.5% wt/vol), consistent with vesicle sizes reported by Tsengam et al. [31]

### 2.2 | Study Design and Procedure

To design a material with predefined T1, T2, and ADC values, it is essential to understand how the different components—Gd-DTPA, agarose, and soy lecithin—affect the relaxation and diffusion properties of water, the base

solvent. Systematic measurements were performed to determine the relaxivities ($r_1$, $r_2$) and ADC-modifying properties of these substances, both individually and in mixtures. To study the MR-specific properties of substance A (e.g., soy lecithin), samples with increasing concentrations of soy lecithin were prepared, while keeping the other substances (agarose and Gd-DTPA) constant. These experiments were repeated for different combinations of constant agarose and Gd-DTPA concentrations to assess whether the diffusion and relaxation properties of soy lecithin are affected by the presence or concentration of the other substances. The same approach was used to determine the relaxation and diffusion-modifying properties of agarose and Gd-DTPA. In total, 47 solutions with different concentrations of each substance were prepared, measured, and analyzed. The combinations of Gd-DTPA, agarose, and soy lecithin ranged from 0 to 0.2 mM (0, 0.05, 0.1, 0.15, 0.2 mM) for Gd-DTPA, from 0% to 4% (0%, 1%, 2%, 3%, 4% wt/vol) for agarose, and from 0% to 5% (0%, 0.5%, 1%, 2%, 3%, 4%, 5% wt/vol) for soy lecithin. The specific composition of each sample is detailed in Table S1. Based on these preliminary experiments, relationships between MR parameters (T1, T2, and ADC) and the concentrations of the ingredients were derived, and a stepwise preparation procedure was developed.

To validate the preparation protocol, samples were prepared to mimic the relaxation times and ADC values of different tissue types: liver (T1 = 812 ms, T2 = 42 ms, ADC = 1.45 [$10^{-3}$] $mm^2/s$), prostate (1597, 80, 1.25 [$10^{-3}$] $mm^2/s$), pancreas (725, 43, 0.98 [$10^{-3}$] $mm^2/s$), fibroglandular tissue (1444, 54, 1.75 [$10^{-3}$] $mm^2/s$), white matter (1084, 69, 0.84 [$10^{-3}$] $mm^2/s$) [14, 18, 20, 34–39]. Note: the liver ADC of $1.45 \cdot 10^{-3}\ mm^2/s$ represents a strongly perfusion-influenced value, but was chosen here to provide gels covering a broad range of different values. To evaluate the accuracy (measured versus target values), reproducibility, and temporal stability of the hydrogels, test phantoms were prepared independently three times and examined over a period of 3 months. Batch 1 was measured weekly. Batches 2 and 3 were measured every 2 weeks. To better assess the temporal stability, a pure water sample was also examined as a reference over the same period.

## 2.3 | Preparation of the Hydrogels

Hydrogels were prepared as shown in Figure 1: First, Gd-DTPA (500 mM) was diluted to the desired concentration with deionized water. Second, soy lecithin was added and dissolved under magnetic stirring at 650 rpm for 10 min. Agarose was then gently stirred into the solution, and the mixture was boiled using a microwave heater until the solution was clear and homogeneous. The solutions were then poured into sterile polypropylene tubes (50 mL, Greiner Bio-One, Germany) and allowed to cool

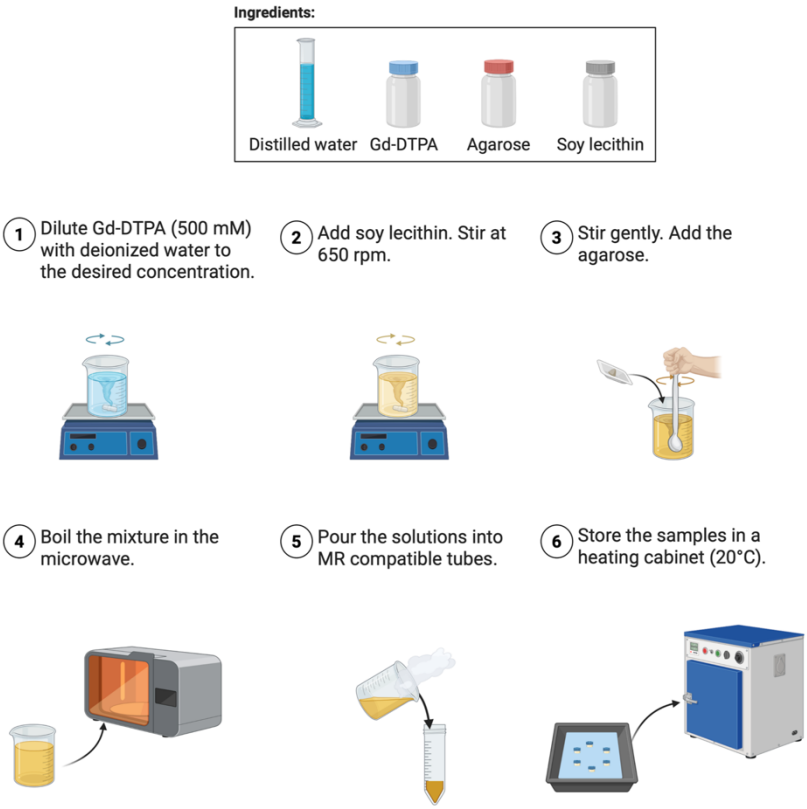


**FIGURE 1** | Scheme of the hydrogel preparation process. Created in BioRender. https://BioRender.com/k1h8vah.

for gelation. Finally, the prepared hydrogel tubes were placed in water-filled MR-compatible housings and stored in a heating cabinet at 20°C.

### 2.4 | Data Acquisition and Analysis

Relaxometry and DWI were performed using a clinical 3.0 Tesla scanner (MAGNETOM Prisma$^{fit}$, Siemens Healthcare, Erlangen, Germany) with an 18-channel body-array coil. Since the room temperature of the scanner can vary on different measurement days (usually between 19°C and 23°C), the samples were tempered to 20°C as described above. To keep the temperature stable during the measurement period, they were placed in a thermally insulated polystyrene box for the measurement.

T1 relaxation times were measured using a 2D inversion recovery prepared turbo spin echo (IR-TSE) sequence with nine different inversion times ranging from 25 to 6400 ms. Other sequence parameters were TR = 10,000 ms, TE = 9.9 ms, FOV = 200 × 200 mm, matrix size = 128 × 128, number of slices = 1 (in coronal plane), slice thickness = 5 mm.

T2 measurements were performed in the same slice using a multi-echo CPMG pulse sequence with 32 echo times ranging from 10 to 320 ms (equally spaced). Imaging parameters were TR = 5000 ms, FOV = 200 × 200 mm, matrix size = 128 × 128, number of slices = 1 (in coronal plane), slice thickness = 5 mm.

DWI was performed using a readout-segmented echoplanar imaging (RESOLVE-DWI) sequence with the following parameters: TR = 5000 ms, TE = 48 ms, FOV = 200 × 200 mm, matrix size = 128 × 128, number of slices = 10 (in coronal plane), slice thickness = 5 mm, bandwidth = 751 Hz/px, b-values = 0, 50, 500, 1000 s/mm$^2$, monopolar diffusion sensitizing gradients.

Image processing, including mapping and analysis, was performed offline in MATLAB (R2022b, MathWorks, Natick, MA, USA). T1 and T2 maps were calculated voxel-wise by mono-exponential fitting of signal intensities as a function of inversion time (for T1) and as a function of echo time (for T2), respectively. ADC maps were calculated voxel-wise by a log-linear fitting of the signal intensities as a function of b-value. T1, T2, and ADC values of each sample were determined from circular regions of interest in the calculated parametric maps. Relaxivities $r_1$ and $r_2$ were calculated from the linear regression of the relaxation rates (R1 = 1/T1, R2 = 1/T2) on the concentration of the substance.

## 3 | Results

### 3.1 | MR Properties of the Ingredients: Gd-DTPA, Agarose, and Soy Lecithin

The dependence of ADC values on soy lecithin concentration was measured under various conditions (in pure water and with different agarose and Gd-DTPA concentrations). A biexponential relationship was observed between soy lecithin concentration and ADC values, consistent with reported findings for pure aqueous soy lecithin solutions [27]. Our results suggest that the influence of soy lecithin on ADC is almost unaffected by the presence of agarose and Gd-DTPA (see Figure 2). However, while the general trend remained stable across the conditions tested, variations in the ADC values were observed: At low concentrations of soy lecithin (≤ 2% wt/vol), the standard deviations (SDs) were small, indicating consistent ADC values over repeated measurements under different agarose–Gd-DTPA compositions. Conversely, at higher concentrations (≥ 3% wt/vol), the SDs were significantly higher, indicating greater variability in ADC values. Unfortunately, this means that the accuracy of the targeted ADC value is lower at higher lecithin concentrations.

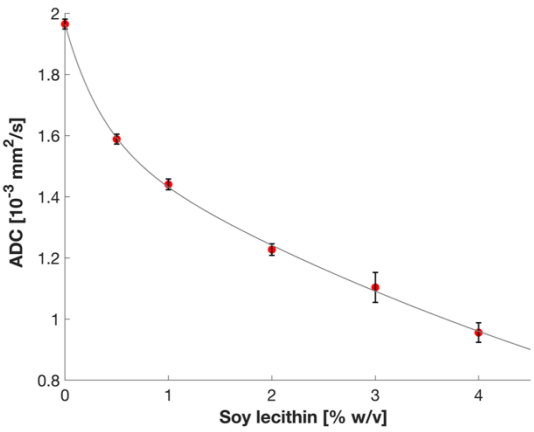


**FIGURE 2** | Dependence of ADC on soy lecithin concentration. Each soy lecithin concentration was measured in the presence of different concentrations of agarose (0%, 1%, 2%, 3%, 4% wt/vol) and Gd-DTPA (0, 0.05, 0.1, 0.15, 0.2 mM). The error bars show the variation in ADC for a given soy lecithin concentration in the presence of different agarose and Gd-DTPA concentrations.

For hydrogels with variable amounts of Gd-DTPA and agarose, the ADC values showed no significant concentration dependence. Therefore, the relationship between ADC and the proposed ingredients is determined only by the soy lecithin concentration with good approximation, as described by the bi-exponential model in Equation (1):

$$ADC\left[10^{-3}\right] = 0.36 \cdot e^{-2.79 \cdot C_{lec}} + 1.60 \cdot e^{-0.13 \cdot C_{lec}} \quad (1)$$

Relaxivities ($r_1$, $r_2$) for soy lecithin, Gd-DTPA, and agarose were determined for pure aqueous solutions with only one ingredient and for mixtures at varying concentrations of the other components (results are summarized in Table 1). For soy lecithin and Gd-DTPA, the relaxivities were $r_{1,lec} = 0.10\ s^{-1}$ (% wt/vol)$^{-1}$, $r_{2,lec} = 0.69\ s^{-1}$ (% wt/vol)$^{-1}$, $r_{1,Gd} = 3.78\ s^{-1}\ mM^{-1}$, and $r_{2,Gd} = 4.24\ s^{-1}\ mM^{-1}$. These values closely match their individual relaxivities (shown in parentheses in Table 1), suggesting that their effects on the relaxation times of water remain unchanged in the presence of the other components. For agarose, however, this is only true for T2. The determined transverse relaxivity of agarose is $r_{2,agarose} = 6.23\ s^{-1}$ (% wt/vol)$^{-1}$, consistent with its individual transverse relaxivity. In contrast, the longitudinal relaxivity $r_{1,agarose}$ could not be reliably determined in the presence of Gd-DTPA and soy lecithin, since no significant

**TABLE 1** | Relaxivities r1 and r2 of Gd-DTPA, agarose, and soy lecithin.

| | Gd-DTPA ($mM^{-1} s^{-1}$) | Agarose ($s^{-1}$ [% wt/vol]$^{-1}$) | Soy lecithin ($s^{-1}$ [% wt/vol]$^{-1}$) |
|---|---|---|---|
| $r_1$ | 3.78 ± 0.14 (3.62) | N/A (0.02) | 0.10 ± 0.02 (0.12) |
| $r_2$ | 4.24 ± 0.16 (4.33) | 6.62 ± 0.47 (5.65) | 0.69 ± 0.04 (0.70) |

dependence of the relaxation rate R1 (1/T1) on the agarose concentration was observed. This means that the contribution of agarose to T1 is negligible in the composite hydrogel. All three ingredients—Gd-DTPA, soy lecithin, and agarose—affect the transverse relaxation time T2, while the longitudinal relaxation time T1 is solely dependent on Gd-DTPA and soy lecithin concentrations. Consequently, the relaxation properties of the composite hydrogel can be mathematically modeled as presented in Equations (2) and (3):

$$R1 = R1_w + r_{1,Gd} \cdot C_{Gd} + r_{1,lec} \cdot C_{lec} \quad (2)$$

$$R2 = R2_w + r_{2,Gd} \cdot C_{Gd} + r_{2,lec} \cdot C_{lec} + r_{2,a} \cdot C_a \quad (3)$$

where R1 and R2 are the relaxation rates ($1/T_{1,2}$) of the gels, $R1_w$ and $R2_w$ are the relaxation rate of pure water, $C_{Gd}$ is the concentration of Gd-DTPA in mM, $C_{lec}$, and $C_a$ are the concentrations of soy lecithin and agarose in % (wt/vol), and $r_1$ and $r_2$ are the longitudinal- and transverse relaxivities of each substance.

### 3.2 | Gel Preparation Protocol

Since the ADC value depends only on the soy lecithin concentration, the T1 value on the concentrations of soy lecithin and Gd-DTPA, and the T2 value on the concentrations of soy lecithin, Gd-DTPA, and agarose, the determination of the component concentrations follows a three-step procedure: (1) the soy lecithin concentration is determined based on the target ADC value using Equation (1) to achieve the desired diffusion characteristics, (2) with the soy lecithin concentration determined, the Gd-DTPA concentration is calculated to achieve the target T1 relaxation time using Equation (2), and (3) finally, the agarose concentration is determined using the calculated soy lecithin and Gd-DTPA concentrations along with the target T2 relaxation time using Equation (3).

### 3.3 | Achievable Combinations of T1, T2, and ADC

Due to the described secondary effects of the ingredients, not all combinations of T1, T2, and ADC can be realized with the proposed approach. Soy lecithin, which is used to adjust the ADC in step (1), also reduces T1 to a non-negligible extent ($r_{1,lec} = 0.10\,s^{-1}$ (% wt/vol)$^{-1}$). As a result, the achievable T1 values are highly dependent on the selected ADC: The lower the ADC value selected, the more limited is the range of achievable T1 times (Figure 3A). For example, if ADC is set to 0.9 $mm^2/s$, only T1 values ≤ 1400 ms can be reached. Nevertheless, the range of combinations (T1, T2, ADC) is very wide and includes most types of tissue in the human body, for example, liver, prostate, and white matter [14, 18, 20, 35, 37–39]. Only a few tissues, such as gray matter (ADC = 0.8–1.0 [$10^{-3}$] $mm^2/s$, T1 = 1500–1850 ms) [18, 34, 36], are outside the range and cannot be well simulated.

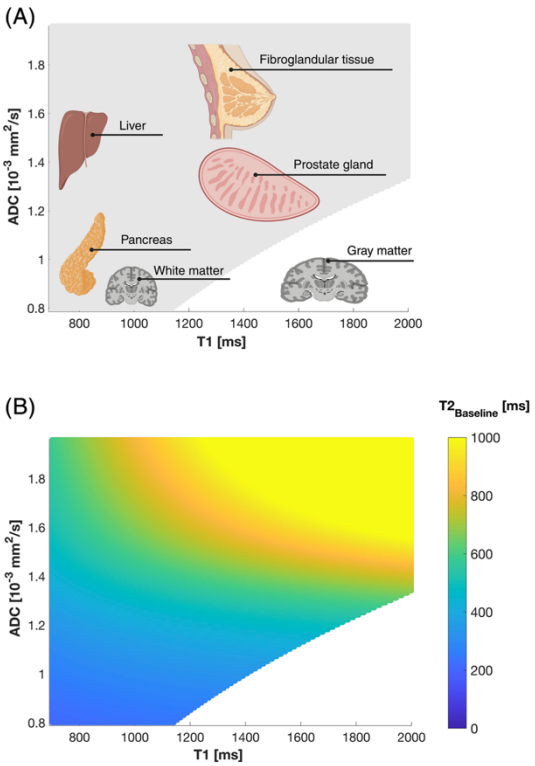


**FIGURE 3** | (A) Achievable combinations of ADC and T1 (gray area) using the proposed recipe. Achievable values cover most human tissues such as liver, prostate, and white matter. Only tissues with low ADC values but long T1 times (e.g., gray matter) are not included in the accessible range. (B) Baseline T2 values as a function of selected ADC and T1 values before addition of agarose. For all combinations of ADC and T1 considered, the baseline values remained above 200 ms, providing sufficient flexibility for further adjustment to physiologically relevant T2 values by adding agarose. Created in BioRender. https://BioRender.com/yu9nc7d.

The adjustable T2 range depends on the preselected ADC and T1. Due to the T2-shortening effects of soy lecithin and Gd-DTPA—used in the preceding steps to set ADC and T1—the baseline T2 is already reduced to some extent without the addition of agarose. Figure 3B illustrates the baseline T2 times as a function of the selected ADC and T1. The ADC range in Figure 3 includes values from 0.8 to 2 [$10^{-3}$] $mm^2/s$ while T1 from 700 to 2000 ms are considered. These ranges cover properties of almost all tissue types. For all (T1, ADC) combinations available, the

**TABLE 2** | Target and measured values for T1, T2, and ADC, presented as mean and standard deviation across the three batches.

| | T1 (ms) | | T2 (ms) | | ADC ($10^{-3}$ mm$^2$/s) | |
|---|---|---|---|---|---|---|
| | **Target** | **Measured** | **Target** | **Measured** | **Target** | **Measured** |
| Pancreas | 725 | $757 \pm 16$ | 43 | $43 \pm 1$ | 0.98 | $0.87 \pm 0.01$ |
| White matter | 1084 | $1143 \pm 3$ | 69 | $66 \pm 1$ | 0.84 | $0.83 \pm 0.04$ |
| Fibroglandular | 1444 | $1396 \pm 13$ | 54 | $50 \pm 1$ | 1.75 | $1.75 \pm 0.02$ |
| Liver | 812 | $809 \pm 14$ | 42 | $41 \pm 1$ | 1.40 | $1.43 \pm 0.03$ |
| Prostate | 1597 | $1721 \pm 28$ | 80 | $80 \pm 2$ | 1.25 | $1.23 \pm 0.02$ |

baseline T2 remained above 200 ms. This provides relatively high flexibility for further T2 adjustments by the addition of agarose, as T2 in most biological tissues is smaller than 100 ms [18].

### 3.4 | Experimental Validation of the Preparation Protocol

Test phantoms with hydrogels mimicking the diffusion and relaxation properties of different tissues (pancreas, white matter, fibroglandular tissue, liver, and prostate) were prepared according to the presented protocol. The composition of the phantoms (three identical phantoms were prepared in order to test variability) is shown in Table S2. The hydrogels were then tested for accuracy (in terms of deviations from targeted values), reproducibility, and temporal stability. The targeted and measured values for ADC, T1, and T2 are listed in Table 2, presented as means and standard deviations across the three batches. The corresponding parametric maps are shown in Figure 4A–D as an example for Batch 1. All hydrogels provided a reasonable agreement between measured and intended values: Deviations were less than 8% for T1, less than 7.5% for T2, and less than 11.5% for ADC. Excluding the pancreas mimicking gel, the deviations were even less than 3% for ADC. In addition, the preparation of the gels showed a reasonable reproducibility, as evidenced by the relatively low standard deviations observed across the three batches (Table 2), underscoring the robustness and accuracy of the preparation protocol.

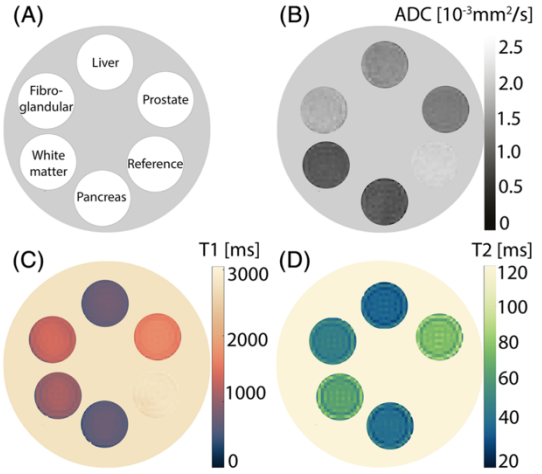


**FIGURE 4** | Parametric maps of gels in the test phantoms mimicking relaxation times of different tissues (pancreas, white matter, fibroglandular tissue, liver, and prostate). (A) Representation of the positions of the hydrogel-filled tubes in the cylindrical housing. (B) Parametric map of ADC values. (C) Parametric map of T1 times. (D) Parametric map of T2 times. The color maps were selected according to the recommendations of the MR Quantitative Study Group of the International Society of Magnetic Resonance in Medicine (ISMRM) [40, 41].

Temporal stability was also acceptable: Over a 12-week storage period, the ADC values and relaxation times of the hydrogel-filled tubes in the phantoms did not change significantly (Figures 5, S1, S2). Small variations were observed between the measurements, but these were also present in the reference sample (pure water) and are therefore expected to be due to measurement uncertainties.

## 4 | Discussion

To date, no instructions have been described for test materials that allow simultaneous and independent adjustment of relaxation and diffusion properties [1]. Most existing materials for test phantoms are designed to mimic only one or two of these parameters, while the other(s) are not controlled. This work presented a practical and reproducible method for the preparation of hydrogels with adjustable T1, T2, and ADC values over a wide range so that many tissue types can be well simulated. The gels are easy to prepare, inexpensive, and show an acceptable temporal stability of at least 3 months. The deviations between measured and target values were less than 8% for relaxation times (T1, T2) and even less than 3% for ADC (except for the pancreas-mimicking gel), confirming the robustness and reliability of the preparation protocol. The comparatively higher deviation observed in the pancreas-mimicking gel (11.5% for ADC) can likely be attributed to the higher variability in ADC measurements at high soy lecithin concentrations. It was shown that at soy lecithin concentrations above 3% (wt/vol), ADC values exhibited a slight dependence on agarose-Gd-DTPA compositions (see *Results, MR Properties of the Ingredients: Gd-DTPA, Agarose, and Soy Lecithin*). This could be due to subtle interactions between soy lecithin and the other substances (agarose and Gd-DTPA), which become more pronounced at higher soy lecithin concentrations and are not accounted for in the parameter adjustment equations. This interpretation is further supported by the high reproducibility of the pancreas-mimicking gel: although the deviation in ADC was larger compared to the other phantom gels,

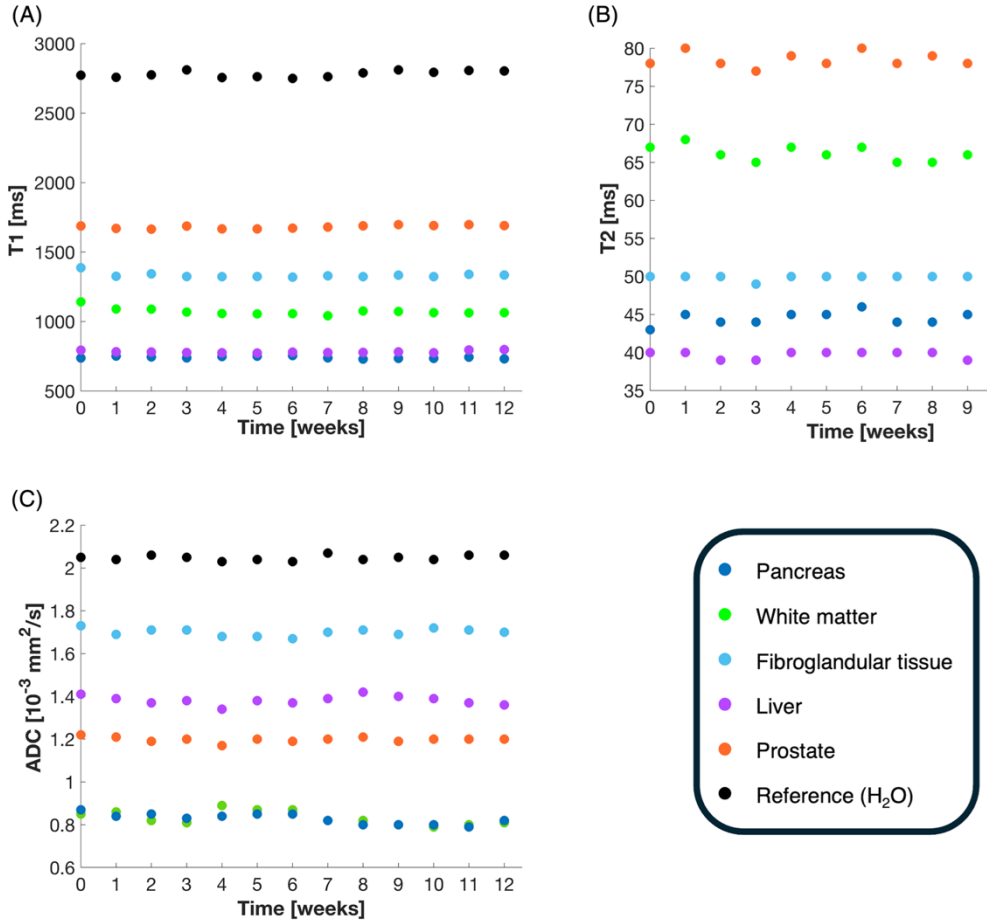


**FIGURE 5** | Temporal stability of the prepared hydrogels (Batch 1) with respect to T1 (A), T2 (B), and ADC (C).

it was consistently observed across repeated preparations (three batches). This suggests that the effect is more likely related to systematic interactions between soy lecithin, agarose, and Gd-DTPA, rather than to reduced reliability of the preparation at higher lecithin concentrations.

Although the hydrogels were successfully produced and allowed for simultaneous and independent adjustment of T1, T2, and ADC values, some limitations remain and must be considered. The presented work focused on developing a formulation that enables relaxation times and ADC to be adjusted largely independently. The range considered includes ADC values from 0.8 to 2 [$10^{-3}$] $mm^2/s$, T1 values from 700 to 2000 ms, and T2 values from 100 to 40 ms. While this covers a broad spectrum of clinically relevant tissue properties, full independence of parameters could not be achieved across the entire range. In particular, the interplay between ADC and T1 proved challenging, since soy lecithin affects both parameters simultaneously. As a result, tissue types characterized by relatively low ADC but long T1 values, such as gray matter, could not be accurately mimicked with the proposed formulation. Furthermore, for certain oncological applications, such as prostate cancer staging, even lower ADC thresholds ($<0.8 \cdot 10^{-3}$ $mm^2/s$) are of interest [42, 43]. In principle, further reduction is possible by increasing the soy lecithin concentration (above 5% wt/vol). A previous study has shown that the addition of soy lecithin can reduce water diffusion to values below $0.5 \cdot 10^{-3}$ $mm^2/s$ at room temperature [27]. This, however, comes with markedly shortened T1 times, which may compromise physiological realism. Additionally, high agarose concentration (3%–4% wt/vol) required for relatively short T2 times becomes challenging when combined with these high soy lecithin concentrations (> 5% wt/vol). This combination leads to a significant increase in gel viscosity, which makes homogeneous mixing difficult and increases the incorporation of air bubbles [25]. This is also the reason why the present study focused on T2 times above 40 ms, which still cover many clinically relevant tissues [18]—shorter T2 times would require even higher agarose concentrations and, as described, become critical for phantom preparation.

The presented design (Equations 1–3) does not account for temperature- and field dependence. In this study, all measurements were performed at a temperature of 20°C and a field

strength of 3 T. However, it is well known that diffusion and relaxation properties are temperature dependent and that relaxation times are also influenced by magnetic field strength [44–47]. These dependencies may lead to discrepancies in measurements under different scanning conditions. Therefore, further measurements at different temperatures and field strengths are needed to systematically study the effects of these factors and to refine the preparation protocol to make it more practical. In addition, research is needed to evaluate potential long-term drifts in relaxation and diffusion properties. Factors such as dehydration or structural changes in agarose or soy lecithin could affect stability over time. Long-term stability (> 12 weeks) is essential when phantoms are used in reproducibility or multicenter studies where measurements are taken over several months or even years. However, for the intended use in research to develop and validate prototype MRI sequences and provide proof of concept, the stability of the hydrogels appears to be sufficient for most applications. Furthermore, the presented gels are designed to mimic specific relaxation and diffusion properties but do not take into account other tissue properties that can significantly affect the MR signal. Effects such as magnetization transfer, non-Gaussian diffusion (kurtosis), susceptibility, or perfusion-related signal contributions are not controlled or specifically adjustable within the current test phantom designs. Future developments could aim to integrate or approximate additional tissue-related parameters to further improve physiological realism. Measurements with higher b-values of up to 3000 s/mm$^2$ could enable a more detailed characterization of the diffusion behavior of the gels, including kurtosis. It is also important to note that Equations (1–3) in the preparation protocol apply only to the product sources used in this study. Soy lecithin and agarose are natural products, so there may be differences in composition or purity from product to product, and thus in MR properties. The authors recommend that when using products other than those presented here, the components should first be characterized by determining their relaxivities and ADC-modifying properties, and constant factors in Equations (1–3) should be adapted appropriately.

Another important aspect, which was beyond the scope of the present study, is a systematic characterization of the morphology and size distribution of the aggregates formed by soy lecithin to better understand the observed restriction of water mobility and MR signal behavior. Preliminary DLS measurements of aqueous soy lecithin solutions indicated mean aggregate sizes ranging from ˜200 nm at a concentration of 0.05% wt/vol to 350 nm at a concentration of 0.5% wt/vol. The observed increase in size with concentration suggests that the aggregates do not simply increase in number but may also undergo changes in morphology and size [32, 33]. This, in turn, supports the finding that the relationship between ADC and soy lecithin concentration is not linear. Future studies should investigate the underlying physicochemical structures in more detail. Additional experiments with small-angle x-ray scattering (SAXS) and cryogenic transmission electron microscopy (cryo-TEM) could provide deeper insights into the underlying mechanisms [31, 48, 49], also at higher concentrations of up to 5% wt/vol.

In summary, the paper presents a step-by-step protocol for the preparation of hydrogels with independently adjustable T1, T2, and ADC values at 3 T using soy lecithin, agarose, and Gd-DTPA. The preparation process is very straightforward, reproducible, and relatively cost-effective. Furthermore, the gels have an acceptable temporal stability of at least 3 months, making them suitable as reference materials for MRI research. Nevertheless, further work is needed to investigate temperature- and field dependency as well as the long-term stability (> 12 weeks) of the materials. To facilitate the practical use of the proposed recipe, we provide a Python-based calculator that determines the required concentrations of Gd-DTPA, agarose, and soy lecithin for user-defined T1, T2, and ADC target values for other users on request (Figure S3).


### Acknowledgments

This work was supported and funded by the German Research Foundation (DFG) under grants SCHI 498/15-1 (package no. 997/2). The authors would like to thank the Physics of Molecular and Biological Matter Group at the University of Tübingen (Institute of Applied Physics) for collaboration, the opportunity to perform the DLS measurements, and for assistance and helpful technical discussions. Open Access funding enabled and organized by Projekt DEAL.


### References


1. K. E. Keenan, K. V. Jordanova, S. E. Ogier, et al., "Phantoms for Quantitative Body MRI: A Review and Discussion of the Phantom Value," *Magma* 37, no. 4 (2024): 535–549, https://doi.org/10.1007/s10334-024-01181-8.

2. K. F. Stupic, M. Ainslie, M. A. Boss, et al., "A Standard System Phantom for Magnetic Resonance Imaging," *Magnetic Resonance in Medicine* 86, no. 3 (2021): 1194–1211, https://doi.org/10.1002/mrm.28779.

3. K. E. Keenan, M. Ainslie, A. J. Barker, et al., "Quantitative Magnetic Resonance Imaging Phantoms: A Review and the Need for a System Phantom," *Magnetic Resonance in Medicine* 79, no. 1 (2018): 48–61, https://doi.org/10.1002/mrm.26982.

4. P. S. Tofts, "QA: Quality Assurance, Accuracy, Precision and Phantoms," in *Quantitative MRI of the Brain*, 1st ed. (Wiley-Blackwell, 2003), 55–81.

5. M. D. Mitchell, H. L. Kundel, L. Axel, and P. M. Joseph, "Agarose as a Tissue Equivalent Phantom Material for NMR Imaging," *Magnetic Resonance Imaging* 4, no. 3 (1986): 263–266, https://doi.org/10.1016/0730-725x(86)91068-4.

6. K. A. Kraft, P. P. Fatouros, G. D. Clarke, and P. R. Kishore, "An MRI Phantom Material for Quantitative Relaxometry," *Magnetic Resonance in Medicine* 5, no. 6 (1987): 555–562, https://doi.org/10.1002/mrm.1910050606.

7. J. O. Christoffersson, L. E. Olsson, and S. Sjöberg, "Nickel-Doped Agarose Gel Phantoms in MR Imaging," *Acta Radiologica* 32, no. 5 (1991): 426–431.

8. P. S. Tofts, B. Shuter, and J. M. Pope, "Ni-DTPA Doped Agarose Gel — A Phantom Material for Gd-DTPA Enhancement Measurements," *Magnetic Resonance Imaging* 11, no. 1 (1993): 125–133, https://doi.org/10.1016/0730-725x(93)90420-i.

9. H. J. Laubach, P. M. Jakob, K. O. Loevblad, et al., "A Phantom for Diffusion-Weighted Imaging of Acute Stroke," *Journal of Magnetic Resonance Imaging* 8, no. 6 (1998): 1349–1354, https://doi.org/10.1002/jmri.1880080627.

10. H. Kato, M. Kuroda, K. Yoshimura, et al., "Composition of MRI Phantom Equivalent to Human Tissues," *Medical Physics* 32, no. 10 (2005): 3199–3208, https://doi.org/10.1118/1.2047807.

11. R. Matsuya, M. Kuroda, Y. Matsumoto, et al., "A New Phantom Using Polyethylene Glycol as an Apparent Diffusion Coefficient Standard

for MR Imaging," *International Journal of Oncology* 35, no. 4 (2009): 893–900, https://doi.org/10.3892/ijo_00000404.

12. C. Pierpaoli, J. Sarlls, U. Nevo, P. Basser, and F. Horkay, Polyvinylpyrrolidone (PVP) Water Solutions as Isotropic Phantoms for Diffusion MRI Studies (2009).

13. A. Hellerbach, V. Schuster, A. Jansen, and J. Sommer, "MRI Phantoms - Are There Alternatives to Agar?," *PLoS One* 8, no. 8 (2013): e70343, https://doi.org/10.1371/journal.pone.0070343.

14. K. E. Keenan, L. J. Wilmes, S. O. Aliu, et al., "Design of a Breast Phantom for Quantitative MRI," *Journal of Magnetic Resonance Imaging* 44, no. 3 (2016): 610–619, https://doi.org/10.1002/jmri.25214.

15. R. Zhao, G. Hamilton, J. H. Brittain, S. B. Reeder, and D. Hernando, "Design and Evaluation of Quantitative MRI Phantoms to Mimic the Simultaneous Presence of Fat, Iron, and Fibrosis in the Liver," *Magnetic Resonance in Medicine* 85, no. 2 (2021): 734–747, https://doi.org/10.1002/mrm.28452.

16. H. L. Cheng, N. Stikov, N. R. Ghugre, and G. A. Wright, "Practical Medical Applications of Quantitative MR Relaxometry," *Journal of Magnetic Resonance Imaging* 36, no. 4 (2012): 805–824, https://doi.org/10.1002/jmri.23718.

17. A. A. Malayeri, R. H. El Khouli, A. Zaheer, et al., "Principles and Applications of Diffusion-Weighted Imaging in Cancer Detection, Staging, and Treatment Follow-Up," *Radiographics* 31, no. 6 (2011): 1773–1791, https://doi.org/10.1148/rg.316115515.

18. J. Z. Bojorquez, S. Bricq, C. Acquitter, F. Brunotte, P. M. Walker, and A. Lalande, "What Are Normal Relaxation Times of Tissues at 3 T?," *Magnetic Resonance Imaging* 35 (2017): 69–80, https://doi.org/10.1016/j.mri.2016.08.021.

19. Y. Cui, H. Dyvorne, C. Besa, N. Cooper, and B. Taouli, "IVIM Diffusion-Weighted Imaging of the Liver at 3.0T: Comparison With 1.5T," *European Journal of Radiology Open* 2 (2015): 123–128, https://doi.org/10.1016/j.ejro.2015.08.001.

20. J. P. Filipe, L. Curvo-Semedo, J. Casalta-Lopes, M. C. Marques, and F. Caseiro-Alves, "Diffusion-Weighted Imaging of the Liver: Usefulness of ADC Values in the Differential Diagnosis of Focal Lesions and Effect of ROI Methods on ADC Measurements," *Magma* 26, no. 3 (2013): 303–312, https://doi.org/10.1007/s10334-012-0348-1.

21. A. Tipirneni-Sajja, S. Brasher, U. Shrestha, H. Johnson, C. Morin, and S. K. Satapathy, "Quantitative MRI of Diffuse Liver Diseases: Techniques and Tissue-Mimicking Phantoms," *Magma* 36, no. 4 (2023): 529–551, https://doi.org/10.1007/s10334-022-01053-z.

22. R. Deichmann, H. Adolf, E. Kuchenbrod, U. Nöth, C. Schwarzbauer, and A. Haase, "Compensation of Diffusion Effects in T2 Measurements," *Magnetic Resonance in Medicine* 33, no. 1 (1995): 113–115, https://doi.org/10.1002/mrm.1910330117.

23. N. Mobini, M. Malekzadeh, H. Haghighatkhah, and H. Saligheh Rad, "A Hybrid (Iron-Fat-Water) Phantom for Liver Iron Overload Quantification in the Presence of Contaminating Fat Using Magnetic Resonance Imaging," *Magma* 33, no. 3 (2020): 385–392, https://doi.org/10.1007/s10334-019-00795-7.

24. M. Woletz, S. Roat, A. Hummer, M. Tik, and C. Windischberger, "Technical Note: Human Tissue-Equivalent MRI Phantom Preparation for 3 and 7 Tesla," *Medical Physics* 48, no. 8 (2021): 4387–4394, https://doi.org/10.1002/mp.14986.

25. V. Fritz, S. Eisele, P. Martirosian, J. Machann, and F. Schick, "A Straightforward Procedure to Build a Non-Toxic Relaxometry Phantom With Desired T1 and T2 Times at 3T," *Magma* 37, no. 5 (2024): 899–907, https://doi.org/10.1007/s10334-024-01166-7.

26. S. Gatidis, H. Schmidt, P. Martirosian, and N. F. Schwenzer, "Development of an MRI Phantom for Diffusion-Weighted Imaging With Independent Adjustment of Apparent Diffusion Coefficient Values and T2 Relaxation Times," *Magnetic Resonance in Medicine* 72, no. 2 (2014): 459–463, https://doi.org/10.1002/mrm.24944.

27. V. Fritz, P. Martirosian, J. Machann, D. Thorwarth, and F. Schick, "Soy Lecithin: A Beneficial Substance for Adjusting the ADC in Aqueous Solutions to the Values of Biological Tissues," *Magnetic Resonance in Medicine* 89, no. 4 (2023): 1674–1683, https://doi.org/10.1002/mrm.29543.

28. P. Walker, R. A. Lerski, R. Mathur-De Vré, J. Binet, and F. Yane, "Preparation of Agarose Gels as Reference Substances for NMR Relaxation Time Measurement. EEC Concerted Action Program," *Magnetic Resonance Imaging* 6, no. 2 (1988): 215–222, https://doi.org/10.1016/0730-725x(88)90452-3.

29. Y. Shen, F. L. Goerner, C. Snyder, et al., "T1 Relaxivities of Gadolinium-Based Magnetic Resonance Contrast Agents in Human Whole Blood at 1.5, 3, and 7 T," *Investigative Radiology* 50, no. 5 (2015): 330–338, https://doi.org/10.1097/rli.0000000000000132.

30. V. Fritz, P. Martirosian, J. Machann, R. Daniels, and F. Schick, "A Comparison of Emulsifiers for the Formation of Oil-In-Water Emulsions: Stability of the Emulsions Within 9 h After Production and MR Signal Properties," *Magma* 35, no. 3 (2022): 401–410, https://doi.org/10.1007/s10334-021-00970-9.

31. I. K. Mkam Tsengam, M. Omarova, E. G. Kelley, et al., "Transformation of Lipid Vesicles Into Micelles by Adding Nonionic Surfactants: Elucidating the Structural Pathway and the Intermediate Structures," *Journal of Physical Chemistry. B* 126, no. 11 (2022): 2208–2216, https://doi.org/10.1021/acs.jpcb.1c09685.

32. T. F. Tadros, "Emulsion Formation, Stability, and Rheology," in *Emulsion Formation and Stability* (Wiley, 2013), 1–75.

33. J. N. Israelachvili, "19 - Thermodynamic Principles of Self-Assembly," in *Intermolecular and Surface Forces (Third Edition)*, ed. J. N. Israelachvili (Academic Press, 2011), 503–534.

34. J. Helenius, L. Soinne, J. Perkiö, et al., "Diffusion-Weighted MR Imaging in Normal Human Brains in Various Age Groups," *AJNR. American Journal of Neuroradiology* 23, no. 2 (2002): 194–199.

35. J. Herrmann, B. P. Schoennagel, M. Roesch, et al., "Diffusion-Weighted Imaging of the Healthy Pancreas: ADC Values Are Age and Gender Dependent," *Journal of Magnetic Resonance Imaging* 37, no. 4 (2013): 886–891, https://doi.org/10.1002/jmri.23871.

36. R. N. Sener, "Diffusion MRI: Apparent Diffusion Coefficient (ADC) Values in the Normal Brain and a Classification of Brain Disorders Based on ADC Values," *Computerized Medical Imaging and Graphics* 25, no. 4 (2001): 299–326, https://doi.org/10.1016/s0895-6111(00)00083-5.

37. S. C. Partridge, W. B. Demartini, B. F. Kurland, P. R. Eby, S. W. White, and C. D. Lehman, "Differential Diagnosis of Mammographically and Clinically Occult Breast Lesions on Diffusion-Weighted MRI," *Journal of Magnetic Resonance Imaging* 31, no. 3 (2010): 562–570, https://doi.org/10.1002/jmri.22078.

38. Y. Cui, S. Han, M. Liu, et al., "Diagnosis and Grading of Prostate Cancer by Relaxation Maps From Synthetic MRI," *Journal of Magnetic Resonance Imaging* 52, no. 2 (2020): 552–564, https://doi.org/10.1002/jmri.27075.

39. T. Tamada, T. Sone, Y. Jo, et al., "Apparent Diffusion Coefficient Values in Peripheral and Transition Zones of the Prostate: Comparison Between Normal and Malignant Prostatic Tissues and Correlation With Histologic Grade," *Journal of Magnetic Resonance Imaging* 28, no. 3 (2008): 720–726, https://doi.org/10.1002/jmri.21503.

40. M. Fuderer, B. Wichtmann, F. Crameri, et al., "Color-Map Recommendation for MR Relaxometry Maps," *Magnetic Resonance in Medicine* 93, no. 2 (2025): 490–506, https://doi.org/10.1002/mrm.30290.

41. M. Fuderer and D. Poot, Resources for Application of Lipari and Navia Color-Maps (2024), https://zenodo.org/records/11185348.

42. Y. Itou, K. Nakanishi, Y. Narumi, Y. Nishizawa, and H. Tsukuma, "Clinical Utility of Apparent Diffusion Coefficient (ADC) Values in Patients With Prostate Cancer: Can ADC Values Contribute to Assess the Aggressiveness of Prostate Cancer?," *Journal of Magnetic Resonance Imaging* 33, no. 1 (2011): 167–172, https://doi.org/10.1002/jmri.22317.

43. G. Thörmer, J. Otto, M. Reiss-Zimmermann, et al., "Diagnostic Value of ADC in Patients With Prostate Cancer: Influence of the Choice of b Values," *European Radiology* 22, no. 8 (2012): 1820–1828, https://doi.org/10.1007/s00330-012-2432-3.

44. T. R. Nelson and S. M. Tung, "Temperature Dependence of Proton Relaxation Times In Vitro," *Magnetic Resonance Imaging* 5, no. 3 (1987): 189–199, https://doi.org/10.1016/0730-725x(87)90020-8.

45. J. P. Korb and R. G. Bryant, "Magnetic Field Dependence of Proton Spin-Lattice Relaxation Times," *Magnetic Resonance in Medicine* 48, no. 1 (2002): 21–26, https://doi.org/10.1002/mrm.10185.

46. F. Wagner, F. B. Laun, T. A. Kuder, et al., "Temperature and Concentration Calibration of Aqueous Polyvinylpyrrolidone (PVP) Solutions for Isotropic Diffusion MRI Phantoms," *PLoS One* 12, no. 6 (2017): e0179276, https://doi.org/10.1371/journal.pone.0179276.

47. K. V. Jordanova, C. C. Fraenza, M. N. Martin, et al., "Paramagnetic Salt and Agarose Recipes for Phantoms With Desired T1 and T2 Values for Low-Field MRI," *NMR in Biomedicine* 38, no. 1 (2025): e5281, https://doi.org/10.1002/nbm.5281.

48. M. T. Ivanović, M. R. Hermann, M. Wójcik, J. Pérez, and J. S. Hub, "Small-Angle X-Ray Scattering Curves of Detergent Micelles: Effects of Asymmetry, Shape Fluctuations, Disorder, and Atomic Details," *Journal of Physical Chemistry Letters* 11, no. 3 (2020): 945–951, https://doi.org/10.1021/acs.jpclett.9b03154.

49. E. Sutherland, S. M. Mercer, M. Everist, and D. G. Leaist, "Diffusion in Solutions of Micelles. What Does Dynamic Light Scattering Measure?," *Journal of Chemical & Engineering Data* 54, no. 2 (2009): 272–278, https://doi.org/10.1021/je800284g.

## Supporting Information

Additional supporting information can be found online in the Supporting Information section. **Figure S1:** Temporal stability of the hydrogels in Batch 2 with respect to T1 (A), T2 (B), and ADC (C). **Figure S2:** Temporal stability of the hydrogels in Batch 3 with respect to T1 (A), T2 (B), and ADC (C). **Figure S3:** Python-based calculator for the determination of the required concentrations of Gd-DTPA, agarose, and soy lecithin for user-defined T1, T2, and ADC target values. **Table S1:** Composition of solutions with different concentrations of soy lecithin, Gd-DTPA, and agarose. A total of 46 solutions were prepared, measured, and analyzed to determine relaxation and diffusion-modifying properties of the ingredients for the hydrogels. **Table S2:** Composition of hydrogels mimicking the diffusion- and relaxation properties of different tissues.